SAINT-PETERSBURG STATE UNIVERSITY

Grishaev Vasily Yurevich

CRYSTAL CHEMISTRY OF NEW MINERAL RELATED SELENITES WITH MONO- AND DIVALENT METAL CATIONS

Scientific speciality 1.6.4. Mineralogy, Crystallography, Geochemistry, geochemical methods of mineral exploration.

DISSERTATION
submitted for the degree of candidate
of chemical sciences

Translation from Russian

Scientific supervisor:
Doctor of Geological and Mineralogical Sciences
Oleg Iokhannesovich Siidra

Saint-Petersburg
2024

Table of contents

Introduction

Topic relevance. The Se^{4+} compounds exhibit a variety of properties which are of interest both for fundamental and applied chemistry, including nonlinear optics, catalysis, separation and exchange, non-trivial magnetism, etc. From the crystal chemical viewpoint, the stereochemically active lone-pair plays a key role in the formation of low-dimensional and non-centrosymmetric structures. Given the presence of magnetically active cations, manifestation of nonlinear magnetism is highly likely. Incorporation of organic cations into the structure is expected to permit their role in the structure formation. Besides, studies in selenium mineralogy allows us to study transformations in natural conditions and predict the possibility of discovering new minerals and their further transformation upon weathering, etc.

The aim of the work is synthesis and development of crystal chemistry of new mineral-related selenites of mono- and divalent metals.

The main objectives of this work are:

1. Synthesis of new selenites with additional anions ReO_4^- and NO_3^- by the evaporation from water solutions.
2. Synthesis of mineral-like selenite chlorides and selenite bromides of Pb^{2+}, Cu^{2+}, Bi^{3+} and Cd^{2+} via gas transport reactions.
3. Study of the effect of the substitution of $SeO_3^{2-} \rightarrow HPO_3^{2-}$ on the symmetry and general motif of the crystal structures thus formed.
4. Determination of crystal structures for the new mineral-like synthetic compounds via the single-crystal X-ray diffraction analysis, development of comparative crystal chemistry of anhydrous and hydrated selenites.

Research methods.

To obtain synthetic compounds the following methods were used:

1. The method of chemical vapor transport reactions. Synthesis was performed in vacuum-sealed silica tubes placed in a furnace with temperature gradient. This approach emulates the mineralization processes in oxidative type fumaroles. Selenites and metal halides play the role of transport agents.
2. Isothermal evaporation method. Crystallization from aqueous solutions at room temperature took place as a result of evaporation of the solution and a change in the concentration of reagents.

A variety of techniques was used to study the new compounds. Data were acquired in the SPbU Resource Centers "Centre of X-ray Diffraction Studies" and "Cente for Microscopy and Microanalysis".

1. Single-crystal X-ray diffraction studies were performed using the Synergy diffractometer with MoKα-radiation at 50 kV and 0.6 mA. The data were integrated and corrected for absorption using the CrysAlis software package (Rigaku Corporation, Tokyo, Japan). Crystal structures were solved and refined using SHELX (Sheldrick 2015).
2. Powder X-ray analysis was performed on the Rigaku MiniFlex II diffractometer (CuKα-radiation) operating at 30 kV and 15mA. X-rays were interpreted using PDXL and Topas 5 software packages.
3. Infrared spectra were obtained using a Bruker Vertex 70 FTIR infrared spectrometer and a standard KBr technique.
4. The semi-quantitative electron miroprobe analysis was performed on a Hitachi TM3000 electron microscope.
5. The second harmonic generation signal was recorded using the Kurtz-Perry method with a powder sample on the Minilite-I Nd:YAG laser with a pulse rate of 10 Hz and primary radiation λ_ω = 1064 nm.
6. Synthetic samples were prepared and photographed using the Leica M205 optical microscope.

Reliability of the results is based on complementary experimental data obtained using modern physico-chemical research methods, reproducibility of experiments and comparison of results with data published by other authors.

Theoretical and practical significance. Synthesis of several series of anhydrous and hydrated selenites by various methods, crystal chemical analysis (tables of coordinates of atoms, interatomic distances, unit-cell parameters and structural features are given). The data obtained from the study of crystal structures of new compounds are included in the Inorganic Crystal Structure Database (ICSD). The results significantly expand the data on crystal chemistry of these groups of compounds. The new data can be used to study relationships linking chemical composition, crystal structures, and physical properties.

Aprobation of the study. The results of the dissertation were reported at international and Russian scientific conferences: Geological International Student Summit (Saint Petersburg, 2023), Lomonosov (Moscow, 2023), XX International Meeting on Crystal Chemistry, X-ray diffraction and Spectroscopy of Minerals (Saint Petersburg, 2024) and XI National Crystal Chemistry Conference (Nalchik, 2024).

Publications. 7 articles have been published on the topic of the dissertation, including journals in Web of Science and Scopus, as well as 5 theses of reports at international and Russian scientific conferences.

Scope and structure of the thesis. The work consists of an introduction, three chapters, a conclusion and a list of cited literature. The total volume of the dissertation is 115 pages, including 44 figures, 21 tables and a list of bibliografic references of 160 titles.

Acknowledgements. The dissertation work was carried out at the Department of Crystallography of Saint-Petersburg State University. The experimental studies were carried out in the resource centers of SPbSU: "Centre of X-ray Diffraction Studies" and "Cente for Microscopy and Microanalysis" and at the Department of Chemical Technology and New Materials (Department of Chemistry) of Lomonosov Moscow State University

The author is deeply grateful to the scientific advisor - Professor of the Department of Crystallography, Prof. Dr. Oleg Siidra for supervision of this work, as well to the Associate Professor at the Department of Inorganic Chemistry, Moscow State University, Dr. Dmitry Charkin for his kind provision of some samples and helpful discussions, Dr. Evgeny Nazarchuk for his help in performing X-ray analisis, and Prof. Dr. Sergey Stefanovich for the measurement of SHG.

The author expresses sincere gratitude for the help in the learning of various crystallographic disciplines by Associate Professor Dr. Tatyana Semenova.

The author expresses special gratitude to the vice director Dr. Natalia Platonova and the collaborators of the SPbSU resource centers for their assistance in conducting experimental research.

Thesis statements to be defended:

1. Electroneutral layers $[M^{II}(HSeO_3)_2]$ are the most stable complex in the compounds of the $A_nX_n \cdot M^{II}(HSeO_3)_2$ series, ($A = Na^+$, enH_2^{2+}, $pipH_2^{2+}$, $M = Mn^{2+}$, $Co^{2+} – Zn^{2+}$, Cd^{2+}, $X = Cl^-$, Br^-) series under conditions of high acidity of the crystallization medium, which is regulated volatile acids. Organic cations for these compounds are structural analogues of alkali metals and participate in the formation of a three-dimensional frame architecture through a system of hydrogen bonds with inorganic layers.
2. The absence of halogen ions in the structures of new hydrated lead selenites leads to weakly asymmetric coordination of the Pb^{2+} cation, which contributes to the formation of frame structures rare for divalent lead oxosols. In the isostructured new compounds $[Pb_2(ReO_4)_2(HPO_3)H_2O](H_2O)$ and $[Pb_2(ReO_4)_2(SeO_3)H_2O](H_2O)$, a proton is replaced by an unshared electron pair on Se^{4+} cations without distortion of symmetry and the main framework structural motif.
3. The structures of 5 new mineral-like selenite halides are organized according to the "guest-host" principle, which is the result of crystallization from gases, and is also determined by the nature of selenophilic and/or halophilic interactions of non-isolated electron pairs. The Br - Cl analogue of sarrabusite was synthesized by the CTP method, where [2O+2O+2X] mixed ligand coordination of the Cu^{2+} cation was revealed.

Main scientific results:

1. 24 new compounds have been synthesized. In the process of decoding and clarifying the structures, 12 new structural types were identified (Charkin *et* al., 2023a, p. 5; Grishaev *et* al., 2023, pp. 182-184; Siidra *et* al., 2024a, pp. 4-5; Charkin *et* al. 2023b, p. 12; Charkin *et* al., 2023c, p. 4; Siidra *et* al., 2023, pp. 288-289).
2. The results obtained showed that selenic acid can form molecular crystals not only with halide complexes, but also with oxoanions (Charkin *et* al., 2023a, p. 5). Oxogroups act as acceptors in the formation of hydrogen bond systems. Selenophilic and/or halophilic interactions are important structural stabilizers in most of the new structures studied.
3. 2 new polymorphs (NaCl)[Cu(HSeO3) were synthesized and structurally characterized for the first time2] (Grishaev *et* al., 2023, pp. 182-184). The preferred crystallization conditions for each of the known modifications are revealed. The high acidity of the medium, regulated by volatile acids, such as trifluoroacetic acid, controls the variety of crystallizing acidic selenites.
4. Anhydrous selenite-cadmium and copper bromide, as well as selenite-bismuth chloride with diselenite groups were obtained for the first time (Siidra *et* al., 2024a, pp. 4-5).
5. The structures of new selenites with organic molecules are low-dimensional and are divided into covalent inorganic and ionic organic layers bonded by hydrogen bonds (Charkin *et* al. 2023b, p. 12).
6. Using the example of new compounds $[Pb_2(ReO_4)_2(SeO_3)H_2O](H_2O)$ and $[Pb_2(ReO_4)_2(HPO_3)H_2O](H_2O)$ demonstrated the possibility of replacing a proton with an unshared electron pair on Se^{4+} cations without distorting the main structural motif (Charkin *et* al., 2023c, p. 4).
7. By the method of chemical gas transport reactions, an analog of sarrabusite was synthesized. The crystal structure has been refined. The type is set [2+2+2] mixed ligand coordination of the Cu^{2+} cation (Siidra *et* al., 2023, pp. 288-289). The formation of sarrabousite on volcanic fumaroles seems very likely, and not only in oxidation zones, from where the mineral is known today.
8. The study of crystallization conditions, as well as the structures of the obtained compounds, allowed not only to expand the understanding of the crystal chemistry of selenites, but also to predict the possibility of formation in nature of certain structural types (e.g. $Cd_7Cu_2(SeO_3)_8Br_2$) (Siidra *et* al., 2024a, pp. 4-5).

The author personal contribution in obtaining all new scientific results: i). Synthesis of new compounds; ii). Performing X-ray diffraction studies; iii). Solving the crystal structure together with the supervisor and other co-authors of scientific publications.

Chapter 1. Literature data

1.1. Mineralogy and geochemistry of selenium

Selenium is a chemical element located in the periodic system of chemical elements in Period 4 group 16. The electron configuration of selenium is [Ar]$3d^{10}4s^24p^4$; the number of valence electrons is 6. Depending on the physico-chemical conditions, oxidation degrees 2-, 4+, 6+ are the most stable.

According to Shannon & Prewitt, 1970, the effective radii of Se^{2-} and S^{2-} are 1.98 Å and 1.84 Å respectively. This similarity of both radii and chemical properties allows the release of sulfur substitution on selenium in chalcogenide minerals (Fischer & Zemann, 1978).

The formation of individual selenium minerals is primarily due to oxidative processes and the difference in ion radii (1.11/1.17Å for Se^{4+}/Se^{6+} versus 0.54/0.43Å for S^{4+}/S^{6+}). According to Krivovichev *et* al., 2019, 2020, mineralogenesis is possible in two ways: oxidation of sulphide ores under aqueous solutions at standard pressures and temperatures (Charykova & Krivovichev, 2017) and in zones of volcanic activity at high temperatures as a result of gas transport reactions in fumaroles. Under these conditions, selenites, like halogenides, can act as a transport agent. The Tolbachik volcano was the site of sofiite $Zn_2(SeO_3)Cl_2$ (Semenova *et* al., 1992), allochalkoseite $Cu^+Cu^{2+}{}_5PbO_2(SeO_3)_2Cl_5$ (Krivovichev *et* al., 2006), and prewittite $KPb_{1.5}Cu_6Zn(SeO_3)_2O_2Cl_{10}$ (Shuvalov *et* al., 2013).

The oxygen-containing compounds of tetravalent selenium adopt a wide variety of crystallochemical forms. They include SeO_2, H_2SeO_3, SeO_3^{2-} anion and its derivatives: diselelenite $Se_2O_5^{2-}$ and $HSeO_3^-$ hydroselenite, its condensation is highly dependent on the pH of the medium (Rugkovin *et* al., 2015c, 2017a). Selenium cation has strong oxidative properties in acidic medium. There are compounds of a wide range of metals among selenite minerals (Krivovichev *et* al., 2019). These compounds are more soluble than sulfites (Séby *et* al., 2001), are more easily absorbed in soils and have less bioavailability compared to selenates.

Selenium, like sulphur, is a chalcopylic non-metal; as a result, selenium minerals often contain copper. Among fumarolic minerals, copper oxocomplexes are often found, e.g. francisite $[Cu_3BiO_2](SeO_3)_2Cl$ (Pring *et* al., 1990), chloromenite $[Cu_9O_2](SeO_3)_4Cl_6$ (Krivovichev *et* al., 1998), georgbokiite α-$[Cu_5O_2](SeO_3)_2Cl_2$ (Krivovichev *et* al., 1999), burnsite $KCd[Cu_7O_2](SeO_3)_2Cl_9$ (Krivovichev *et* al., 2002), allochalcoseite $Cu^+[PbCu_5^{2+}O_2](SeO_3)_2Cl_5$ (Vergasova *et* al., 2005), parageorgbokiite β-$[Cu_5O_2](SeO_3)_2Cl_2$ (Krivovichev *et* al., 2017), prewittite $KPb_{0.5}Cu[PbCu_5O_2]Zn(SeO_3)_2Cl_{10}$ (Shuvalov *et* al., 2013) and nyxobolevite $[Cu_7O_2](SeO_3)_2Cl_6$

(Vergasova *et* al., 2014), formed at temperatures below 1000 °C (Krivovichev *et* al., 2020; Missen *et* al., 2020).

Selenium is a common by-product of processing copper and sulphide ores. In industry, it is extracted as dioxide from the insoluble copper anode sludge which is formed upon refining copper from ores and concentrates with a content of selenium from 5 to 25%, together with small amounts of tellurium (Hoffmann 1989). Selenium is mainly extracted from copper, nickel or lead sulphide ores. Selenium minerals are mainly found in hydrothermal deposits (Grundmann & Förster, 2017) and ore oxidation zones (Charykova & Krivovichev, 2017; Krivovichev *et* al., 2017), but these have but little industrial significance.

1.2.Crystal chemistry of selenium

Tetravalent selenium stands out among other "incomplete valent" cations in that it possesses a stereochemically active electron lone-pair. The anion $(Se^{4+}O_3E)^{2-}$ (E – the lone-pair electrons) forms a trigonal pyramidal complex in which selenium has an “umbrella” coordination and the pair is located at the apex. When a selenite anion is protonated, hydrogen is attached to one of the oxygen vertices to form a hydrogenite anion $HSe^{4+}O_3^-$. In this case protonation lengthens the bond Se - O by about 0.2Å. The hydroselenite anion can be incorporated into the crystal strucutures *per se* or transform into a diselenite anion. Addition of a second proton is possible leading to a neutral $H_2Se^{4+}O_3$ molecule.

The arrahgement of selenite anions in the crystal structures depends on a variety of factors. The first is the presence of metal cations, coordinated by oxygen of the selenite group. The second one is the presence of additional anions in the structure, as usual halogens, that orient themselves to lone-pair electrons. Third, the presence of hydrogen bonds in the structure.

The absence of a centre of symmetry of very the selenite anion enhances formation of selenite-containing non-centrosymmetric structures. The absence of a center of symmetry of the crystal structure is a necessary condition for the occurrence of dielectric and nonlinear optical properties. The presence of "one-sided" polyhedra and "boundary surfaces", "curved" lone-pair electrons (and halide anions) often results in open and/or porous structures, including salt inclusion ones. The charge of anions is commonly compensated by cations with regular coordination environments, which often form sublattices with unusual topologies, being of interest for targeting materials with non-trivial magnetic properties based on *d*- and *f*-element cations. Derivatives of cations with a d^0 configuration are also of interest due to manifestation of the second-order Jahn-Teller effect which significantly increases the probability of forming non-centrosymmetric structures with prominent dielectric and non-linear optical properties

(Zimmerman *et* al 2014b, Halasyamani *et* al 1998). The stereochemical activity due to lower oxidation states and presence of lone-pair is also common for *p*-metal cations, particularly Tl^{+}, Pb^{2+}, and Bi^{3+} (Mudring, 2006), due to the asymmetry of coordination environment, as well as cations with Jahn-Teller effect (Jahn & Teller, 1937).

The Pb atom has four electrons on the valence shell corresponding to the configuration $[Xe]4f^{14}5d^{0}6s^{2}6p^{2}$. The most common oxidation states are 0, 2+, 4+. The coordination of Pb^{2+} cations, the most stable form of lead in both the solution and the solid, is diverse, often unsymmetrical, resulting in a wide range of structural motifs and properties. The Pb^{2+} cation also possesses a lone pair which however may be either stereochemically active or completely inert (Siidra *et* al., 2012).

The neutral Cu possesses one electron on outer shell with configuration $[Ar]3d^{10}4s^{1}$, but it is very easilt excited into a divalent state with $3d^{9}$ configuration. Together with the low crystal field stabilization energy, causes a particularly pronounced Jahn-Teller effect manifested in very strong distirtions of the CuX_6 octahedra, very commonly towards CuX_4 planar squares (Charkin *et* al., 2019; Markovski *et* al., 2019, 2020 a, b, c). Of all *d*-metal cations, Cu^{2+} has the most structurally non-rigid coordination sphere.

The compounds represented in this work can be divided into three groups. The first includes compounds obtained by solution methods containing once or twice protonated selenite anions, wherein complex systems of hydrogen bond are observed. These mostly composed of neutral $[M(HSeO_3)_2]$ layers (M = Mn, Co – Zn, Cd), decorated with halide anions. The second group includes compounds containing “normal” selenite anions (SeO_3^{2-}), lead cations, water and extra anions (perrenate or nitrate) obtained from aqueous solutions at elevated temperatures. The third group consists of anhydrous compounds containing lead, bismuth, copper, and cadmium, obtained by chemical vapor transport reactions. The $(AX)[Cu(HSeO_3)_2]$ (*A* = Na, K, NH_4, Rb, Cs; *X* = Cl, Br) series of copper compounds was previously studied in detail (Charkin *et* al., 2019; Markovski *et* al., 2019, 2020 a,b). The structure of the layers is formed by hydrogen-bonded dimers $(HSeO_3)_2^{2-}$ which coordinate the copper cations forminf slightly distorted planar squares. These squares may be supplemented by one or two halied or nitrate anions to square pyramids or tetragonal bipyramid (stretched octahedron) dependent essentially on the size of the A^{+} cation (alkali or ammonium). At present, there are several known structures illustrating the analogy between selenite and phosphite (Kovrugin *et* al., 2016b), however, this does not apply to lead compounds, including structures with “extra” anions. The hitherto reported compounds are constructed in the form of a framework, where metal polyhedra are connected by bridges SeO_3^{2-} and HPO_3^{2}-, and the cavities are formed by "micelles" from lone-pairs of selenium or phosphate hydrogens. Known selenite nitrates exhibit 3D arrangements and, unlike layered copper hydroselenites, do not include additional cations. The relationships in the Cu-Pb-SeO_3-Cl/Br system are therefore appealing. At least nine compounds were obtained therein (Siidra *et* al., 2018). Thus, the above families are promising both for new structures and new properties.

Chapter 2. New acidic selenites of alkali and transition metals

2.1. Crystal chemistry of new acid selenites of copper and alkaline metals

2.1.1. Synthesis of new compounds

Structural design of layered structures relies on several approaches whereof one of the most successful among inorganics relies on the use of lone-pair cations and halide anions, as well as their crystal chemical analogs (e.g. nitrates). When transition metals are involved, this often leads to compounds exhibiting low-dimensional magnetism (Asai & Kiriyama, 1973; Berdonosov *et* al., 2013), other intriguing phenomena are expected to be manifested. Several families are hitherto known based on the stable 2D "building blocks" e.g. in arsenites, selenites, and tellurites. The two former anions can also contribute to the structure formation in partially or even fully protonated states (Tellgren & Liminga, 1973; Vinogradova, 1981; Shuvalov *et* al., 1984; Sheldrick & Häusler, 1985, 1987; Effenberger *et* al., 1990)), giving rise to hydrogen-bonded networks recently considered as "molecular inorganic polymers" (Markovski *et* al., 2020a). Perhaps the most numerous (i.e. more thoroughly studied) is a family of copper hydrogen selenites based on $[Cu(HSeO_3)_2$ slabs (Baran *et* al., 1991; Feng *et* al., 2006; Markovski *et* al., 2019; Charkin *et* al., 2019). Recent studies of the $(AX)[Cu(HSeO_3)_2]$ ($A = Na^+$, K^+, Rb^+, Cs^+, NH_4^+; $X = Cl^-$, Br^-) has revealed that the nature of the halide anion has no effect on the structure, but the size of the cation strongly affects the interlayer (*AX*) arrangement. As a result, Na^+ and K^+ give rise to two different monoclinic structures (the latter being isostructural to $(RbX)[Zn(HSeO_3)_2]$) (Spirovski *et* al., 2007) while the larger Rb^+, Cs^+, and NH_4^+ contribute to an orthorhombic polumorph first reported for $(NH_4Cl)[Cu(HSeO_3)_2]$ (Trombe *et* al., 1997). These arrangements also differ by the copper coordination CuO_4X_n, where $n = 0 – 2$ dependent on the size of the interlayer A^+ cation.

All members of the copper hydroselenite family were prepared by the slow evaporation of strongly acidic aqueous solutions at ambient temperature which generally leads to multiphase products/ This is not surprising since the respective halide (or nitrate) of monovalent or divalent cation is present in large (6- to 10-fold) excess. The target crystals are formed and exist in relatively narrow pH ranges, *i.e.* within a certain period of evaporation after which, at least in case of halides, they undergo various transformations (Charkin *et* al., 2019).). In addition, copper-free compounds with peculiar structures are also formed at the later evaporation stages (Markovski *et* al., 2020a,b).

Synthesis of (NaCl)[$Cu(HSeO_3)_2$] from freshly prepared aqueous solutions yielded blue acicular crystals of the compound first prepared in sealed silica tubes upon vapour transport (Kovrugin *et* al., 2015b).). However, revision of the polycrystalline mass after *ca.* one-year keeping in a closed vial (to avoid complete drying) revealed the presence of yet another type of coloured crystals (yellowish green) which were found to belong to a new polymorph of the title compound. Further on, we refer to the previously described compound as to (NaCl)[$Cu(HSeO_3)_2$]-I while the new compound is referred to as (NaCl)[$Cu(HSeO_3)_2$]-II. As it was found to be isostructural to (KCl)[$Cu(HSeO_3)_2$] (*vide infra*), a new study was undertaken in the search of possible mixed '(NaCl,KCl)[$Cu(HSeO_3)_2$]' crystals. Instead, a new (third) polymorph of the sodium compound, which is named (NaCl)[$Cu(HSeO_3)_2$]-III, was serendipitously observed with another new structure type. Hereby we report and briefly discuss the structural details of these polymorphs of the (NaCl)[$Cu(HSeO_3)_2$] compound.

The crystals of (NaCl)[$Cu(HSeO_3)_2$]-II were selected from the same sample whereof the crystals of previously known (NaCl)[$Cu(HSeO_3)_2$]-I were picked out (Charkin *et* al., 2019) after ca. 1-year standing in a closed vial under small amount of mother liquor at ambient temperature. A photo of the crystals (wherein the blue ones most likely refer to (NaCl)[$Cu(HSeO_3)_2$]-I) is presented in Fig.2.1.

Greenish-blue single crystals of (NaCl)[$Cu(HSeO_3)_2$]-III were produced in a series of experiments aimed at possible mixed (NaCl,KCl)[$Cu(HSeO_3)_2$] compounds. Five starting solutions, containing 5-*n* mmol NaCl, *n* mmol KCl (*n* = 0 – 4), 1 mmol $CuCl_2$, and 3 mmol H_2SeO_3 in 50 ml of distilled water, were prepared. The precipitates of copper selenite were dissolved by adding 0.3 – 0.5 ml of trifluoroacetic acid and gentle heating for a few minutes on a hotplate (not above 45 °C). As in the previous cases, the color of the solutions changed gradually upon room-temperature evaporation from bluish to green and yellowish; green and blue acicular crystals were formed within three to five weeks.

Studies in the chemically related NaBr – KBr – $CuBr_2$ – H_2SeO_3 systems did not produce any new copper-bearing compounds. The crystal structures of two new copper-free species will be reported in a separate communication.

Qualitative electron microprobe analysis of two compounds reported herein (LINK AN-10000 EDS system) revealed no other elements, except Na, Cu, Se and Cl with atomic number greater than 11 (Na).

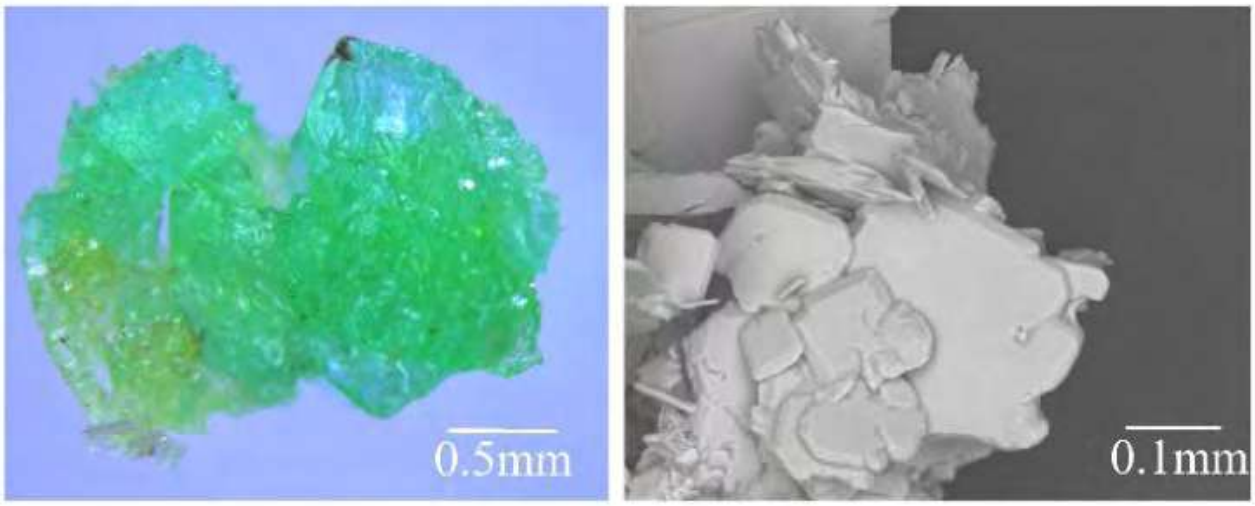

Fig. 2.1. Mint green crystals of (NaCl)[Cu($HSeO_3$)$_2$]-II overgrowing on blue crystals of (NaCl)[Cu($HSeO_3$)$_2$]-I under optical microscope (left) and SEM image (right).

2.1.2. Single crystal X-ray experiments

Single-crystal X-ray data of the new compounds were collected using a Rigaku XtaLAB Synergy-S diffractometer equipped with a PhotonJet-S detector operating with Mo*K*α radiation at 50 kV and 1 mA. A single crystal of each compound was chosen and more than a hemisphere of data collected with a frame width of 0.5° in ω, and 10 s spent counting for each frame. The data were integrated and corrected for absorption applying a multi-scan type model using the Rigaku Oxford Diffraction programs CrysAlis Pro. The structures of compounds were successfully refined with the use of SHELX software package (Sheldrick, 2015). All H atoms were located from the analysis of difference Fourier electron density maps and were refined with the imposed O–H distance restraints of 1.00 ± 0.005 Å. Atom coordinates and thermal displacement parameters are collected in the corresponding cif files; experimental parameters are provided in Table 2.1 and selected interatomic distances in Table 2.2-2.3.

Table 2.1 Crystallographic and structure refinement data for (NaCl)[$Cu(HSeO_3)_2$]-**II** and (NaCl)[$Cu(HSeO_3)_2$]-**III**.

compound	(NaCl)[$Cu(HSeO_3)_2$]-**II**	(NaCl)[$Cu(HSeO_3)_2$]-**III**
space group	*P*2/*c*	$P2_1/c$
a, Å	6.1754(5)	11.1204(3)
b, Å	5.3823(4)	29.0105(7)
c, Å	10.4442(8)	9.0128(2)
β, °	100.3420(10)	93.236(2)
V, $Å^3$	567.0(2)	2902.97(12)
Z	2	16
F(000)	350	2800
radiation	Mo*K*α	Mo*K*α
h, k, l ranges	$-8 \le h \le 7$,	$-16 \le h \le 17$,
	$-4 \le k \le 7$,	$-46 \le k \le 45$,
	$-13 \le l \le 13$	$-14 \le l \le 9$
total number of reflections	2528	45315
number of unique reflections	805	6474
R_1 [$F > 4\sigma(F)$]	0.014	0.038
wR_1 [$F > 4\sigma(F)$]	0.037	0.060
GOF	1.164	1.037
CCDC	2236369	2236370

Table 2.2. Selected bond distances (Å) in structure of (NaCl)[$Cu(HSeO_3)_2$]-**II**.

Cu1-O2	1.9757(14) ×2
Cu1-O1	2.0291(14) ×2
Cu1-Cl1	2.6058(9)
Cu1-Cl1	2.7765(9)
Na1-O3	2.4898(19) ×2
Na1-O1	2.5426(16) ×2
Na1-O2	2.6165(16) ×2
Na1-Cl1	3.3302(6) ×2

Se1-O2	1.7026(15)
Se1-O1	1.7068(14)
Se1-O3	1.7490(16)
Se1-Cl1	3.1474(4)
Se1-Cl1	3.4530(5)

Table 2.3. Selected bond distances (Å) in the structure of (NaCl)[$Cu(HSeO_3)_2$]-**III**.

Se1-O1	1.670(3)	Cu1-O2	1.955(3)	Na1-OH8	2.251(3)
Se1-O2	1.691(3)	Cu1-O9	1.963(3)	Na1-OH5	2.257(3)
Se1-OH1	1.746(3)	Cu1-O10	1.967(3)	Na1-O7	2.487(3)
Se1-Cl3	3.4860(11)	Cu1-O5	1.983(3)	Na1-O8	2.736(3)
Se1-Cl4	3.5875(11)	Cu1-Cl2	2.7180(10)	Na1-Cl1	2.881(2)
		Cu1-Cl4	2.8490(11)	Na1-Cl2	2.969(2)
Se2-O3	1.681(3)				
Se2-O4	1.690(3)	Cu2-O13	1.947(3)	Na2-OH1	2.310(3) ×2
Se2-OH2	1.738(3)	Cu2-O14	1.963(3)	Na2-O15	2.685(3) ×2
Se2-Cl3	3.3729(11)	Cu2-O4	1.970(3)	Na2-Cl3	2.8654(11) ×2
		Cu2-O7	1.981(3)		
Se3-O5	1.682(3)	Cu2-Cl4	2.6938(11)	Na3-OH4	2.272(4)
Se3-O6	1.688(3)	Cu2-Cl2	2.8702(10)	Na3-OH3	2.287(4)
Se3-OH3	1.753(3)			Na3-O9	2.546(4)
Se3-Cl4	3.5068(12)	Cu3-O11	1.940(3)	Na3-O10	2.905(4)
		Cu3-O1	1.959(3)	Na3-Cl4	2.865(2)
Se4-O7	1.685(3)	Cu3-O16	1.962(3)	Na3-Cl4	2.934(3)
Se4-O8	1.693(3)	Cu3-O6	1.977(3)		
Se4-OH4	1.737(3)	Cu3-Cl1	2.7634(10)	Na4-OH7	2.288(4)
Se4-Cl4	3.3659(12)	Cu3-Cl3	2.8543(10)	Na4-OH6	2.310(3)
Se4-Cl3	3.5796(11)			Na4-O3	2.637(3)
		Cu4-O12	1.951(3)	Na4-O5	2.804(3)
Se5-O9	1.680(3)	Cu4-O8	1.977(3)	Na4-Cl1	2.882(2)
Se5-O10	1.687(3)	Cu4-O15	1.978(3)	Na4-Cl2	2.859(2)
Se5-OH5	1.763(3)	Cu4-O3	1.988(3)		
Se5-Cl2	3.3627(11)	Cu4-Cl3	2.7199(10)	Na5-Na5*	1.274(8)
Se5-Cl2	3.6282(11)	Cu4-Cl1	2.7884(10)	Na5-OH2	2.213(5)
				Na5-OH2	2.330(5)

Se6-O11	1.685(3)	Na5-O11	2.500(5)
Se6-O12	1.688(3)	Na5-O12	2.757(5)
Se6-OH6	1.765(3)	Na5-Cl3	2.932(4)
Se6-Cl1	3.4449(11)	Na5-Cl3	2.935(4)
Se6-Cl1	3.5728(11)		
Se7-O13	1.685(3)		
Se7-O14	1.698(3)		
Se7-OH7	1.769(3)		
Se7-Cl2	3.4866(11)		
Se7-Cl2	3.6008(11)		
Se8-O15	1.683(3)		
Se8-O16	1.694(3)		
Se8-OH8	1.773(3)		
Se8-Cl1	3.4270(11)		

* occupancy of Na5 site = 50%

2.1.3. Crystal structures of new polymorphic forms of (NaCl)[Cu(HSeO$_3$)$_2$]

In the structure of (NaCl)[Cu(HSeO$_3$)$_2$]-II, Na^+ cations are coordinated to six oxygen atoms (two of which belong to OH groups) and two chlorine atoms (d(Na–O) = 2.490(2) Å -2.617(2) Å, d(Na–Cl) = 3.3302(6) Å). The Cu^{2+} centers a [4 + 2] octahedron with mixed-anion coordination CuO_4Cl_2 formed by a planar square with Cu-O distances in the range 1,976(1) Å - 2,029(1) Å and two longer apical bonds, Cu - Cl 2.6058(9) Å – 2.7765(9) Å. Hence, the structure of the II polymorph differs from that of (KCl)[Cu(HSeO$_3$)$_2$] wherein the Cu - Cl separations are 2.623(5) Å and 3.184(1) Å, i.e. the Jahn-Teller distortion (Jahn & Teller, 1937) of the CuO_4Cl_2 octahedron in the sodium compound is less pronounced. The probable reason is the size difference between K^+ and Na^+; in the first case, the distance between the [Cu(HSeO$_3$)$_2$] layers is longer, and formation of Cu - Cl - Cu bridges is not favored. In addition, the Cu - Cu distances within the [Cu(HSeO$_3$)$_2$] layer are longer in (KCl)[Cu(HSeO$_3$)$_2$] compared to (NaCl)[Cu(HSeO$_3$)$_2$]-II (Fig. 2.2 and 2.3).

The selenium atoms form the classical SeO_3E cores; the distances Se-O are different due to protonation of one vertex. The distances Se - O and Se – OH, centered around 1.70 Å and 1.75Å relatevely, vary just slightly within the family.

In the more complex structure of (NaCl)[Cu(HSeO$_3$)$_2$]-III, five symmetrically independent Na^+ cations adopt two different coordinations dissimilar to those in (NaCl)[Cu(HSeO$_3$)$_2$]-II. The square planar coordinanet Na5 is eqiprobably disordered over two possible position. Na1, Na3 and Na5 center irregular $NaO_2(OH)_2Cl_2$ polyhedra while Na2 and Na4 center other distorted $NaO_2(OH)_2Cl_2$ octahedra. The Na – Cl distanses lie in range of 2.859(2) – 2.969(2) Å which is essentially less compared to 3.3302(6) Å in (NaCl)[Cu(HSeO$_3$)$_2$]-II. (Fig. 2.2 and 2.3)

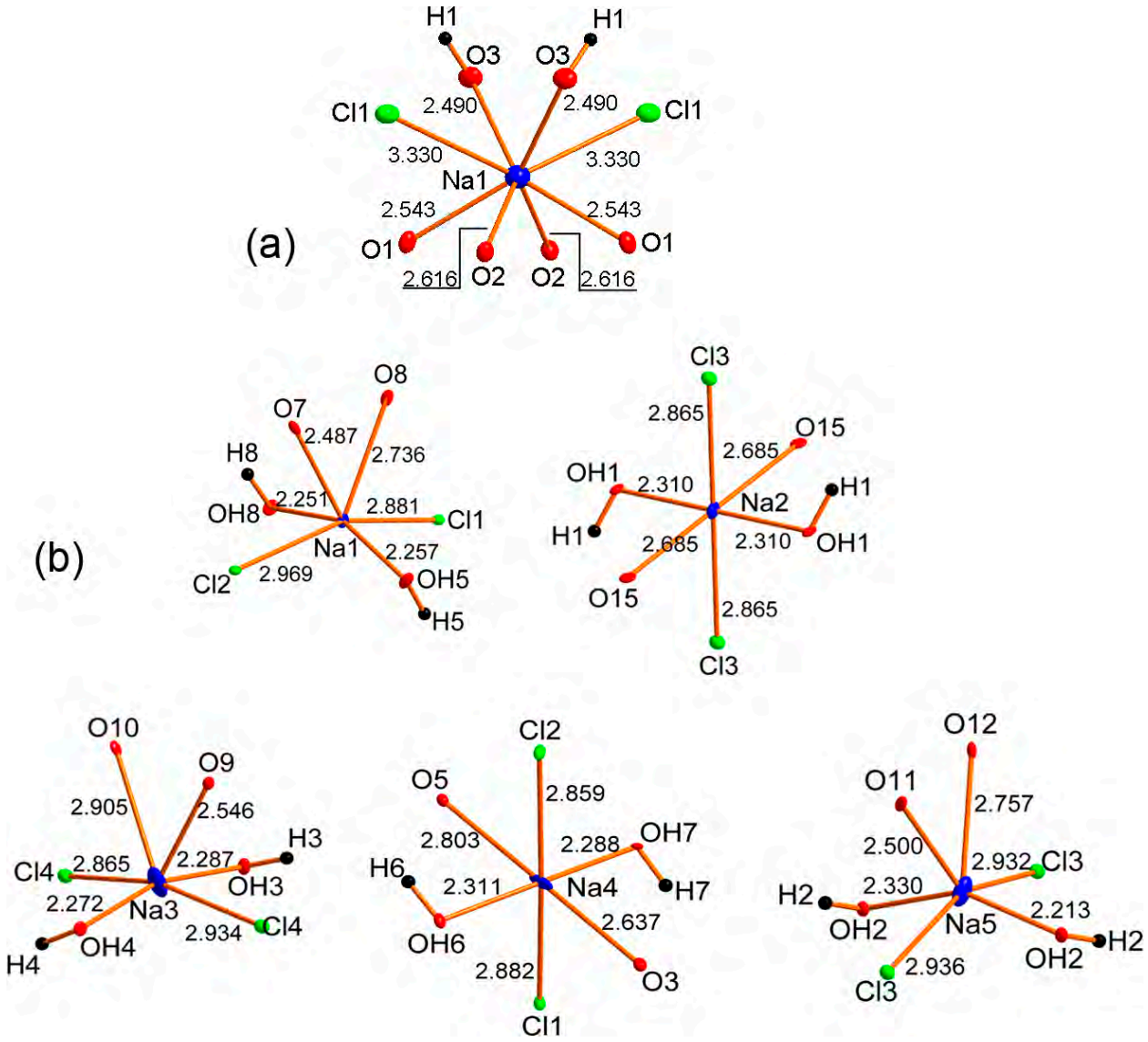

Fig. 2.2. Coordination environments of Na^+ cations in (NaCl)[Cu(HSeO$_3$)$_2$]-**II** (a) and (NaCl)[Cu(HSeO$_3$)$_2$]-**III** (b). Displacement ellipsoids are drawn at the 50 % probability level.

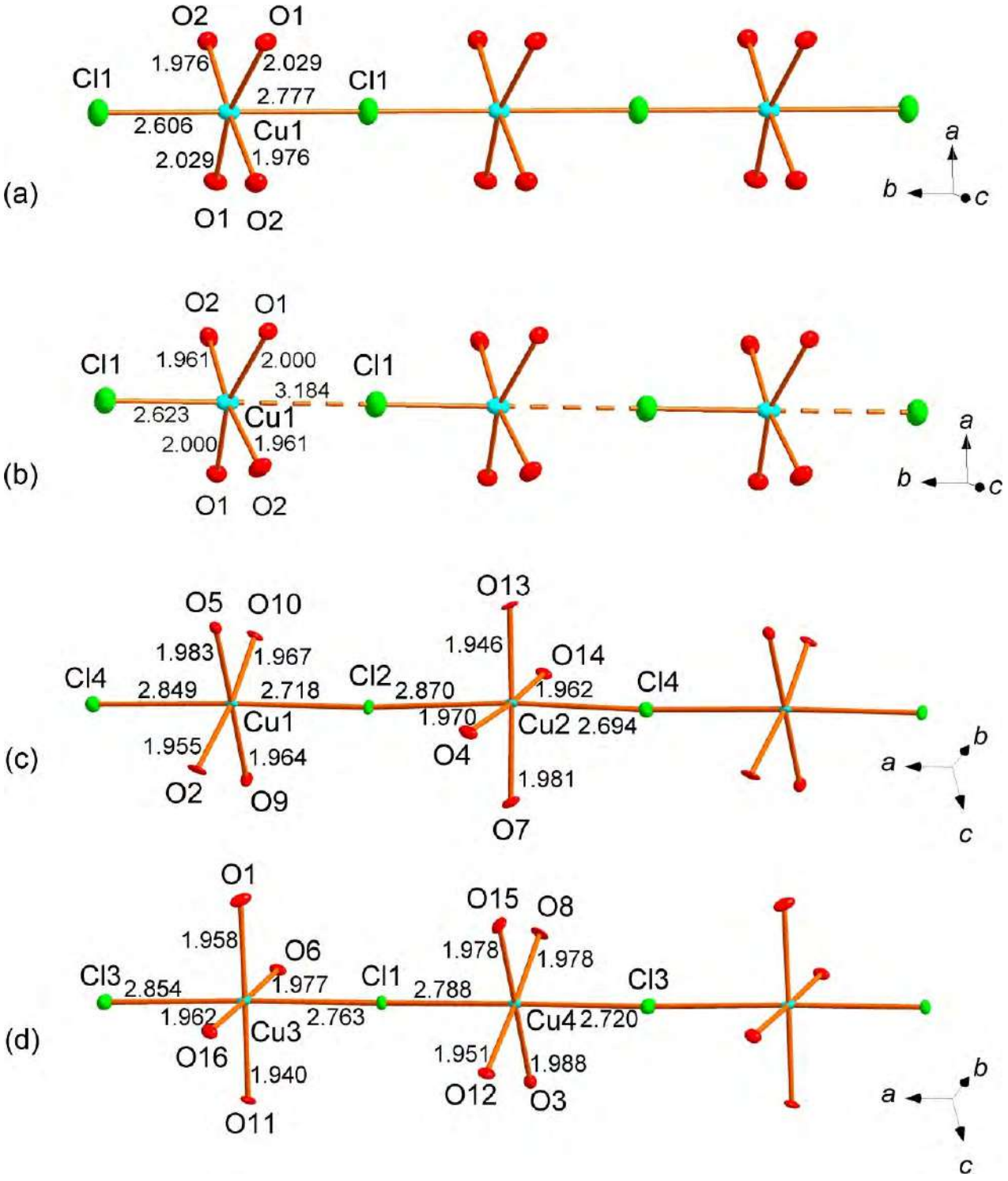

Fig. 2.3. Cu^{2+} coordination environments in the structures of (NaCl)[$Cu(HSeO_3)_2$]-**II** (a), (KCl)[$Cu(HSeO_3)_2$] (Cu-Cl bonds > 3.0 Å are shown by dashed lines) (b) and (NaCl)[$Cu(HSeO_3)_2$]-**III** (c,d). Displacement ellipsoids are drawn at the 50 % probability level.

All four symmety independent Cu atoms in (NaCl)[$Cu(HSeO_3)_2$]-III are coordinated by four oxygen atoms at nearly equal distances Cu – O ≈1.95 Å forming planar CuO_4 squares, augmented by two Cl^- anions in apical positions, which reaults in distorted CuO_4Cl_2 octahedra similar to those in (NaCl)[$Cu(HSeO_3)_2$]-II (Fig. 2.4). The Cu – Cl distances lie in the range of 2.694(1) – 2.870(1) Å. These octahedra share Cl voertices to form chains. Overall, the [$Cu(HSeO_3)_2$] layers in (NaCl)[$Cu(HSeO_3)_2$]-III exnibit a new mutual orientation of the $HSeO_3^-$ contrary to those observed in other members of the (AX)[$Cu(HSeO_3)_2$] family (Charkin *et* al 2019).

The (NaCl)[$Cu(HSeO_3)_2$]-II is formally isostructural to (KCl)[$Cu(HSeO_3)_2$]. The largest difference concerns the environment of Cu^{2+}. Generally, the coordination number of Cu^{2+} cation decreases with the increase of ionic radius of A^+. As noted earlier (Charkin *et* al. 2019), the structures (*AX*)[$Cu(HSeO_3)_2$] can be described as a [$Cu(HSeO_3)_2Cl]^-$ three-dimensional framework, wherein the Cl^- anions "stitch" the [$Cu(HSeO_3)_2$] layers and the voids are filled by the alkali metal or ammonium cations. In the case of Na^+, which has the smallest radius, the Cu-Cu distance is the shortest. In the structure of (KCl)[$Cu(HSeO_3)_2$, these are longer and the asymmetry copper of the coordination increases, so the pattern can be considered to be intermediate between distorted octahedral and square-pyramidal coordination Cu^{2+}. Finally, in the structure of (RbCl)($Zn(HSeO_3)_2$] (Spirovski *et* al. 2007), Zn^{2+} adopts the classical square-pyramid coordination, which corresponds to its tendency to have smaller coordination numbers compared to Cu^{2+}. It is possible that this trend will be observed in the structures of yet not yet reported (AX)[$Zn(HSeO_3)_2$] with A = K and Cs.

The common feature of both new polymorphs if (NaCl)[$Cu(HSeO_3)_2$] is a copperhydroselenite-selenite architecture with the “boundary” of lone-pairs oriented towards the chloride anions. The Se-Cl interactions, weak as they may seem, are likely to make an important contribution into the stability of the resulting structural architectures. The shortest Se-Cl contacts of 3.1474(4) Å are observed in the structure of (NaCl)[$Cu(HSeO_3)_2$]-II (table 2.2). Such sepatations aresignificantly larger in (NaCl)[$Cu(HSeO_3)_2$]-III wherein the shortest is 3.366(1) Å for Se4-Cl4 (table 2.3).

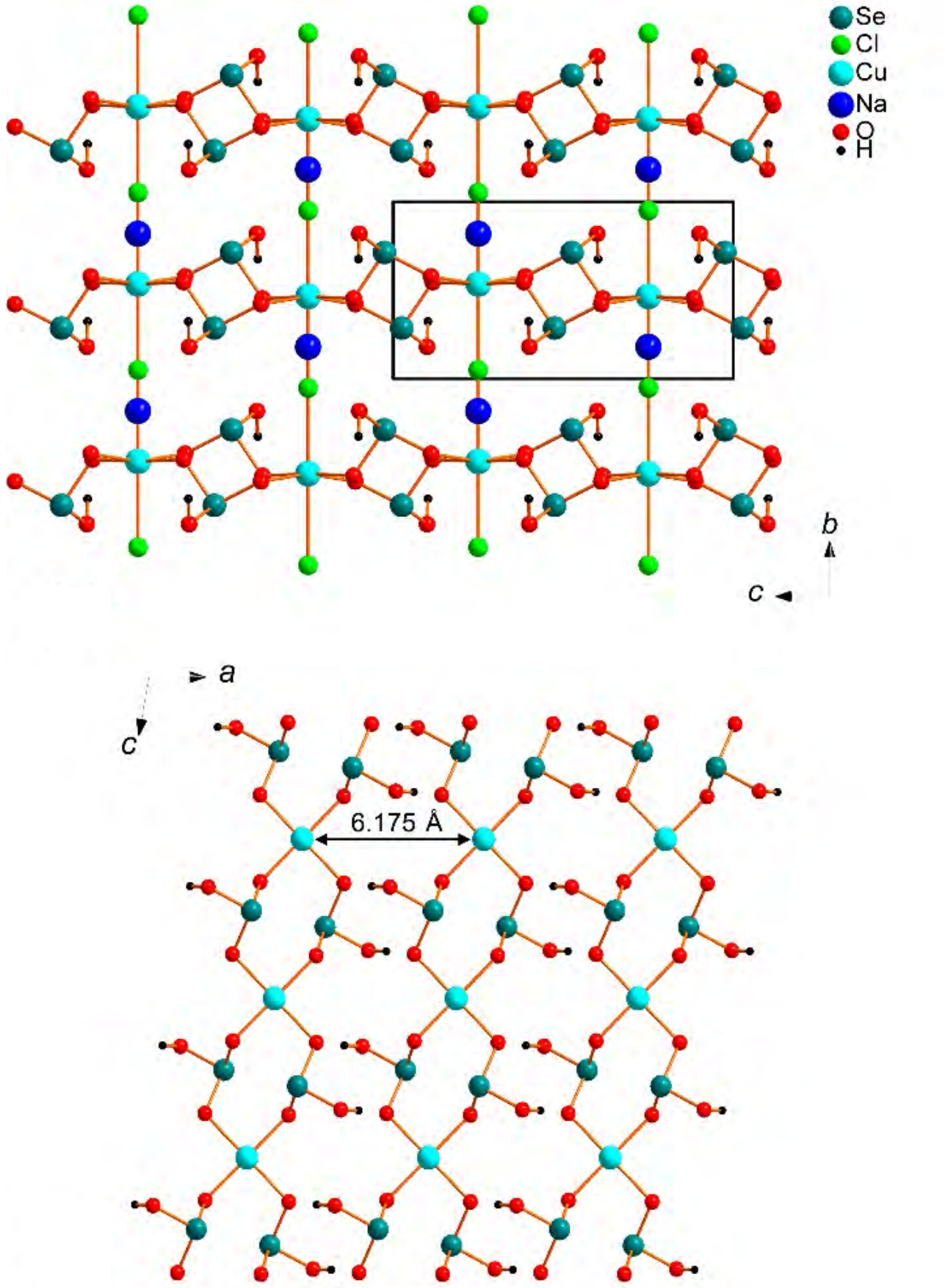

Fig. 2.4. General projection of the crystal structure of (NaCl)[$Cu(HSeO_3)_2$]-**II** (above) and [$Cu(HSeO_3)_2$] layers (Cu^{2+} = blue balls; Se^{4+} = cyan balls; O^{2-} = red balls; H^+ = black balls) in (NaCl)[$Cu(HSeO_3)_2$]-**II** (below).

The structural organization of (NaCl)[$Cu(HSeO_3)_2$]-III is relatively similar to that of (NaCl)[$Cu(HSeO_3)_2$]-I (Kovrugin *et* al. 2015c) wherein the Na^+ cations are disordered. In the intermediate layer of (NaCl)[$Cu(HSeO_3)_2$]-I and (NaCl)[$Cu(HSeO_3)_2$]-III (Fig. 2.5), the lone-pairs of Se^{IV} are directed towards each other, forming kind of "micelles". Thus, the cavities in the three-dimensional frames of these structures adopt a staggered order filled with either sodium cations or lone-pairs of Se^{IV}. In the structure of (NaCl)[$Cu(HSeO_3)_2$]-II, formation of such “lone pair micelles” is less pronounced.

The (NaCl)[$Cu(HSeO_3)_2$]-III exhibits the most complex architecture among the whiole family of “layered hydroselenites”. Despite presence of potassium chloride in the growing media, no indication of K^+ being incorporased was found. Instead, potassium is deposited in the early stages of crystallization, probably as less soluble (KCl)[$Cu(HSeO_3)_2$], which in turn does not include any noticeable amounts of Na^+, probably due to the size difference between Na^+ and K^+. Thus, the sodium chloride system echibits the highest structural diversity. The relatively poor agreement of Na^+ and the cavities in the $[Cu(HSeO_3)_2Cl]^-$ framework retards crystallization which becomes more sensitive to the external factors such as evaporation rate or presence of other species in the mother liquor. Note that the deposition times of the (NaCl)[$Cu(HSeO_3)_2$] polymorphs increase in the order I < III < II. The structures of polymorphs I and III are close, but somewhat longer crystallization time of III (probably due to the depletion of Cu^{2+} and $HSeO_3$ as (KCl)[$Cu(HSeO_3)_2$] is deposited the low initial content of Na^+) contributes to the formation of a more ordered motif corresponding to a well-developed superstructure. Finally, the very long crystallization time required to form the II polymorph results in a completely ordered, however different, structure. Similar polymorphism may be suggested for some chemically related systems, for example, AX – (ZnX_2 or CdX_2) – H_2SeO_3.

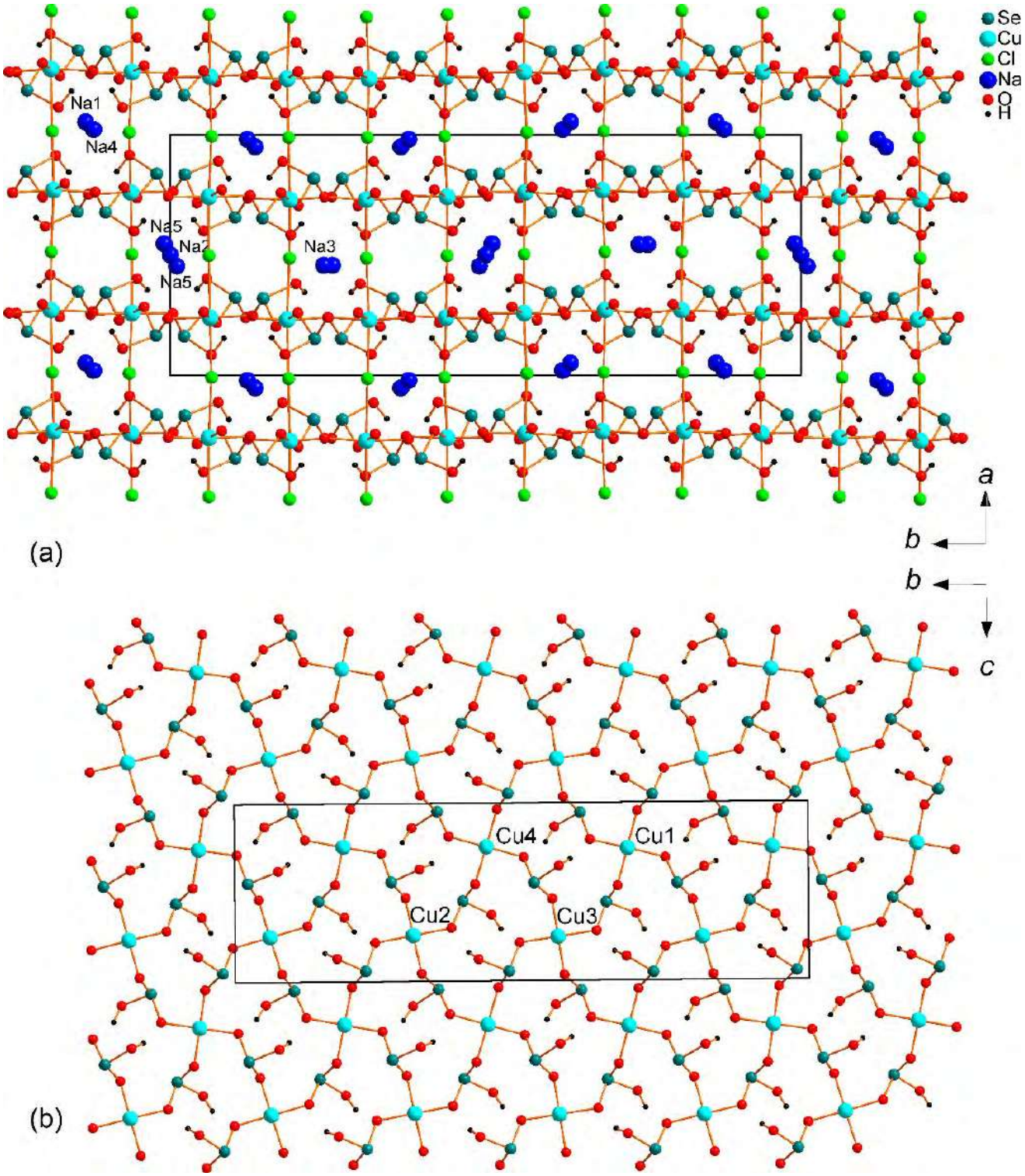

Fig. 2.5. General projection of the crystal structure of (NaCl)[Cu(HSeO$_3$)$_2$]-**III** along the *c* axis (a) and [Cu(HSeO$_3$)$_2$] layer (b).

2.1.4. Infrared spectroscopy

The IR spectrum of (NaCl)[$Cu(HSeO_3)_2$]-II (Fig. 2.6) was acquired at ambient conditions on a Bruker Vertex 70 FTIR spectrometer with a resolution of 4 cm^{-1}. A powdered sample was added to a dried KBr pellet using another pure KBr pellet as a reference. The band at 453 cm^{-1} can be tentatively attributed to the Cu–O stretching vibrations by analogy to the $[Cu(H_2O)_4]^{2+}$ cation (Berger, 1976). The bending Cu–O vibrations lie beyond the range studied.Strong vibrations in the range 1205-787 cm-1 and 509 cm^{-1} correspond to the $[(HSeO_3)_2]^{2-}$ dimers linked by hydrogen bonds (Kretzschmar *et* al., 2015). The Se-O stretching vibrations lie usually in the 754-679 cm^{-1} range (Valkonen *et* al., 1986; Kretzschmar *et* al., 2015), while Se-OH modes are observed at 480 cm^{-1} (Nakamoto, 2009) The bands at 2829-2292 cm_{-1} correspond to O-H vibrations.

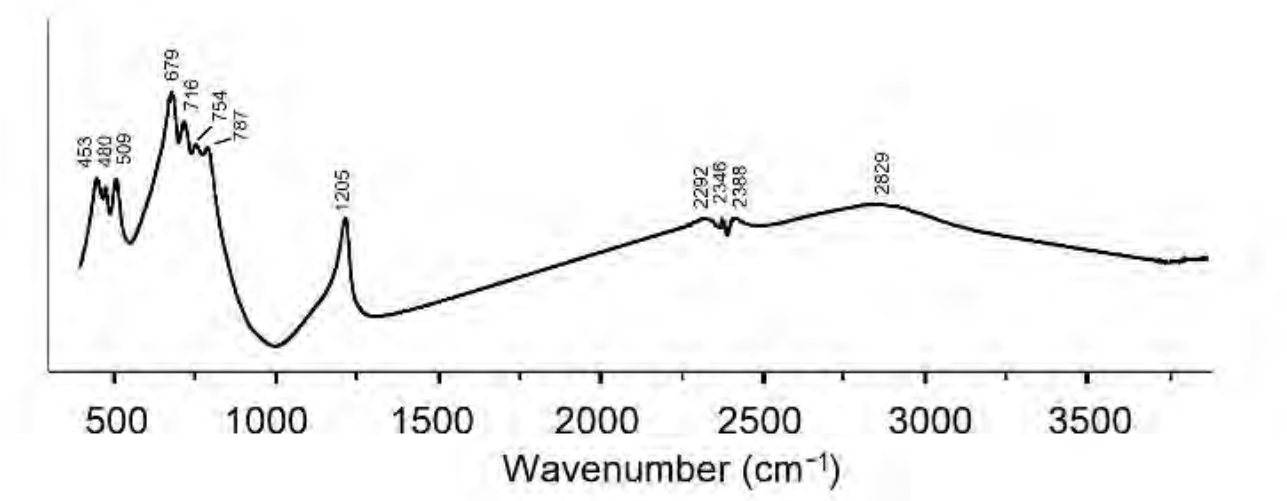

Fig. 2.6. IR absorbtion spectra of (NaCl)[$Cu(HSeO_3)_2$]-II

2.2. Crystal chemistry of new acid selenites of transition metals and organic cations

2.2.1. Synthesis of new compounds

The compounds which feature simultaneously organic and inorganic parts are often used in zeolite synthesis (Xiao *et* al., 2020), wherein the organic part of the structure acts as a template for formation of cavities with given size and shape in the inorganic framework. Another application of organo-inorganic compounds is medicine, primarily the targeted delivery of microelements and sonetimes drugs. Furthermore, the template molecule commonly serves as a donor of hydrogen bonds donated to the inorganic framework which may affect its substructure. Among the previously considered copper hydroselenite halides, the compounds of ammonium, rubidium, and cesium are isostructural (Charkin *et* al., 2019, Spirovski *et* al., 2007); yet, among nitrates the ammonium compouns contribute to most complex interlayer structure, $(NH_4NO_3)_3[Cu(HSeO_3)_2]$ (Lafront & Trombe, 1995). The NH_4^+ cations form strong directed hydrogen bonds with the nitrate anions. This suggests that some other compounds, such as organic ammonium species, may also be incorporated into the interlayer space. This was initially demonstrated by a cadmium-containing compound $(enH_2)[Cd(HSeO_3)_2Cl_2]$ (enH_2^{2+} = ethylenediammonium cation, $H_3NCH_2CH_2NH_3^{2+}$) (Pasha *et* al., 2003); later, isostructural cobalt and copper compounds were reported (Feng *et* al., 2006). The topology of layers therein is nearly the same as in $[M(H_2O)_4][Cu(HSeO_3)_2Cl_2]$, $[Co(H_2O)_4][Co(HSeO_3)_2Cl_2]$ and $[A_2(H_2O)_n][Co(HSeO_3)_2Cl_2]$ (A = K, n = 2; A = Cs, n = 0). The existence of a related piperazinium compound was also noted in (Pasha *et* al., 2003), however, no data were provided and possible analogs were not mentioned. However, the ethylenediammonium and piperazinium cayopns have very similar distances between the ammonium hydrogen bond donor centers, although the number of "active" N-H bonds is different (6 instead of 4). In this study, we have conducted an extensive search for possible analogues for selenite halides of hydrogen, diprotonated ethylenediamine (enH_2^{2+}), piperazine ($pipH_2^{2+}$), N,N'-dimethylendediamine ($dmedaH_2^{2+}$) and N-methylpiperazine ($mpip_2^{2+}$) (Fig. 2.7) and transition metals and Cd, reported earlier, to form layers $[M^{II}(HSeO_3)_2]$. Similar experiments were also made with magnesium, manganese cobalt, zinc, and nickel halides.

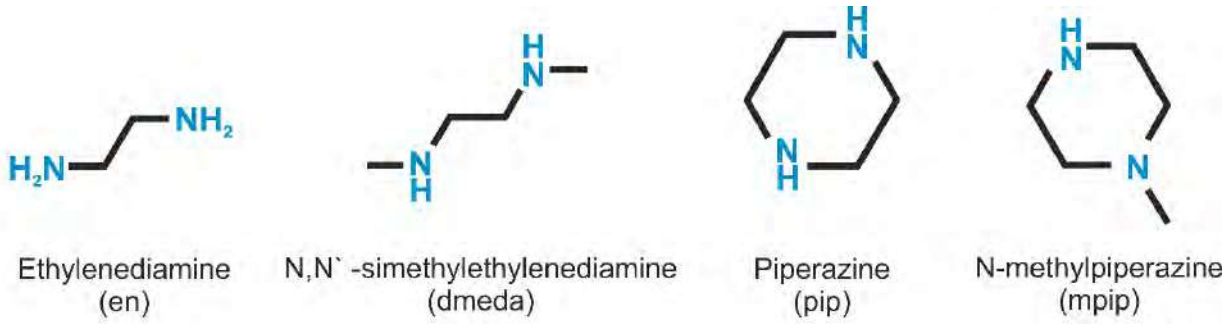

Fig. 2.7. Structural formulas of organic complexes (from left to right): ethylenediamine (en), N, N'-dimethyl ethylendediamine (dmeda), piperazine (pip), N-methylpiperazine (mpip).

The synthesis was performed by isothermic evaporation of strongly acidic aqueous solutions. The reagents used were selenious acid, divalent metal halide, and organic diamine in the 1:1:3 ratio. As a rule, 1 ml of MX_2 solution was mixed with 3 ml 1 M of H_2SeO_3 solution. Then, 1 ml of diamine solution was added by the drops then mixed with a small glass rod. It was demonstrated earlier (Charkin *et* al., 2019, Lafront *et* al., 1995, Pasha *et* al., 2003) a 50% excess of selenious acid is necessary to suppress the formation of insoluble metal selenites and competitive formation of halometallates, which are easily formed with the addition of halogen acid (Charkin *et* al., 2019). Typically, after addition of ethylenediamine, precipitation or turbidity was observed due to the formation of $MSeO_3$ aq, which mostly disappeared after addition of ethylenediamine, mixing and heating to a temperature of 50-60°C for 5-10 minutes on a hotplate. To suppress premature evaporation, a few drops of water were added. With M = Cu or Cd, which form less soluble selenites, green and white precipitates formed, respectively, which dissolved after heating and adding 0.1-0.7 ml trifluoroacetic acid for halides and 0.1-0.5 ml 50% nitric acid for nitrates according to the previously reported protocols (Charkin *et* al., 2019, Grishaev *et* al., 2023). In just few cases, traces of $CdSeO_3 \cdot aq$ remained but dissolved when the crystals of the target compounds began to form. The halide solutions (colorless in the case of M^{II} = Mg, Zn and Cd, originally pink for Mn, purple for Co, green in the case of Ni and blue in the case of Cu) were left to evaporate at ambient conditions. Crystallization started a few weeks after the color of halide-containing solutions became lilac (Co), green (Cu-Cl) or brownish (Cu-Br); the color of the crystals containing Cu and Co was blue green and dark violet, respectively. The intermediate color change of the solution likely indicates transient formation of $[MX_4^{2-}]$ halometallate due to extra hydrohalic acid in solution. For solutions containing Mn and Ni (as well as for all nitrate experiments), no color change was observed. The crystals containing Mn and Ni were grayish pink and brownish yellow. Crystals grown in solutions containing Mg were of relatively low quality. Sometimes small amounts of red selenium precipitated due to the reduction of selenic acid, which did not affect the formation and growth of the target crystals. The exception was dmeda, which was rapidly oxidized with selenistic acid; therefore, no further studies were conducted with this component. The crystals were collected and stored in closed vials under a drop

of mother iquor. Further evaporation resulted in deposition of crystals of similar color and appearance. Most of these experiments produced target comounda with en, only a few for pip and none for mpip. In most cases, crystals of some by-products were also observed, either due to the non-stoichiometric reagent ratio in the initial solution or instead of the target compound. Based on a combination of diamine, metal cation and anions, these by-products can contain either all or only some of the components.

2.2.2. Single crystal X-ray experiments

The single crystal X-ray analysis was performed on a Rigaku XtaLAB Synergy-S (Tokyo, Japan) diffractometer, equipped with PhotonJet-S detector (Tokyo, Japan) operating on MoKα-radiation at 50 kV and 1 mA. A single crystal was chosen, and a more than hemisphere with a frame width of 0.5° by ω was collected, each frame took 5-15 seconds to count. The data were integrated and corrected for absorption using the multiscan model in Oxford's Rigaku CrysAlis Pro (Rigaku OD, 2015) (Tokyo, Japan). The experiments were carried out at 150 K. The unit cell parameters were calculated by least-squares fite. The structures were solved using direct methods implemented into WinGX 2020.1 software (Glasgow, UK) (Farrugia *et* al., 1999) and Olex2 version 1.3.0 (Regensburg, Germany) (Dolomanov *et* al., 2009). Final solutions include coordinates and anisotropic thermal parameters of atoms, except for hydrogens which were localized using the mathematical part of the program Olex2.

Experimental data for the $(enH_2)[M(HSeO_3)_2X_2]$series are collected in table 2.4 (except M = Mg, where crystals were of low quality). All these compounds are isostructural; some trends are discussed below. The corresponding data for the piperazinium compounds are given in Table 2.6. Unlike the alkali metal hydroselenite-halide family, we have not observed the formation of layered nitrate-hydroselenites containing organic cations. With en and pip, new compounds were discovered, $(BH_2)(NO_3)_2•2H_2SeO_3$.

Table 2.4. Crystallographic data and refinement parameters for the $(enH_2)[M(HSeO_3)_2X_2]$ series

M-X	Cd-Cl	Co-Br	Co-Cl	Cu-Br	Cu-Cl
space group			$P2_1/c$		
a (Å)	8.8222(4)	8.2957(5)	8.9395(6)	8.6750(4)	9.1833(4)
b (Å)	7.6140(3)	7.8094(3))	7.3147(4)	7.3277(3)	7.1548(3)
c (Å)	10.2481(5)	9.9433(5)	9.7558(8)	9.6812(4)	9.4845(5)
β (°)	114.196(6)	112.430(6)	111.904(9)	113.093(6)	110.608(5)
V ($Å^3$)	627.91(6)	595.44(6)	591.88(8)	566.10(4)	583.30(5)
h, k, l |range	-12→12	-12→12	-15→15	-9→13	-13→12

	-11→9	-8→12	-11→12	-10→10	-10→10
	-15→14	-14→13	-15→16	-12→12	-12→12
total number of reflections	2119	2019	4713	2319	1992
number of unique reflections	1885	1702	3061	2009	1710
R_1	0.023	0.025	0.047	0.029	0.035
wR	0.051	0.053	0.084	0.056	0.070
Gof	1.053	0.984	0.989	1.056	1.095
CCDC	2,271,293	2,271,295	2,271,296	2,271,297	2,271,298

Continuation of the table 2.4.. Crystallographic data refinement parameters for series $(enH_2)[M(HSeO_3)_2X_2]$:

M-X	Cu-Cl	Mn-Br	Mn-Cl	Zn-Br	Zn-Cl	Ni-Cl
space group			$P2_1/c$			
a (Å)	8.9953(3)	8.9465(4)	8.2958(3)	9.1862(4)	8.6699(4)	8.6420(8)
b (Å)	7.1677(2)	7.4460(3)	7.6712(2)	7.1516(2)	7.3448(2)	7.3081(4)
c (Å)	9.3819(4)	10.0240(5)	9.5977(4)	9.4849(4)	9.6996(4)	9.6000(9)
β (°)	111.215(4)	112.720(6)	111.293(4)	110.624(4)	113.228(5)	112.999(11)
V ($Å^3$)	563.91(3)	615.94(5)	569.09(3)	583.19(4)	567.59(4)	558.11(8)
h, k, l range	-12→12	-12→12	-15→15	-9→13	-13→12	-11→11
	-11→9	-8→12	-11→12	-10→10	-10→10	-9→9
	-15→14	-14→13	-15→16	-12→12	-12→12	-12→12
total number of reflections	2395	2091	2362	2414	2339	1349
number of reflections	2101	1791	2109	2128	2089	1048
R_1	0.024	0.030	0.022	0.028	0.028	0.039
wR	0.057	0.073	0.049	0.062	0.058	0.076
Gof	1.026	1.107	0.981	1.125	1.047	1.058
CCDC	2,271,307	2,271,300	2,271,301	2,271,306	2,271,305	2,271,304

Table 2.5. Geometrical parameters of MO_4X_2 polyhedra in $(enH_2)[M^{II}(HSeO_3)_2X_2]$.

Polyhedron	CdO_4Br_2	CdO_4Cl_2	CoO_4Cl_2	CuO_4Br_2	CuO_4Cl_2
Bond valence M^{2+}	2.04	2.08	2.00	1.89	2.09
Average bond length (Å)	2.4387	2.3950	2.2243	2.2807	2.2329
Polyhedra volume ($Å_3$)	19.063	18.177	14.453	15.083	14.271
distortion index	0.0768	0.0546	0.0884	0.1686	0.1532

Continuation of the table 2.5. Geometrical parameters of MO_4X_2 polyhedra in $(enH_2)[M^{II}(HSeO_3)_2X_2]$:

Polyhedron	MnO_4Br_2	MnO_4Cl_2	ZnO_4Br_2	ZnO_4Cl_2	NiO_4Cl_2
Bond valence M^{2+}	2.11	2.04	2.09	1.90	2.01
Average bond length (Å)	2.3587	2.3032	2.2806	2.2318	2.1973
Polyhedra volume ($Å_3$)	17.124	16.131	15.081	14.611	13.9603
distortion index	0.1086	0.0735	0.1689	0.0866	0.08296

Table 2.6. Crystallographic data refinement parameters for $(pipH_2)[Cd(HSeO_3)_2X_2]$ (X = Cl, Br) and $(pipH_2)[M(HSeO_3)_2(Se_2O_5)]_2$ (M = Mn, Co).

M-X	Cd-Cl	Cd-Br	Co-Se_2O_5	Mn-Se_2O_5
space group	*P*-1			
a (Å)/ α (°)	7.6207(3)/ 77.077(4)	7.7373(2)/ 76.646(3)	7.4411(3)/ 114.766(4)	7.5632(3)/ 115.300(4)
b (Å)/ β (°)	9.4337(4)/ 88.138(4)	9.4999(3)/ 88.778(2)	8.5623(4)/ 93.329(3)	8.7844(3)/ 92.985(3)
c (Å)/ γ (°)	10.0207(4)/ 68.552(4)	10.1340(3)/ 68.472(3)	9.2460(4)/ 114.568(4)	9.4451(3)/ 114.829(4)
V ($Å^3$)	652.57(5)	672.53(4)	466.85(4)	493.96(4)
h, k, l range		-10→10 -12→12 -13→13	-10→11 -13→12 -13→13	-11→10 -13→13 -13→14
total reflection number		3084	3120	3331
unique reflection number		2748	2624	2724
R_1		0.035	0.025	0.038
wR		0.085	0.045	0.087
Gof		1.024	1.030	1.150
CCDC		2,275,377	2,275,344	2,275,377

Table 2.7. Crystallographic data refinement parameters for $(BH_2)(NO_3)_2 \cdot 2H_2SeO_3$ (B = en, pip), $(enH_2)(H_2SeO_3)Br_2$ and $(pipH_2)[Cd(HSeO_3)_2Cl_2](H_2O)_2$

M-X	en-NO_3	pip-NO_3	en-Br	pip-Cd-Cl-H_2O
space group	$P2_1/c$	$P2_1/n$	$P2_1/c$	P-1
a (Å)/ α (°)	5.9386(3)	5.61000(10)	8.0012(5)	7.14040(10)/ 107.419(2)
b (Å)/ β (°)	5.2221(3)/ 90.669(4)	6.8184(2)/ 98.024(2)	11.1514(7)/ 90.012(5)	7.5642(2)/ 95.832(2)
c (Å)/ γ (°)	21.0732(11)	18.7159(5)	6.8168(4)	9.0469(2)/ 106.206(2)
V (Å^3)	653.48(6)	708.90(3)	608.23(6)	438.464(18)
h, k, l range	-8→7 -7→7 -32→27	-8→9 -10→11 -27→31	-10→12 -17→15 -10→6	-12→12 -12→12 -14→15
total reflection number	2234	3622	2335	4484
unique reflection number	1827	3046	1887	3997
R_1	0.053	0.028	0.033	0.025
wR	0.14	0.62	0.076	0.56
Gof	1.081	1.029	1.004	1.026
CCDC	2,275,256	2,275,366	2,275,047	2,275,336

2.2.3. Crystal structures of new compounds $(BH_2)[M^{II}(HSeO_3)_2X_2]$, (B = en, pip, M^{II} = Mn, Co, Ni, Cu, Zn, Cd, X = Cl, Br)

Representatives of this structure type have been found among compounds of Co, Cu, Zn, and Cd, that is, for all M^{2+} cations where the formation of $[M(HSeO_3)_2]$ layers had been reported (vide supra); the new contributors to this series are Mn^{2+}, Ni^{2+}, and probably Mg^{2+} (Table 2.4). Similar to $(AX)[M(HSeO_3)_2]$ (M = Cu, Zn) and in contrast to $[M'(H_2O)_4][M(HSeO_3)_2]$, both chlorides and bromides were found to exist. Bromides have not been observed yet for Mg^{2+} and Ni^{2+}; most likely these compounds exist but are less stable and more sensitive to the preparation conditions. Numerous attempts to prepare acceptable quality crystals for the elusive $(enH_2)[Mg(HSeO_3)_2Cl_2]$ have not been successful; the cell metrics and positions of non-hydrogen atoms correspond to the same arrangement.

In the structures of $(enH_2)[M(HSeO_3)_2X_2]$ (M = Cd, Co, Cu, Mn, Zn; X = Cl, Br), the metal cations center slightly distorted trans-MO_4X_2 octahedra (Fig. 2.8). The bond valence sums on M^{2+} cites agree well with the oxidation state of 2. The distortion indices for the octahedra (table 2.5) were calculated using the Vesta suite (Momma *et* al., 2011).

The largest anisotropy in the bond lengths is observed among the Cu and Zn compounds. The difference between the apical and equatorial bonds in $[CuO_4Br_2]$ is as much as 0.871Å (distortion index = 0.168). In the most symmetrical $[CdO_4Cl_2]$ octahedron, this difference drops to 0.293 Å (distortion index = 0.055). The strong distortion of the Cu and Zn polyhedral can be explained considering the low CFSE values and the Jahn–Teller effect (first order for the former and second order for the latter). Another reason for the distortion of the MO_4X_2 octahedra is extrinsic and caused by hydrogen bonds, both to oxygen and halogen vertices, from the $(enH_2)^{2+}$ or $(pipH_2)^{2+}$ templates, where the size of halogen also matters. The volumes of the MO_4X_2 octahedra vary from 14.27 $Å^3$ (CuO_4Cl_2) to 19.06 $Å^3$ (CdO_4Br_2). The M-X bond distances agree well with the reported values, e.g., Cd-Br distances of 2.7198(3) Å are only slightly shorter than those in the $CdBr_6$ octahedra in $CdBr_2$ (2.785(4) Å); the same applies to the Cd–Cl bond distances in $(enH_2)[Cd(HSeO_3)_2Cl_2]$ (2.5910(7) Å) and $CdCl_2$ (2.637(4) Å). Selenium forms the expected SeO_3*E*-tetrahedron with two shorter (1.67–1.69 Å) and one longer (1.75–1.77 Å) bond to the OH group (Fig. 2.8) as expected for the $HSeO_3^-$ anion.

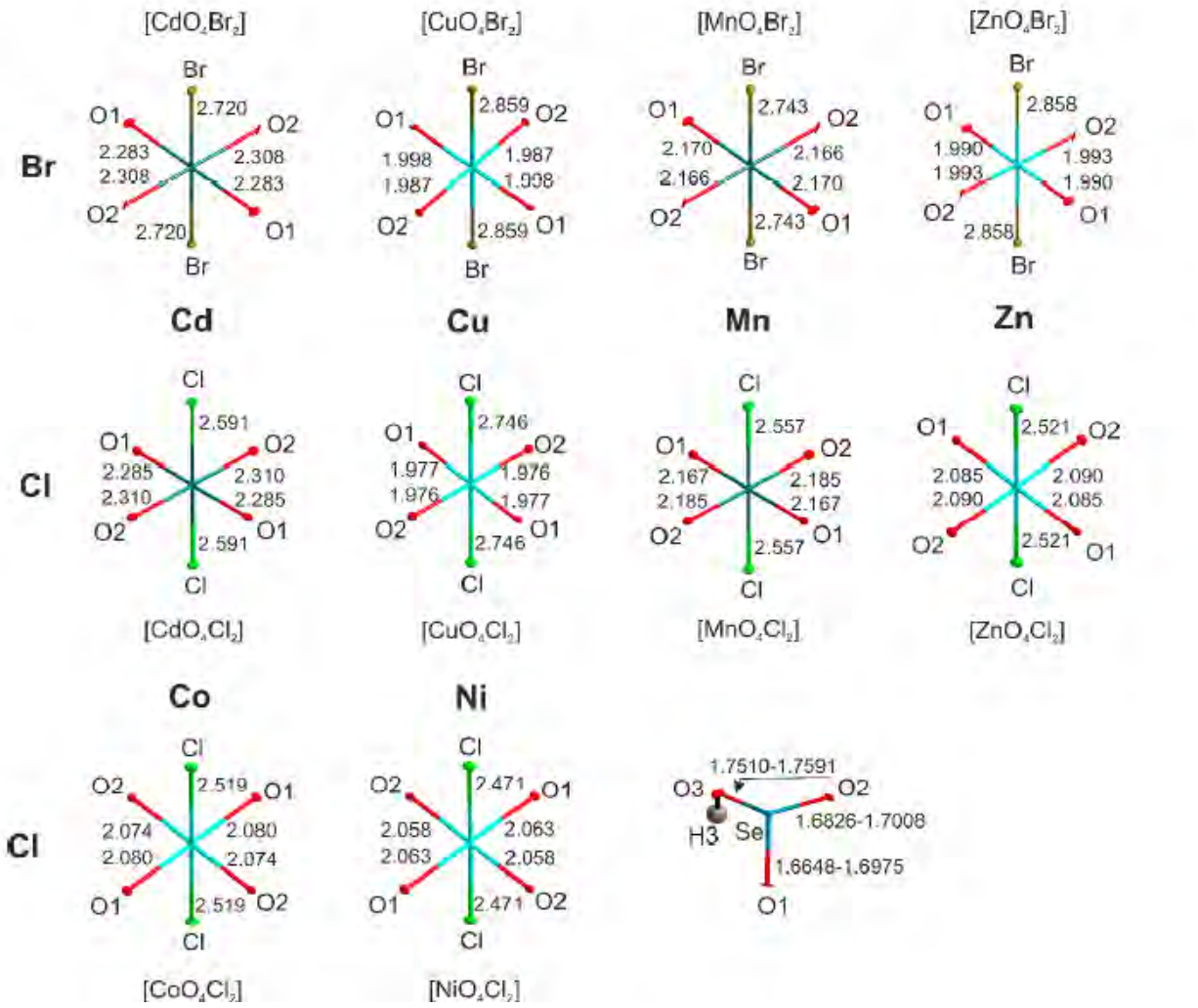

Fig. 2.8. Cations coordination environment in $(enH_2)[M^{II}(HSeO_3)_2X_2]$, ($M^{II}$ = Mn, Co, Ni, Cu, Zn, Cd, X = Cl, Br)

A typical crystal structure of the $(enH_2)[M(HSeO_3)_2X_2]$ (M = Cd, Co, Cu, Mn, Zn, Ni; X = Cl, Br) is shown in Fig. 2.9. The M^{2+} cations reside in centers of MO_4X_2 octahedra formed by the non-protonated oxygen atoms of the four $HSeO_3^-$ anions; these are very similar to those in the corresponding chloride compound (2.2881(17) and 2.3082(18) Å, respectively (Pasha *et* al., 2003)). Each of the protonated nitrogen atoms of the enH_2^{2+} cation forms hydrogen bonds: two to the bromide anion and one to the oxygen atoms of two $HSeO_3^-$ species (Fig. 2.9). The halide anions' hydrogen bonds are weakest (3.196(5)–3.435(3)Å). Therefore, the enH_2^{2+} cation forms the maximal number (6) of possible hydrogen bonds. Very similar environments are also observed in the compounds of manganese, cobalt, nickel, copper, and zinc.

The $[MO_4X_2]$ octahedra are stitched by the hydrogen-bonded $(HSeO_3^-)_2$ pairs into the $[M(HSeO_3)_2X_2]^{2-}$ layers (Fig. 2.9). In the structures of $(enH_2)[M(HSeO_3)_2X_2]$, the O3-H1···O1 bond lengths change within 2.616(2)–2.653(4) Å. The enH_2^{2+}-$HSeO_3^-$ hydrogen bonds are rather insensitive to the nature of M^{2+} cations (2.798(2)–2.971(1)Å).

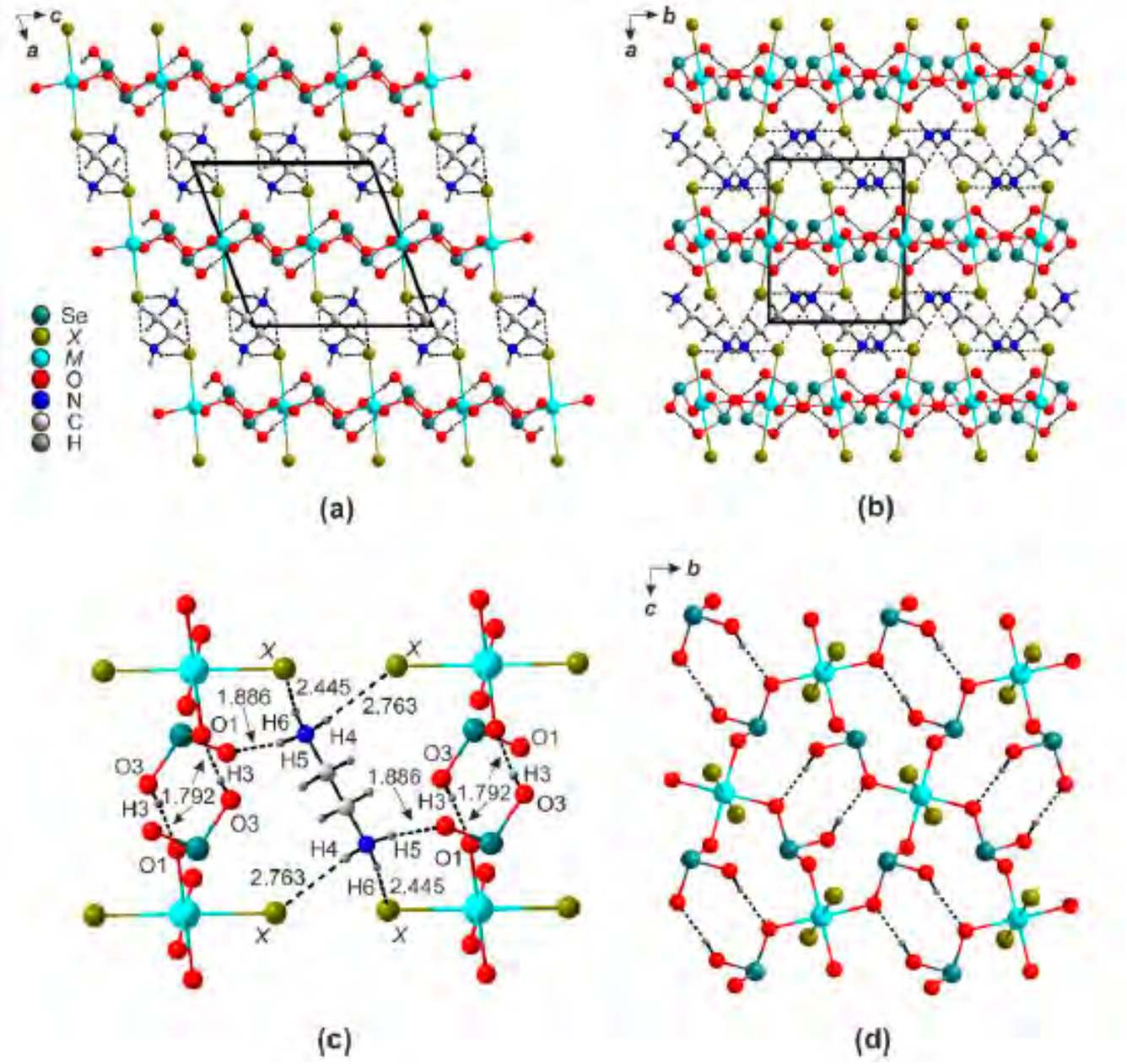

Fig. 2.9. General projection of the structure of $(enH_2)[M(HSeO_3)_2X_2]$ (M = Cd, Co, Cu, Mn, Zn, Ni; X = Cl, Br) (a, b). Hydrogen bonding system enH_2^{2+} - $HSeO_3^-$ (c) and $HSeO_3^-$ - $HSeO_3^-$(d).

2.2.4. Crystal structures of new compounds from series $(pipH_2)[Cd(HSeO_3)_2X_2]$ (X = Cl, Br)

In the structures of $(pipH_2)[Cd(HSeO_3)_2X_2$ the Cd atoms also center the $[CdO_4X_2]$ octahedra (Fig. 2.10). The mean Cd-O separations in the $[CdO_4Br_2]$ (2.335(3) Å) and $[CdO_4Cl_2]$ (2.293(4) Å) in $(enH_2)[M(HSeO_3)_2X_2]$ and $(pipH_2)[Cd(HSeO_3)_2X_2]$ are rather close :<Cd-Br> = 2.653 Å, <Cd-Cl> = 2.587 Å.

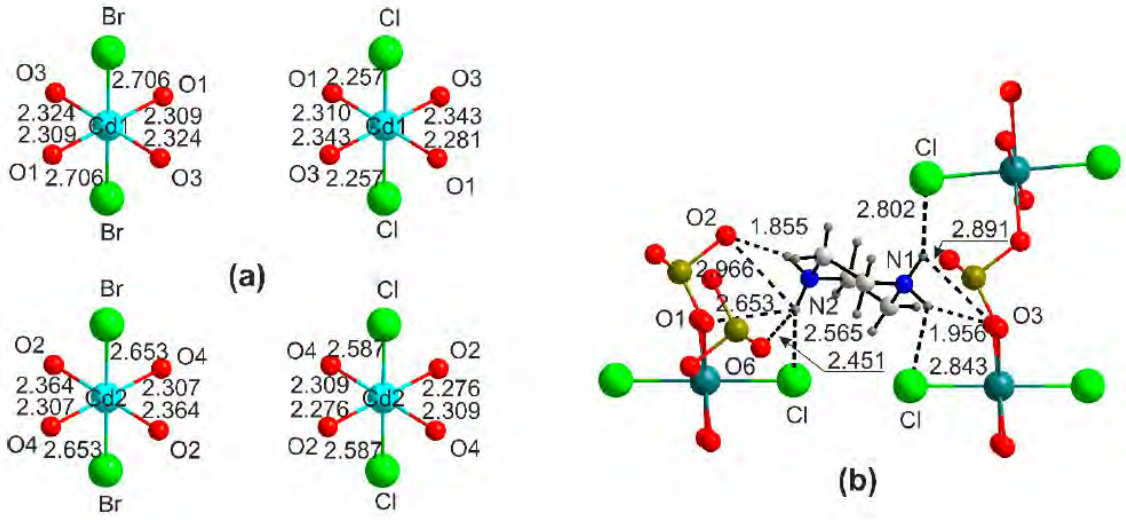

Fig. 2.10. Cd coordination environment in structure $(pipH_2)[Cd(HSeO_3)_2X_2]$ (X = Cl, Br) (a). Hydrogen bonding system $pipH_2^{2+}$ - $HSeO_3$ (b)

The bond differences in the CdO_4X_2 octahedra (0.318 and 0.577 Å for $[CdO_4Br_2]$ and $[CdO_4Cl_2]$, respectively) are smaller in $(pipH_2)[Cd(HSeO_3)_2X_2]$ compared to $(enH_2)[Cd(HSeO_3)_2X_2]$. The piperazinium cations form five hydrogen bonds of varying strength exclusively to the oxygen atoms of the $HSeO_3^-$ anions (Fig. 2.10) which are better recipients than the halides. The $[Cd(HSeO_3)_2X_2]^{2-}$ layers in the en and pip structures are nearly the same (Fig. 2.11). As the quality of the $(pipH_2)[Cd(HSeO_3)_2Cl_2]$ crystals was relatively low, several attempts were made to produce better ones.

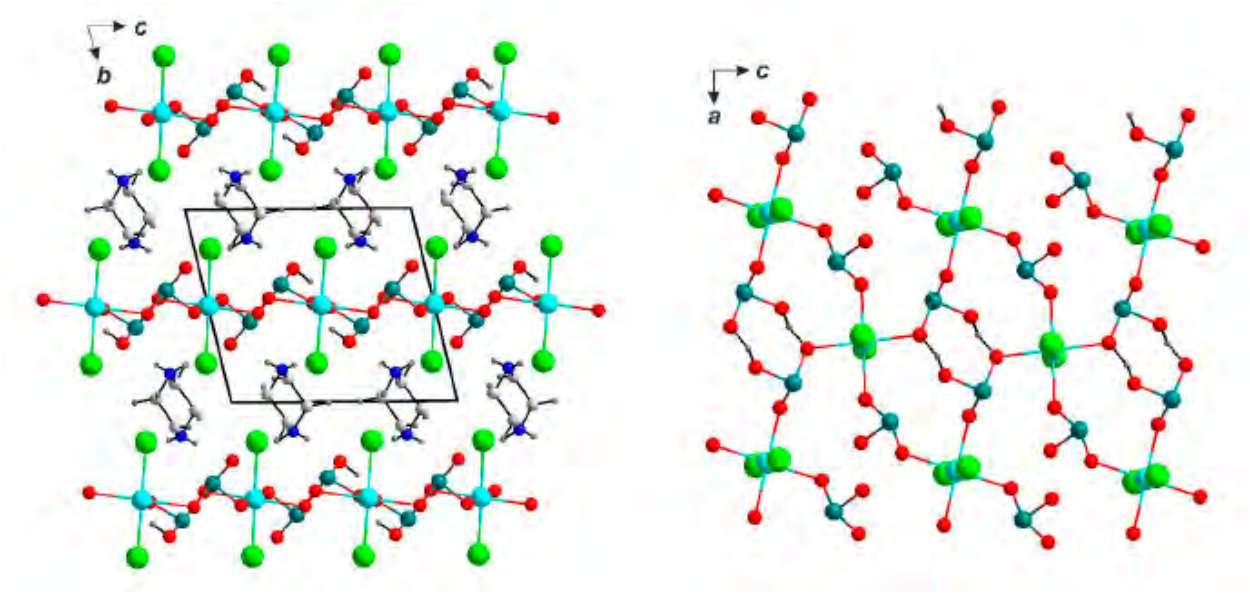

Fig. 2.11. General projection of the structure $(pipH_2)[Cd(HSeO_3)_2X_2]$ (X = Cl, Br) (a). The layer $[Cd(HSeO_3)_2X_2]^{2-}$ in $(pipH_2)[Cd(HSeO_3)_2X_2]$ (X = Cl, Br).

In a single case, a crystal with quite different metrics was picked, which was found to belong to a new compound $(pipH_2)[Cd(HSeO_3)_2Cl_2]\bullet 2H_2O$ (Table 2.6) with a related composition but a totally different structure (Fig. 2.12).In this case, two symmetry-independent Cd^{2+} cations reside in *trans*-CdO_2Cl_4 octahedra which share common Cl-Cl edges to form chains The $HSeO_3^-$ anions do not form pairs; they act as hydrogen bond acceptors from the $pipH_2^{2+}$ cations. The $[CdCl_2(HSeO_3)_2]^{2-}$ chains are also involved in hydrogen bonding with water molecules.

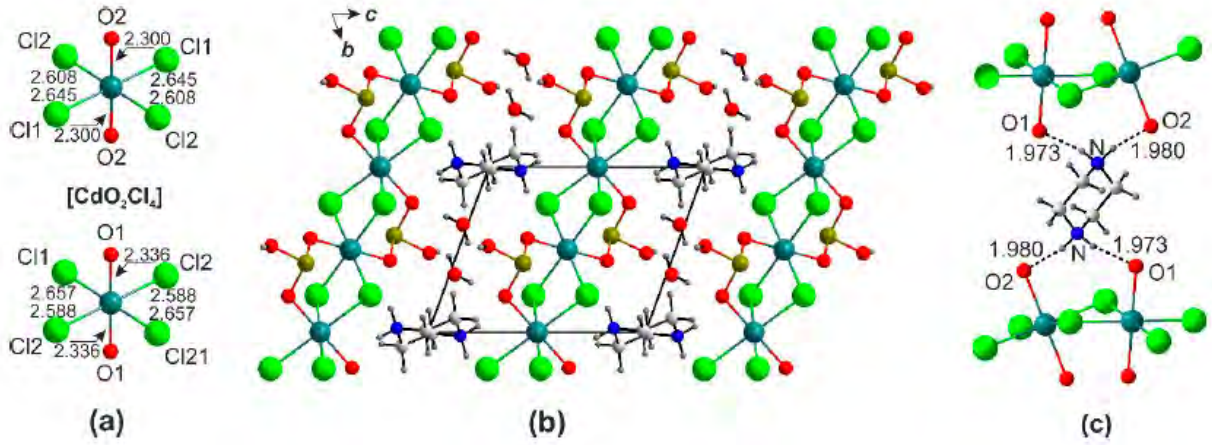

Fig. 2.12. Coordination environment of Cd^{2+} in $(pipH_2)[Cd(HSeO_3)_2Cl_2]\bullet 2H_2O$ (a). General projection of the structure $(pipH_2)[Cd(HSeO_3)_2Cl_2]\bullet 2H_2O$ (b). Hydrogen bonding system $pipH_2^{2+}$ - $HSeO_3^-$ (c).

2.2.5. Crystal structures of the new compounds $(BH_2)[M(HSeO_3)(Se_2O_5)]_2$ (B = en, pip, M = Cd, Co, Mn, Zn)

The organic templates also contribute to formation of halide-free complex selenite diselenites of the $(enH_2)[M(HSeO_3)(Se_2O_5)]_2$ (M = Cd, Co, Mn, Zn) family (Table 2.7). These frameworks have been reported earlier for $(NH_3(CH_2)_4NH_3)[M(HSeO_3)(Se_2O_5)]_2$ (M = Zn, Co or Ni) series templated by tetramethylenediammonium cations (Udayakumar *et* al., 2003). These frameworks also seem to be rather elastic and readily incorporate cyclic piperazinium cations.

The newcomer to this family is Mn^{2+}. Overall, combinations of (protonated) SeO_3^{2-} and $Se_2O_5^{2-}$ are rather common in inorganic frameworks based on various *s*-, *d*-, and *f* -metals (Koskenlinna & Valkonen, 1977a,b, Rao *et* al., 2006, Wickleder, 2006, Jiang & Mao, 2008, Jones *et* al., 1981). Their templating by various organic species is very likely to result in a variety of complex and elegant architectures. In the meantime, such species were not observed with the branched $mpipH_2^{2+}$ cation. A likely reason for this is the same as in the previous case: either the branched structure or the shape of the organic moiety.

In the $(pipH_2)[M(HSeO_3)(Se_2O_5)]_2$ (M = Co, Mn), the divalent cations center nearly regular MO_6 octahedra (Fig. 2.13), with a mean distance of 2.1039(18) and 2.181(4) Å, respectively. Three symmetry-independent Se atoms contribute to the $Se1Se2O_5^{2-}$ and $HSe3O_3^-$ anions (Fig. 2.13). The latter associate into chains aligned along *a*. The $Se1O_3$ and $Se2O_3$ polyhedra share vertices with the MO_6 octahedra to form layers aligned in parallel. Overall, a porous framework is formed with cavities filled by the piperazinium cations. The latter are for hydrogen bonds to the oxygen atoms of the framework. The channel size, estimated as the distance between the opposite oxygen atoms, is 4.13 × 5.58 Å.

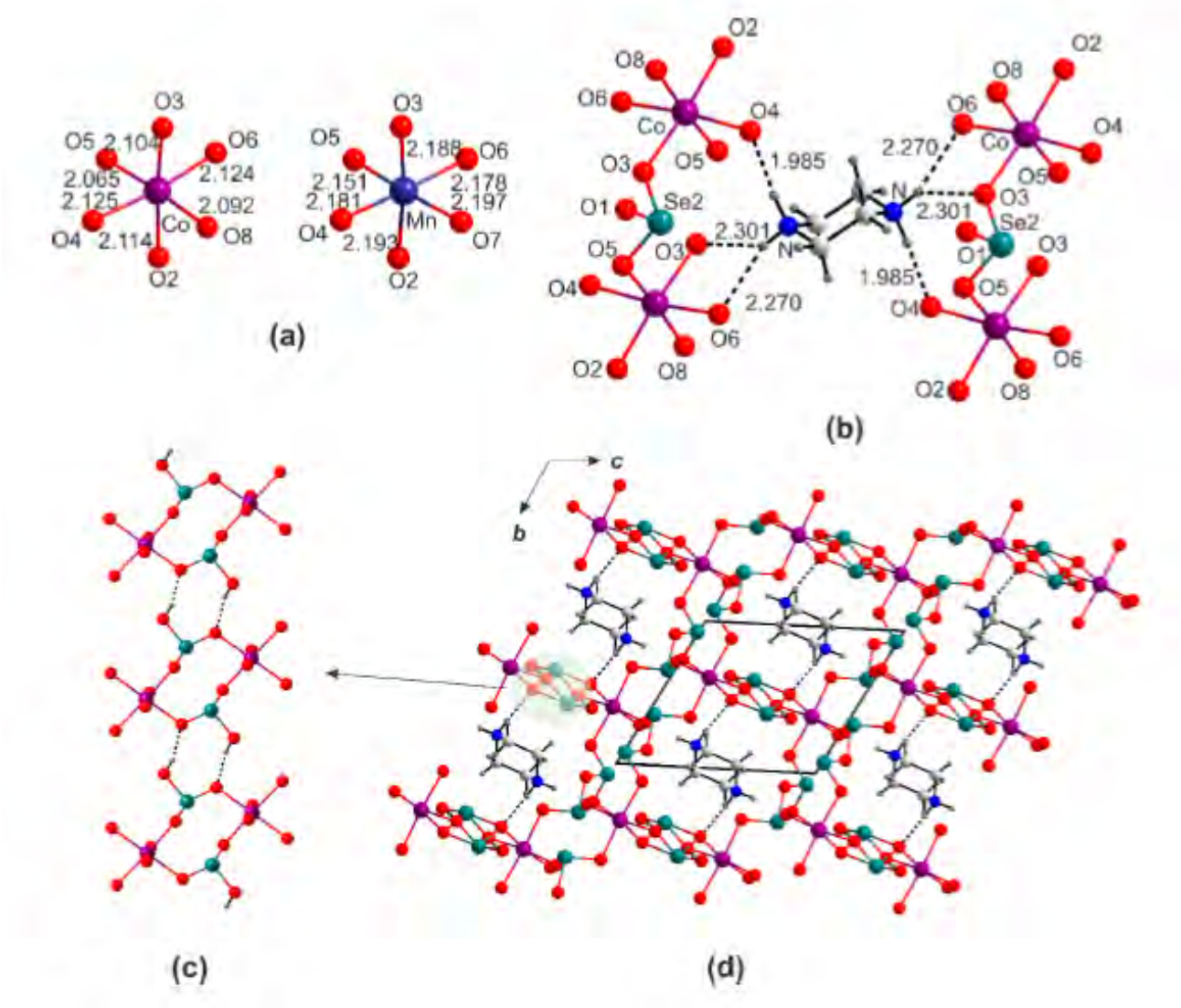

Fig. 2.13. Coordination enviroment of Co^{2+} and Mn^{2+} in structures $(pipH_2)[M(HSeO_3)(Se_2O_5)]_2$ (M = Co, Mn) (a). Hydrogen bonding system $pipH_2^{2+}$ - $HSeO_3^-$ (b). Layer $[M(HSeO_3)(Se_2O_5)]_2^{2-}$ (M = Co, Mn) (c). General projection of the structure of $(pipH_2)[Co(HSeO_3)(Se_2O_5)]_2$ (d).

2.2.6. Crystal structures of $enH_2X_2 \cdot 2H_2SeO_3$ (X = Cl, Br), $(enH_2)(NO_3)_2 \cdot 2H_2SeO_3$ and $(pipH_2)(NO_3)_2 \cdot 2H_2SeO_3$

The metal-free structure of $(enH_2)X_2 \bullet 2H_2SeO_3$ (X = Cl and Br) (Fig. 2.14) is the first "organic analog" of the $AX \bullet nH_2SeO_3$ compounds (A is an alkali cation) (Markovski *et* al., 2020, Wang *et* al., 2023), wherein the Se atom is also coordinated to three oxygen atoms, two of which are protonated to form the H_2SeO_3 molecule. In the structure of halides (take X = Br for example), these species and the enH_2^{2+} cations, as well as Br^-, link via hydrogen bonding to form a framework wherein the organic and inorganic parts form sublayers distantly reminiscent of the $AX \bullet nH_2SeO_3$ (Markovski *et* al., 2020b, Wang *et* al., 2023). The H_2SeO_3 molecules also form hydrogen bonds between each other.

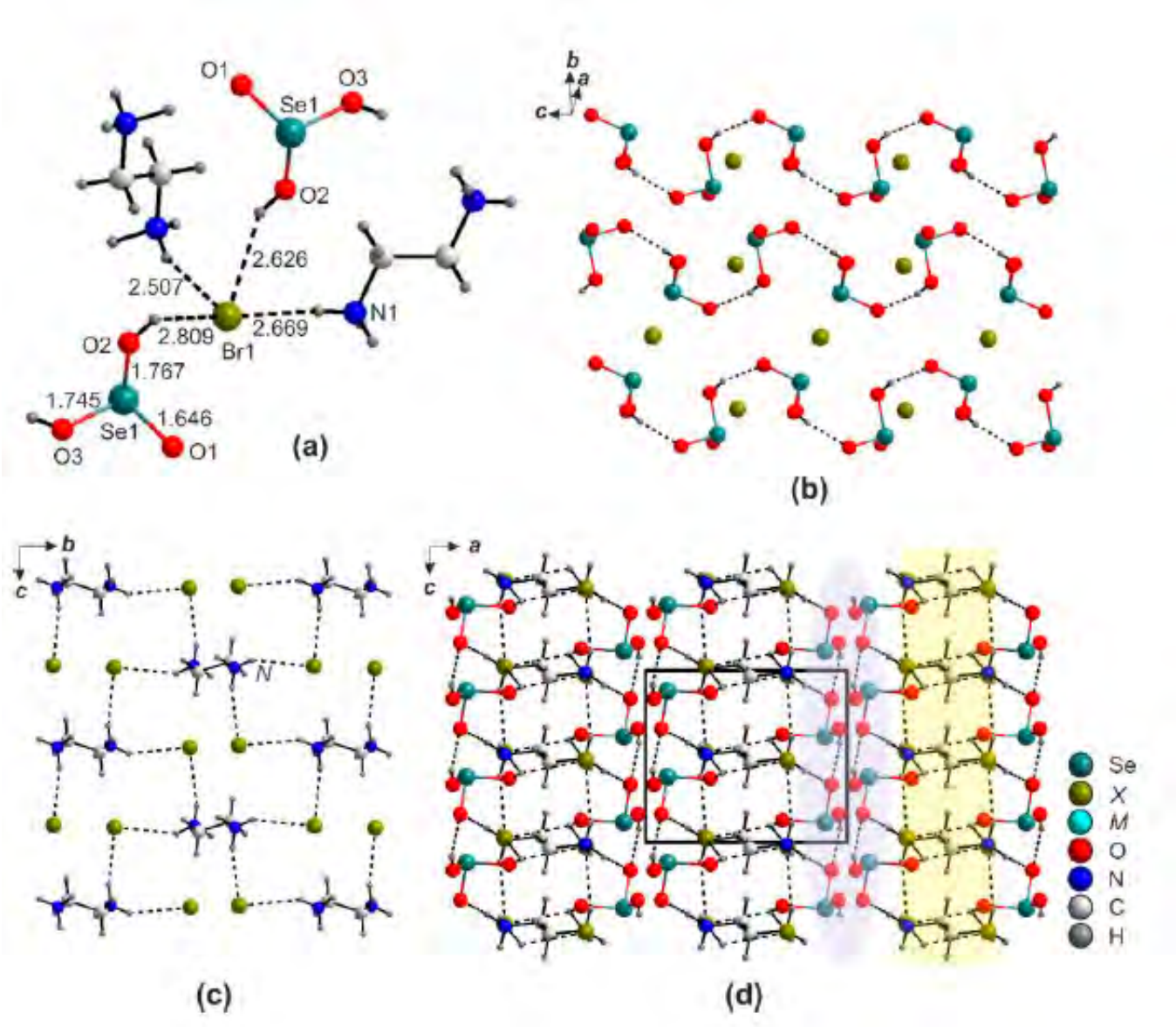

Fig. 2.14. Hydrogen bonding system in the structure of $enH_2X_2 \cdot 2H_2SeO_3$ (X = Cl, Br) (a-c). General projection of the structure of $enH_2X_2 \cdot 2H_2SeO_3$ (X = Cl, Br) (d).

The nitrate derivatives, $(enH_2)(NO_3)_2 \cdot 2H_2SeO_3$ and $(pipH_2)(NO_3)_2 \cdot 2H_2SeO_3$, have close chemical compositions but also different crystal structures (Fig. 2.15). In the former structure, the H_2SeO_3 species form chains aligned along *b*. They are decorated by the nitrate groups attached via hydrogen bonds to form ribbons. The enH_2^{2+} cations are situated between these. As in the previous case, both architectures can be considered to be pseudo-layered, yet with a different topology; the layers are formed by changed and neutral moieties. Both organic species form hydrogen bonds to oxygens of both NO_3^- and H_2SeO_3 moieties.

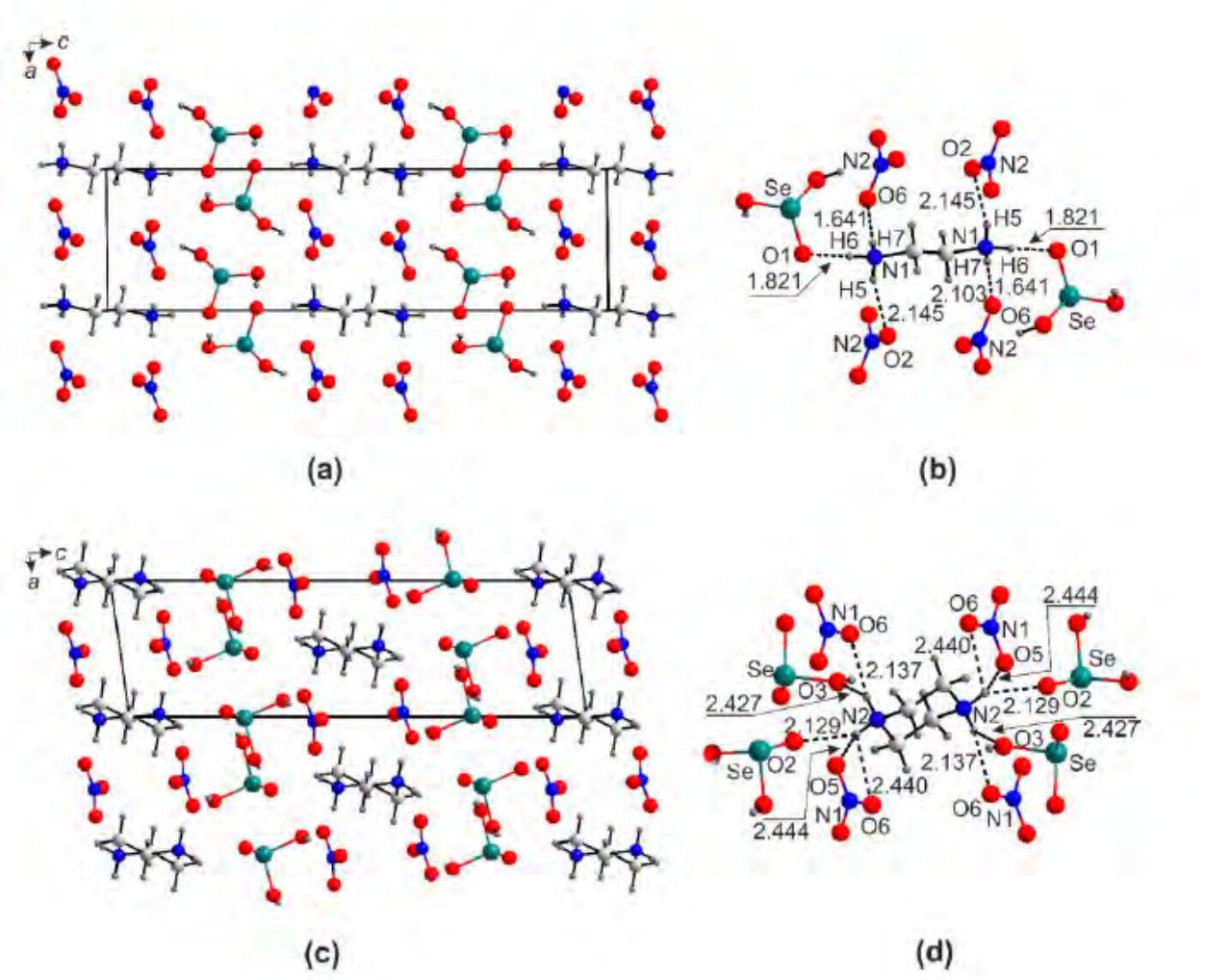

Fig. 2.15. General projection of crystal structure of $(enH_2)(NO_3)_2 \cdot 2H_2SeO_3$ (a). Hydrogen bonding system enH_2^{2+} - $HSeO_3^-$ in $(enH_2)(NO_3)_2 \cdot 2H_2SeO_3$ (b). General projection of crystal structure of $(pipH_2)(NO_3)_2 \cdot 2H_2SeO_3$ (c).). Hydrogen bonding system enH_2^{2+} - $HSeO_3^-$ in $(pipH_2)(NO_3)_2 \cdot 2H_2SeO_3$ (d).

2.3. Crystal chemistry of new non-centrosymmetric compounds $KNO_3 \cdot 3H_2SeO_3$ and $NaHSeO_3 \cdot 3H_2SeO_3$

2.3.1. Synthesis of new compounds

Hydrogen bonding is an efficient tool in constructing organic and metal-organic frameworks which exhibit great variability in composition, structures, and applications (see Brammer, 2004 and references therein). In the meantime, purely inorganic hydrogen-bonded frameworks were extensively studied mostly in the realm of acid salts due to their attractive properties like superionic proton conductivity (Colodero *et al* 2022, Chisholm & Haile, 1999) or nonlinear optical activity (Nelmes, 1984). Less attention is paid to the structures containing neutral molecules of inorganic hydrogen bond donors, mostly acids. Selenious acid, H_2SeO_3, received essential attention as a constituent of its acid salts as $M^IHSeO_3 \cdot nH_2SeO_3$ (M^I – alkali and thallium cation or ammonium, n = 1 – 3 (Soda & Chiba, 1969, Loub *et* al., 1992, Chomniplan *et* al., 1977, Lehmann & Larsen, 1971, Tellgren & Liminga, 1973, Hiltunen *et* al., 1987, Vinorgadova, 1981, Tellgren *et al* 1974, Shuvalov *et al* 1984), due to their ferroelectric properties, as well as some more complex compounds, *e.g.* non-centrosymmetric $Na_2SeO_4 \cdot H_2SeO_3 \cdot H_2O$ (Baran *et* al., 1991).. Among chemically related species, *e.g.* copper hydrogen selenites, nitrates commonly behave as crystal chemical analogs of halide anions (Charkin *et* al., 2019, Markovski *et* al., 2019).. Therefore, formation of hydrogen-bonded species based on nitrate anions and selenious acid is very likely.

The synthesis was peformed by isothermal evaporation of aqueous solutions at room temperature. 1 mmol KNO_3 and 3 mmol H_2SeO_3 were used as the startin greagents for the preparation of KNO_3 $3H_2SeO_3$. These were dissolved in 9 ml of distilled water and acidified by 1ml 1M HNO_3 to suppress the dissociation of selenous acid (Levanov *et* al., 2017, Wilcox & Prideaux., 1925) used for the synthesis of related compounds (Wang *et* al., 2023, Charkin *et* al., 2019). Within a few weeks, crystals of both target and initial compounds fell out of the resulting matrix with increased viscosity. The crystals were collected during several precipitation stages from different parts of the reaction vessel. They were all colorless, easily soluble in water. Similar experiments were carried out with other alkali metal nitrates, but crystals were mostly of insufficient quality. In the Na-containing solutions. However, in addition to the target compounds, crystals of a known compound $NaHSeO_3 \bullet 3H_2SeO_3$ were found for which a better quality structure solution could be cobtained compared to the reference data (Loub *et* al., 1992).

Qualitative electron microprobe analysis (Hitachi TM3000) revealed no other elements, except K and Se in $KNO_3 \cdot 3H_2SeO_3$ and Na and Se in and $NaHSeO_3 \cdot 3H_2SeO_3$ with the atomic number greater than 11 (Na).

2.3.2. Single crystal X-ray experiments

Single crystals of $KNO_3 \cdot 3H_2SeO_3$ and $NaHSeO_3 \cdot 3H_2SeO_3$ selected for X-ray diffraction analysis were glued onto glass filaments and arranged in a Rigaku XtaLAB Synergy-S diffractometer equipped with a PhotonJet-S detector operating with MoKα radiation at 50 kV and 1 mA. A single crystal of each mineral was chosen and more than a hemisphere of data collected with a frame width of 0.5° in ω, and 20 s spent counting for each frame. The experiments were performed with cooling to 120 K. The unit cell parameters were calculated by the least-squares method. The structures were solved by direct methods. The parameters of the X-ray diffraction experiment and structure refinement are given in Table 2.8. The final model includes the coordinates and anisotropic thermal parameters of all atoms, hydrogen atoms are refined in the isotropic approximation. All H atoms were located from the analysis of difference Fourier electron density maps and were refined with the imposed O–H distance restraints of 1.00 ± 0.005 Å.

Table 2.8. Crystallographic data and refinement parameters for $KNO_3 \cdot 3H_2SeO_3$ and $NaHSeO_3 \cdot 3H_2SeO_3$

	$KNO_3 \cdot 3H_2SeO_3$	$NaHSeO_3 \cdot 3H_2SeO_3$
Crystal system	Monoclinic	monoclinic
Space group.	$P2_1$	Pc
a (Å)	10.2709(8)	5.7803 (3)
b (Å)	6.2840 (3)	4.9390 (2)
c (Å)	10.3886 (8)	21.2827 (11)
β (°)	118.825 (10)	111.836 (6)
V (Å^3)	587.43 (7)	564.00 (5)
Radiation (Å)	MoKα, 0.71073	MoKα, 0.71073
total reflection number	5147	5875
number of unique reflections $F > 4\sigma(F)$	2315	2684
R_1	0.036	0.028
wR_1	0.092	0.058
Gof on F^2	1.093	1.024

Table 2.9. Selected bond lengths in crystal structures $KNO_3 \cdot 3H_2SeO_3$ and $NaHSeO_3 \cdot 3H_2SeO_3$

$KNO_3 \cdot 3H_2SeO_3$		$NaHSeO_3 \cdot 3H_2SeO_3$	
bond	*d*, Å	Bond	*d*, Å
K1–O1	2.718(5)	Na1-O2	2.377(4)
K1–O8	2.739(6)	Na1-O7	2.398(4)
K1–O4	2.756(5)	Na1-O11	2.403(4)
K1–O2	2.794(5)	Na1-O5	2.435(5)
K1–O5	2.800(5)	Na1-O3	2.467(4)
K1–O7	2.835(5)	Na1-O4	2.498(5)
K1–O9	3.034(4)		
K1–O3	3.131(5)	Se1-O2	1.674(4)
K1–O6	3.278(5)	Se1-O1	1.677(4)
Se1–O4	1.780(4)	Se2-O10	1.643(4)
Se1–O1	1.620(5)	Se2-O3	1.741(4)
Se1–O2	1.711(5)		
Se1–O3	1.744(4)	Se3-O7	1.643(4)
Se2–O6	1.757(4)	Se3-O12	1.732(4)
Se2–O4	1.640(5)		
Se2–O5	1.727(5)	Se4-O5	1.636(4)
Se2–O6	1.748(4)	Se4-O9	1.737(4)
Se3–O8	1.756(4)		
Se3–O7	1.625(5)		
Se3–O8	1.739(5)		
Se3–O9	1.754(4)		
Se4–O11	1.755(4)		
N1–O10	1.244(7)		
N1–O11	1.247(8)		
N1–O12	1.245(7)		

2.3.3. Crystal structures of new non-centrosymmetric $KNO_3 \cdot 3H_2SeO_3$ and $NaHSeO_3 \cdot 3H_2SeO_3$

The cation coordination in the new compound $KNO_3 \cdot 3H_2SeO_3$ is shown in Fig. 2.16. There are one potassium, one nitrogen, and three symmetrically independent selenium sites. The potassium cation coordinates six oxygen atoms at 2.718(5) – 2.835(5) Å and three at longer distances of 3.034(4) – 3.278(5) Å thus forming a strongly distorted tricapped trigonal prism The calculated bond valence sums for K, Se1, Se2, Se3, and N are very close to the expected formal valences of +1, +4, and +5 (Table 1 in Appendix).

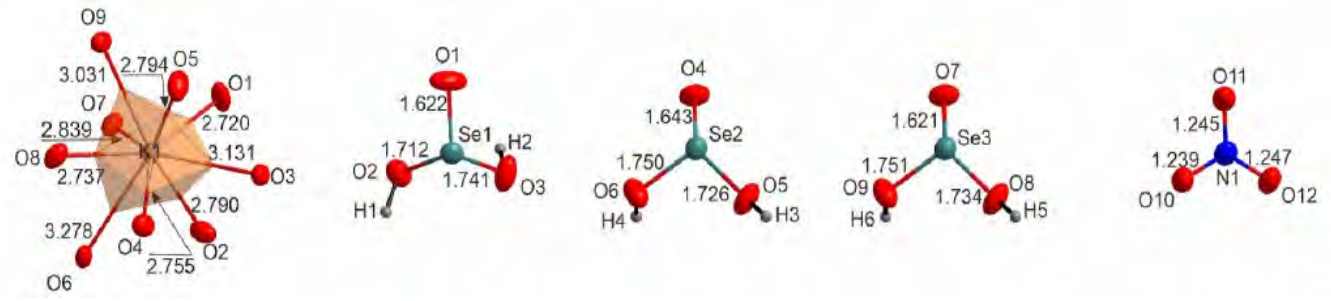

Fig. 2.16. Coordination of atoms in crystal structures $KNO_3 \cdot 3H_2SeO_3$

The structure of $KNO_3 \bullet 3H_2SeO_3$ contains 1 symmetrically independent position of K^+, 1 position of N^{5+} and 3 positions of Se^{4+}. The potassium atom is surrounded by 6 oxygen atoms at 2.718(5) – 2.835(5) Å and 3 oxygen ‘atoms at 3.034(4) – 3.278(5) Å, forming an essentially distorted three-capped trigonal prism. All three symmetrically independent H_2SeO_3 molecules contain one short Se=O bond with of 1.620(5) – 1.640(5) Å and two longer Se–OH bonds of 1.711(5) – 1.754(4) Å. The potassium cation is coordinated by oxygen atoms belonging to nine molecules of selenous acid. All oxygen atoms of the latter are invoilved into linking the KO_9 tricapped prisms into a pseudo-hexagonal lattice with channels running along (001). These channels are filed by the nitrate groups bond N-O length 1.244(7) - 1.245(7) Å, located on the 2_1-axis and arranged relative to each other in a neasrly stalled configuration. The stability of the structure is further provided by formation of hydrogen bonds between nitrate anions and hydroxyl groups of the selenious acid molecules located on the channel "walls”.

The selenious acid *per se* is known to be a relatively strong hydrogen bond donor (Soda & Chiba, 1969, Loub *et* al., 1992, Chomniplan *et* al., 1977, Lehmann & Larsen, 1971, Tellgren *et* al., 1973, Hiltunen *et* al., 1987, Vinorgadova *et* al., 1981, Tellgren & Liminga, 1974, Shuvalov *et* al., 1984, Baran *et* al., 1991, Markovski *et* al., 2020, Wang *et* al., 2023, Charkin *et* al., 2019, Markovski *et* al., 2019). In the structure of $KNO_3 \cdot 3H_2SeO_3$, all molecules are active in the formation of hydrogen bonds (Fig. 2.17 and 2.18). One hydroxyl group of one molecule H_2SeO_3 and one end oxygen atom and the other form six-membered cycles that resemble those in the structures of layered copper hydroselenites (Charkin *et*

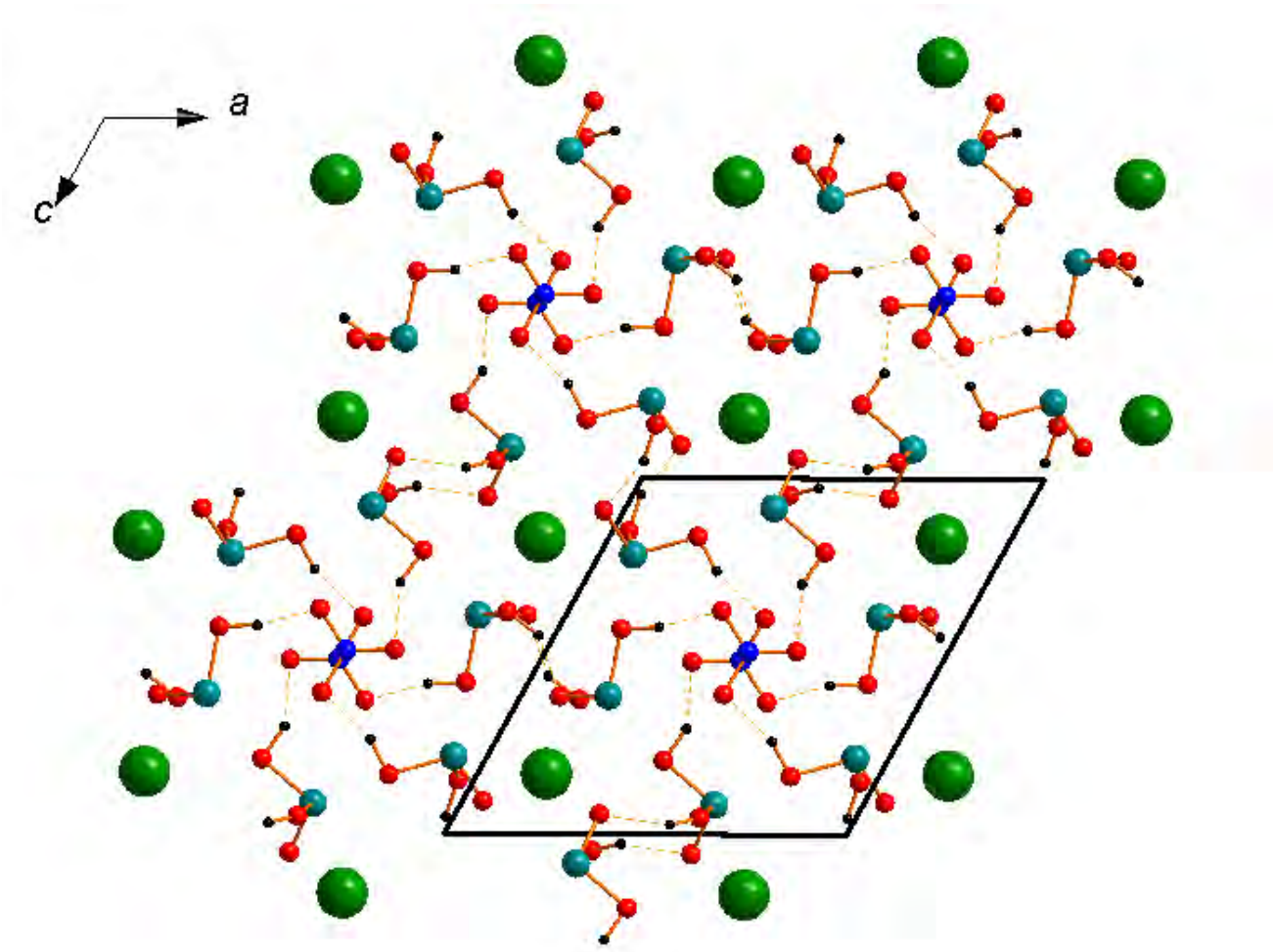

Fig. 2.17. General projection of $KNO_3 \cdot H_2SeO_3$

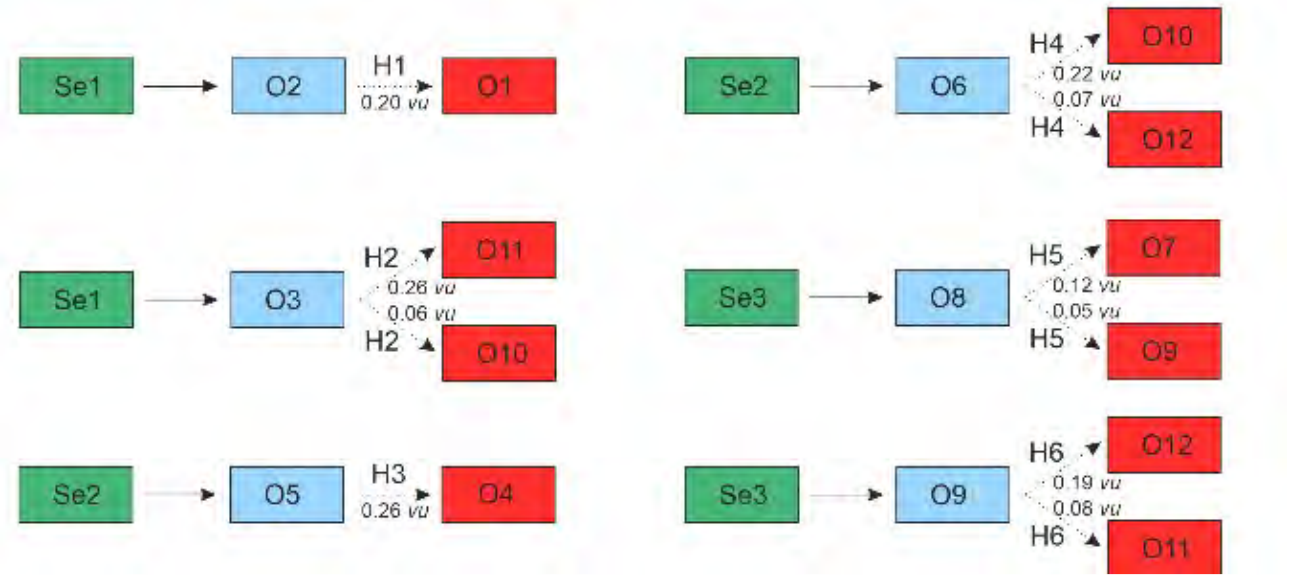

Fig. 2.18. Hydrogen bonding system in $KNO_3 \cdot H_2SeO_3$

al., 2019, Markovski *et* al., 2019). The hydrogen atom of the second hydroxyl group forms a relatively strong bond with the nitrate anion. Investigator o, the hydrogen bond is involved both in the structure and fixation of nitrate-anions in the inner part of the channel. Overall, the crystal structure of

$KNO_3 \cdot 3H_2SeO_3$ is a monoclinically distorted version of a hypothetical archetypal centrosymmetric hexagonal structure. (Fig. 2.17 and 2.18).

In the structure of $NaHSeO_3 \cdot 3H_2SeO_3$, there are one Na^+ and three Se^{4+} sites among which Se1 belongs to the hydrated anion group $HSeO_3^-$. $HSeO_3^-$ anions and H_2SeO_3 molecules are easily distinguishable by analyzing bond lengths and hydrogen interactions, as the bond of selenium to the hydrated oxygen atom is longer than to the non-hydrated. Cation Na^+ has an octahedral environment that is formed by two oxygen atoms belonging to the $HSeO_3$-group and four oxygen atoms belonging to H_2SeO_3. Environment of sodium resembles potassium environment in structure $KNO_3 \cdot H_2SeO_3$ except that the radius of Na^+ is less than K^+ (0.189 *vs* 0.236 Å), that only 2 of 3 oxygen selenistic acid are used. (Fig. 2.19).

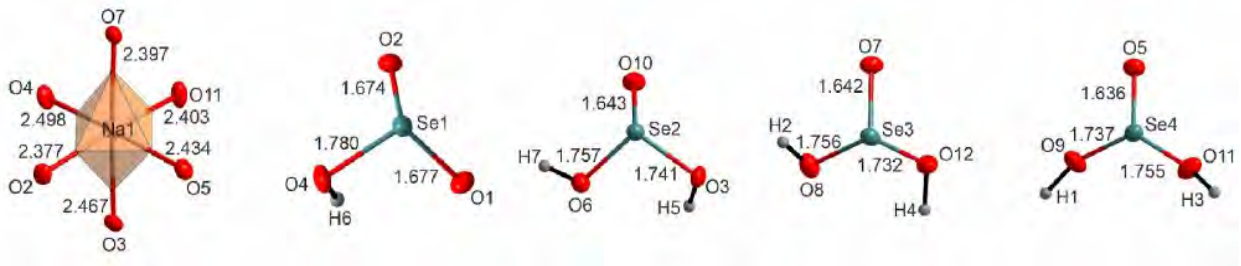

Fig. 2.20. Coodrination environment of Na and Se in $NaHSeO_3 \bullet 3H_2SeO_3$

The sodium-oxygen octahedra are linked by the hydrogen bonds into chains, which are further organized into layers so that the structure of $NaHSeO_3 \cdot 3H_2SeO_3$ can be considered as pseudo-two-dimensional (Fig. 2.21). The hydrogen bonds link the chains into layers and further into a 3D framework. In the mantime, the $HSeO_3^-$ anions do not participate in the formation of hydrogen bonds like those in

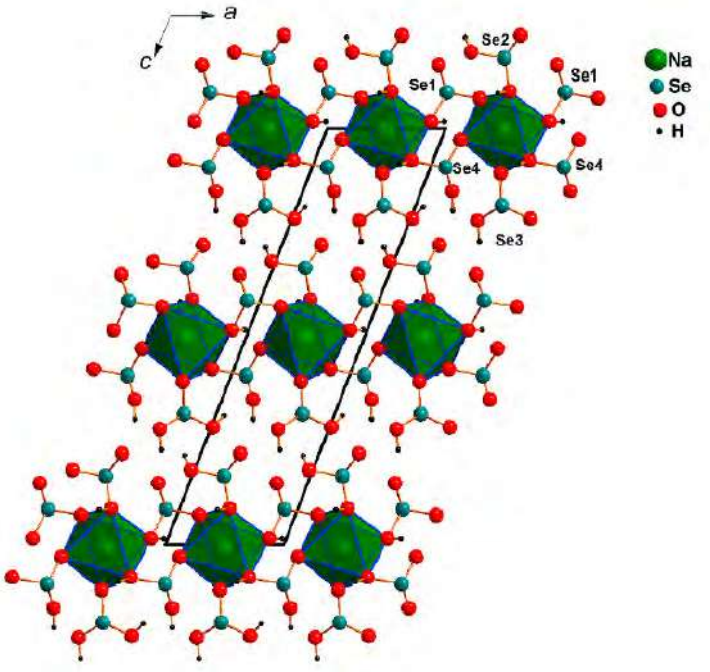

Fig. 2.21. General projection of $NaHSeO_3 \cdot 3H_2SeO_3$

$Ca(HSeO_3)Cl$, copper hydroselenites and related compounds (Markovski *et* al., 2020, Wang *et* al., 2023, Kurtz & Perry, 1968). It is likely that the H_2SeO_3 molecule with more polar O-H bonds is a better hydrogen bond donor compared to $HSeO_3^-$, particulatly when coordinated to weak Lewis acids like Na^+ or Ca^{2+}. It is possible that coordination with to Lewis acids, such as Zn^{2+}, Co^{2+} or Cu^{2+}, would affect the O - H bonds, so they become more polar. (Fig. 2.22).

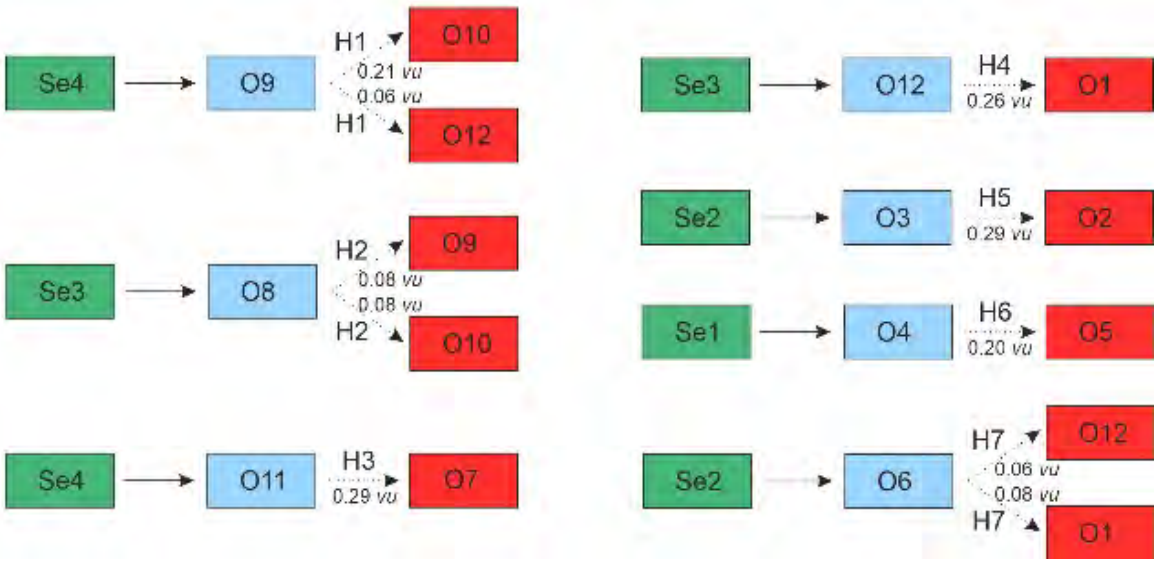

Fig. 2.22. Hydrogen bonding system in $NaHSeO_3 \cdot 3H_2SeO_3$

2.3.4. Second harmonic generation

The SHG signal from $KNO_3 \cdot 3H_2SeO_3$ was registered using the Kurtz – Perry technique (Kurtz & Perry, 1968). The material was softly ground to obtain a powder. A Minilite-I Nd:YAG laser, operating in Q-switched mode with repetition rate 10 Hz, produced the radiation at λ_ω = 1064 nm. Green light of the second harmonic, $\lambda_{2\omega}$ = 532 nm, was collected in reflection mode and detected by a photomultiplier tube equipped by a narrow band-pass interference filter. A moderate SHG signal of 5-6 SiO_2 units was observed confirming the non-centrosymmetric character of the crystal structure.

Chapter 3. New aqueos lead selenites

3.1. Crystal chemistry of $Pb_2(ReO_4)_2(SeO_3)\cdot 2H_2O$ and $Pb_2(ReO_4)_2(HPO_3)\cdot 2H_2O$

3.1.1. Synthesis of new compounds

The incorporation of stereochemically active lone- electron pairs into inorganic frameworks is considered to be a powerful tool for construction of low-dimensional, porous and non-centrosymmetric crystal structures (Walsh *et* al., 2011; Xiao *et* al., 2006; He *et* al., 2018; Dai *et* al., 2021). Larger low-velence cations such as Tl^{I}, Pb^{II}, Bi^{III} and Sn^{II} with flexible coordination environments exhibit relatively high coordination numbers and form asymmetric polyhedra, while smaller cations with rigid environments such as As^{III}, S^{IV}, Se^{IV}, Te^{IV}, Br^{V} and ^{IV}, form stable molecular anions used as structural units. While chemical bonding is not possible in the vicinity of lone-pairs and electrostatic interactions with the adjacent anions, especially halides, are weak yet active (the so-called phenomenon of halophilic electron pair (Mayerová *et* al., 2006; Siidra *et* al., 2013) These combinations were widely used as a tool for "chemical scissors" (Jo *et* al., 2010), mainly in the construction of low-dimensional complexes (e.g., chains and layers), often with the aim of producing low-dimensional magnetic subcells (Chakraborty *et* al., 2013). To date, the most commonly used lone-pair anions are relatively thermally and redox stable complexes such as AsO_3^{3-}, SeO_3^{2-} and TeO_3^{2-} (or TeO_4^{4-}) which can be used in both solution (hydrothermal) and solid-state (including chemical vapor transport) synthetic approaches (Shen *et* al., 2005, Lin *et al*,. 2013, Siidra *et al*,. 2018, Goerigk *et* al., 2019, Markovski *et* al., 2020, Charkin *et* al., 2022). For less stable complexes like BrO_3^-, IO_3^- (IO_4^{3-}) or SO_3^{2-}, aqueous syntheses were mainly employed (Liu *et* al., 2008, Chilas *et* al., 2010, Zhao *et* al., 2013). There is at least one less common analog of these compounds, the hydrophosphonate, or phosphite, anion, HPO_3^{2-}, wherein the nearly nonpolar P-H bond sometimes behaves in a similar way to the lone pair of electrons, preventing any interaction with neighboring compounds on its side. Structural analogies of phosphites were reported mainly to selenites (Handlovic, 1969, Robinson *et* al., 1992, Boldt *et* al., 2000; Kovrugin *et* al., 2016b), despite significant differences in the lengths of Se - O and P – O bonds.

Single crystals of $Pb_2(ReO_4)_2(SeO_3)\cdot 2H_2O$ were first produced when a saturated solution of lead perrhenate was poured accidentally into a vial containing some seleniuous acid. Formation of small transparent needles was observed and the structure solution (*vide infra*) provided a new compound described below. Targeted synthesis was performed using a similar scheme. 2 mmol of lead perrhenate

(obtained by annealing 1:2 mixture of PbO and NH_4ReO_4 at 350 and, after grinding, at 450°C) were dissolved in 10 ml of distilled water and heated to boiling, after which 1 mmol of solid selenious acid was added. A heavy white precipitate was immediately formed. After several minutes of boiling, the solution was decanted and let cooling naturally. After a *ca.* one-hour induction period, a mass of colorless needle crystals was produced within several minutes. The crystals are stable under mother liquor for at least one year. Subsequent single-crystal and powder X-ray studies indicated that single-phase $Pb_2(ReO_4)_2(SeO_3)\cdot 2H_2O$ was formed both in the initial microcrystalline precipitate and during later precipitation in larger amounts.

Attempts to prepare phosphite analog of $Pb_2(ReO_4)_2(HPO_3)\cdot 2H_2O$ followed the same protocol using H_3PO_3 instead of H_2SeO_3. The same sequence of events was observed with successful production of $Pb_2(ReO_4)_2(HPO_3)\cdot 2H_2O$. However, when $Na_2S_2O_5$ was added to hot (ca. 80 °C) solution of $Pb(ReO_4)_2$, evolution of sulfur dioxide was instantly observed with formation of white precipitate; the decanted solution provided no sulfite analog of $Pb_2(ReO_4)_2(SeO_3)\cdot 2H_2O$ or $Pb_2(ReO_4)_2(HPO_3)\cdot 2H_2O$ after standing for several weeks. Interaction of $Pb(ReO_4)_2$ and HIO_3 produced only $Pb(IO_3)_2$.

Qualitative electron microprobe analysis (Hitachi TM3000) revealed no other elements, except Pb, Re and Se in $Pb_2(ReO_4)_2(SeO_3)\cdot 2H_2O$ and Pb, Re and P in $Pb_2(ReO_4)_2(HPO_3)\cdot 2H_2O$ with the atomic number greater than 11 (Na).

3.1.2. Single crystal X-ray experiments

Single-crystal X-ray studies of $Pb_2(ReO_4)_2(SeO_3)\cdot$and $Pb_2(ReO_4)_2(HPO_3)\cdot 2H_2O$ were performed on a Synergy S single-crystal diffractometer equipped with a Hypix detector using monochromatic MoKα radiation (λ = 0.71069 Å) at 120 K temperature. More than a hemisphere was collected with scanning step of 1◦, and an exposure time of 10 s for each crystal. The data were integrated and corrected by means of the CrysAlis (Rigaku Corporation, Tokyo, Japan) program package, which was also used to apply empirical absorption correction using spherical harmonics. The structure was refined using the SHELXL software package (Sheldrick, 2015). All H atoms were located from the analysis of difference Fourier electron density maps and were refined with the imposed O–H distance restraints of 1.00 ± 0.005 Å and for some H-H pairs in H_2O molecules with restraints of 1.65 ± 0.05 Å. The isotropic displacement parameters for several hydrogen atoms were held constant at 0.05 $Å^2$. H1A···H2A distances in $Pb_2(ReO_4)_2(SeO_3)$ and $Pb_2(ReO_4)_2(HPO_3)\cdot 2H_2O$ are relatively short, whereas their elongation and restraining result in strong distortions of the geometry of the water molecules. The atom coordinates for the solved structure of $Pb_2(ReO_4)_2(SeO_3)\cdot 2H_2O$ were used as starting point for the refinement of the

structure of $Pb_2(ReO_4)_2(HPO_3)\cdot 2H_2O$. Crystal data, data collection information, and refinement details are given in Table 3.1. Bond valence sum (BVS) values (Tables 3.2 and 3.3) were calculated using the parameters from Gagné & Hawthorne, 2015. All of the BVS are in good agreement with the expected oxidation states in both structures. The three oxygen atoms add BVS of 4.15 to the phosphorus atom.

Table 3.1. Crystallographic data and refinement parameters for $Pb_2(ReO_4)_2(SeO_3)(H_2O)_2$ and $Pb_2(ReO_4)_2(HPO_3)(H_2O)_2$

	$Pb_2(ReO_4)_2(SeO_3)(H_2O)_2$	$Pb_2(ReO_4)_2(HPO_3)(H_2O)_2$
Crystal system	monoclinic	monoclinic
Space group	$P2_1/c$	$P2_1/c$
a (Å)	7.6609(2)	7.6571(3)
b (Å)	19.0260(4)	18.9189(6)
c (Å)	9.1437(2)	9.2745(3)
β (°)	108.167(3)	109.075(4)
V (Å^3)	1266.32(5)	1269.77(8)
Radiation	Mo*Kα*	Mo*Kα*
Total reflections collected	4359	3049
Unique reflections	3655	2676
R_1	0.028	0.029
wR_1	0.048	0.083
Goodness-of-fit	1.049	1.066
CCDC	2194258	2194259

Table 3.2. Selected interatomic distances (Å) in $Pb_2(ReO_4)_2(SeO_3)(H_2O)_2$ and $Pb_2(ReO_4)_2(HPO_3)(H_2O)_2$.

$Pb_2(ReO_4)_2(SeO_3)(H_2O)_2$				$Pb_2(ReO_4)_2(HPO_3)(H_2O)_2$			
Pb1-O3	2.370(4)	Pb2-O2	2.424(4)	Pb1-O3	2.326(6)	Pb2-O2	2.372(6)
Pb1-O1	2.548(4)	Pb2-O3	2.532(4)	Pb1-O1	2.485(6)	Pb2-O5	2.527(7)
Pb1-OW1	2.604(4)	Pb2-O5	2.534(5)	Pb1-O8	2.590(7)	Pb2-O10	2.572(7)
Pb1-O8	2.606(5)	Pb2-O10	2.615(4)	Pb1-OW1	2.623(7)	Pb2-O3	2.637(6)
Pb1-O2	2.654(4)	Pb2-O1	2.676(4)	Pb1-O4	2.790(7)	Pb2-O1	2.673(6)
Pb1-O9	2.791(5)	Pb2-OW1	2.818(4)	Pb1-O9	2.823(7)	Pb2-O7	2.834(8)
Pb1-O4	2.795(5)	Pb2-O7	2.894(5)	Pb1-O2	2.832(6)	Pb2-OW1	2.871(7)
Pb1-O11	2.907(5)	Pb2-O6	2.921(4)	Pb1-O11	2.941(7)	Pb2-O6	2.966(7)
Pb1-O6	3.388(5)	Pb2-O4	3.336(5)	Pb1-O6	3.282(7)	Pb2-O4	3.328(8)

<Pb1-O>	2.740	<Pb2-O>	2.750	<Pb1-O>	2.744	<Pb2-O>	2.753
Re1-O9	1.713(4)	Re2-O10	1.707(4)	Re1-O9	1.709(7)	Re2-O10	1.705(7)
Re1-O6	1.714(4)	Re2-O11	1.713(4)	Re1-O7	1.721(7)	Re2-O4	1.717(7)
Re1-O7	1.721(5)	Re2-O8	1.724(4)	Re1-O6	1.722(7)	Re2-O11	1.721(7)
Re1-O5	1.726(5)	Re2-O4	1.732(4)	Re1-O5	1.727(7)	Re2-O8	1.728(7)
<Re1-O>	1.719	<Re2-O>	1.719	<Re1-O>	1.720	<Re2-O>	1.718
Se1-O2	1.690(4)			P1-O3	1.511(6)		
Se1-O3	1.691(4)			P1-O2	1.511(7)		
Se1-O1	1.716(4)			P1-O1	1.540(6)		
<Se1-O>	1.699			P1-HP1	1.200(5)		
				<P1-O>	1.521		

3.1.3. Crystal structures of $Pb_2(ReO_4)_2(TO_3)(H_2O)](H_2O)$ ($TO_3 = SeO_3^{2-}$, HPO_3^{2-})

Both structures of $Pb_2(ReO_4)_2(SeO_3)\cdot 2H_2O$ and $Pb_2(ReO_4)_2(HPO_3)\cdot 2H_2O$ contain two symmetrically independent Pb^{2+} cations (Fig. 3.1) which are coordinated by eight oxygen atoms from the perrhenate anions and one H_2O molecule (OW1 site). The coordination spheres of Pb^{2+} in both structures are characterized by a rather uniform distribution of shorter and longer bonds. Eight of nine Pb-O bonds in both polyhedra centered by Pb1 and Pb2 atoms lie in the range 2.3-3.0 Å. Only for one Pb-O bond (Pb1-O9 in $Pb_2(ReO_4)_2(SeO_3)\cdot 2H_2O$ and Pb2-O4 in $Pb_2(ReO_4)_2(HPO_3)\cdot 2H_2O$ the distance exceeds 3.2 Å. The presence of the lone pairs does not appear to have a significant influence on the structural features of $Pb_2(ReO_4)_2(SeO_3)\cdot 2H_2O$ and $Pb_2(ReO_4)_2(HPO_3)\cdot 2H_2O$, an observation in agreement with the general pattern that the activity of a lone electron pair on Pb^{2+} cation is correlated with the presence of strong Lewis bases and decreases with increasing coordination number. The largest differences in Pb-O bond-distance values, between $Pb_2(ReO_4)_2(SeO_3)\cdot 2H_2O$ and $Pb_2(ReO_4)_2(HPO_3)\cdot 2H_2O$, are observed for Pb1-O2 and Pb2-O3 bonds, i.e. those involved in pseudotetrahedral $SeEO_3^{2-}$ and HPO_3^{2-} groups (Fig. 3.1). Interestingly, relatively weak Pb-OW1 bond is almost the same in $Pb_2(ReO_4)_2(SeO_3)\cdot 2H_2O$ and $Pb_2(ReO_4)_2(HPO_3)\cdot 2H_2O$.

The Se atom, in the structure of $Pb_2(ReO_4)_2(SeO_3)\cdot 2H_2O$, forms three nearly equal Se-O bonds (<Se-O> = 1.699 Å) with O1, O2 and O3 atoms and occupies an apex of an SeO_3 pyramid. This one-sided pyramidal configuration is typical of a Se^{IV} cation possessing a $5s^2$ lone pair of electrons.

In the structure of $Pb_2(ReO_4)_2(HPO_3)\cdot 2H_2O$., the pseudo-tetrahedral HPO_3 oxoanion has three P-O bonds in the narrow range 1.511(6) -1.540(6) Å and a relatively short hydrogen P-H bond of 1.200(5) Å. The latter bond length was fixed on the final stages of refinement due to very low scattering of hydrogen in the vicinity of medium scatterer like phosphorus. The P-O bond-distance values in $Pb_2(ReO_4)_2(HPO_3)\cdot 2H_2O$ are different to those observed in H_3PO_3 (Furberg& Landmark, 1957) with the double P=O = 1.47 Å and single P–OH 1.54 Å. A similar scatter of P-O distances is observed in the structure of $PbHPO_3$ (1.49(2)-1.53(2) Å) (Song *et* al., 2015); on the contrary, the HPO_3^{2-} anion is almost regular in the structure of $Pb_2(NO_3)_2(HPO_3)$ (Ouarsal *et* al., 2009).

There are two symmetrically independent Re^{VII} cations in each structure, which are tetrahedrally coordinated by four O atoms. The Re-O bonds in ReO_4 tetrahedra are in the range of 1.705(7)-1.732(4) Å (Fig. 3.1, Table 3.2). The O-Re-O bond angles are very close to the ideal tetrahedral values. The structural near-equality of the perrhenate tetrahedra in $Pb_2(ReO_4)_2(SeO_3)\cdot 2H_2O$ and $Pb_2(ReO_4)_2(HPO_3)\cdot 2H_2O$ is reflected by almost coinciding positions of their vibrational bands in the IR spectra. The ReO_4^- are therefore the most rigid species in the structures of $Pb_2(ReO_4)_2(SeO_3)\cdot 2H_2O$ and $Pb_2(ReO_4)_2(HPO_3)\cdot 2H_2O$.

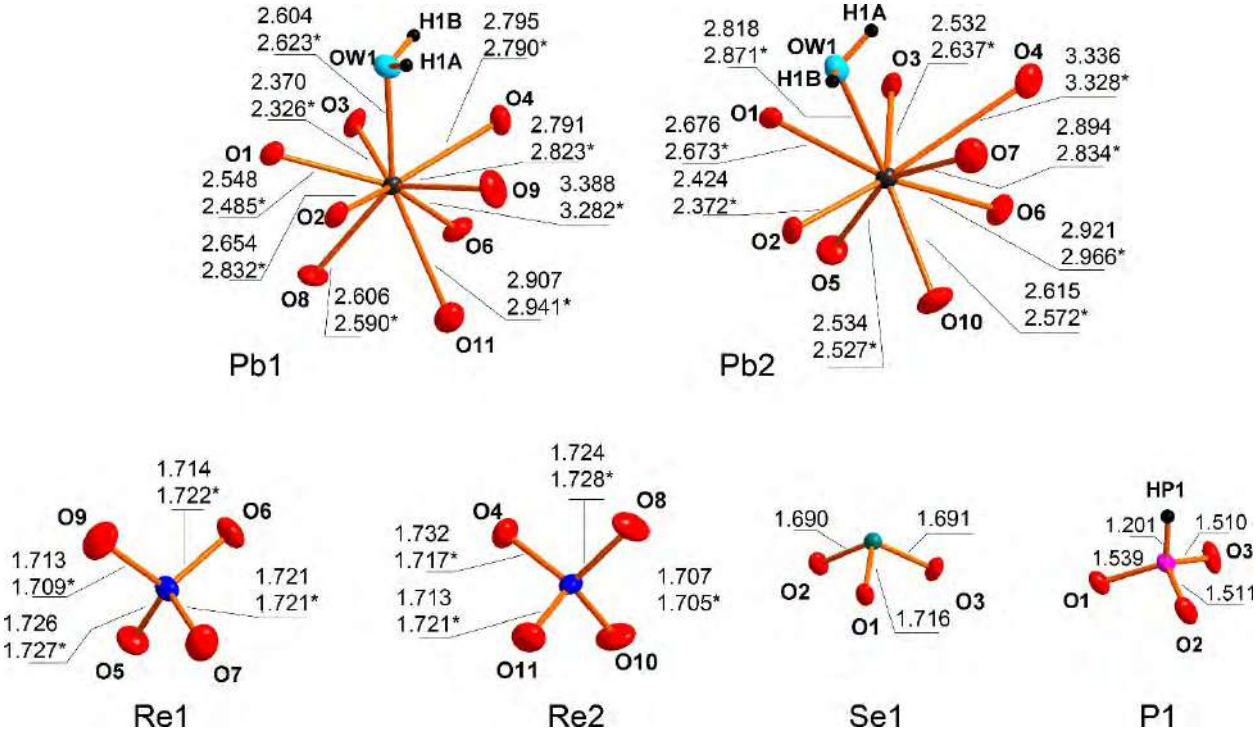

Fig. 3.1. Cation coordination in the structures $Pb_2(ReO_4)_2(SeO_3)\cdot 2H_2O$ and $Pb_2(ReO_4)_2(HPO_3)\cdot 2H_2O$

There are two symmetrically independent water molecules ($OW1H_2$ and $OW2H_2$) in each crystal structure. It is worth noting that the $OW2H_2$ molecules are not bonded to the Pb^{2+} cations but linked exclusively via hydrogen bonds OW1–H1A···OW2 and OW1–H1B···OW2 with $OW1H_2$ (Fig. 3.2). Hence, the structural formulas for both compounds can be represented as $[Pb_2(ReO_4)_2(SeO_3)H_2O]H_2O$

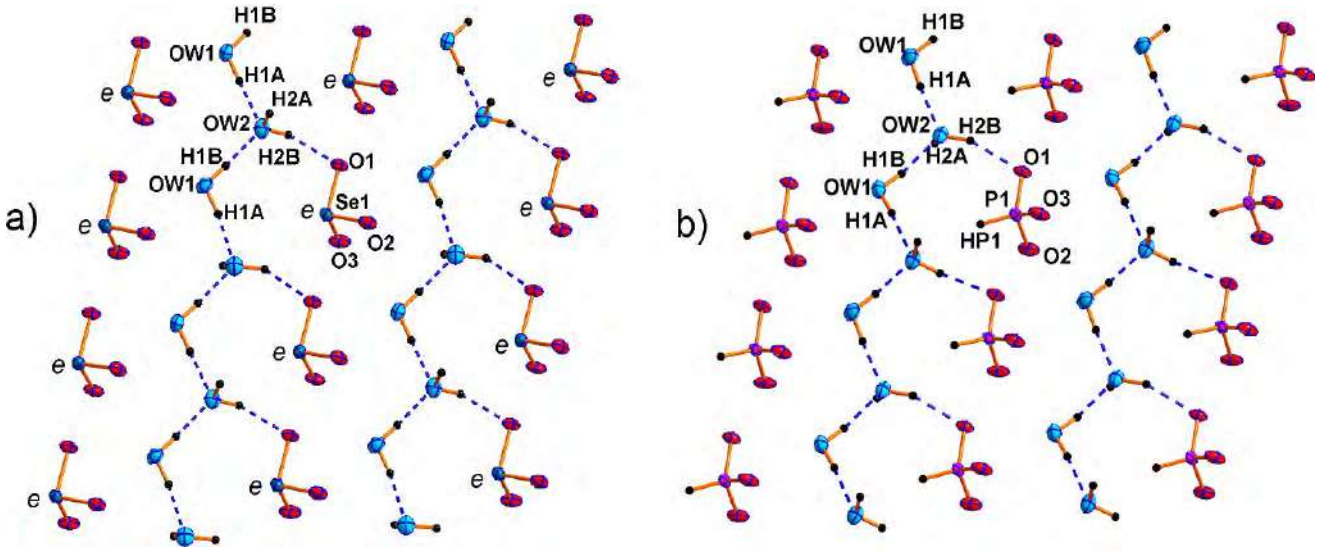

Fig. 3.2. Hydrogen bonding system in $Pb_2(ReO_4)_2(SeO_3)\cdot 2H_2O$ and $Pb_2(ReO_4)_2(HPO_3)\cdot 2H_2O$

and $[Pb_2(ReO_4)_2(HPO_3)H_2O]H_2O$. The $OW1H_2$ molecule, coordinated to the Pb^{2+} cations, bears more acidic hydrogens and forms two relatively strong hydrogen bonds to two $OW2H_2$ molecules. The protons of the 'free' $OW2H_2$ are less acidic and form weaker bonds to the oxygen atoms of $SeEO_3^{2-}/HPO_3^{2-}$ (Fig. 3.2) and perrhenate groups. The hydrogen atoms of OW_2H_2 are directed towards the 'lone pairs' of $SeEO_3^{2-}$ or the nearly nonpolar P–H bond of HPO_3^{2-}. In the latter case, the distance between the corresponding hydrogen atoms is 2.77 Å, which is too large for supposing any agostic-like interactions. Therefore, the lone pair of the selenite and the nonpolar P–H bond of the phosphite play the same role in structure formation. Note however that this distance has the lowest precision due to the very weak contribution of hydrogen in the overall scattering dominated by Pb and Re. The $PbO_8(H_2O)$ polyhedra and ReO_4 tetrahedra share common corners forming single sheets depicted in Fig. 3.3. The lead-perrhenate two-dimensional units are connected into double layers, which are further linked via SeO_3^{2-} or HPO_3^{2-} groups into frameworks with channels occupied by $OW2H_2$ water molecules (Fig. 3.4). Both new compounds $Pb_2(ReO_4)_2(SeO_3)H_2O]H_2O$ and $[Pb_2(ReO_4)_2(HPO_3)H_2O]H_2O$ adopt a new structure type.

The complete structural analogy between $Pb_2(ReO_4)_2(SeO_3)H_2O]H_2O$ and $[Pb_2(ReO_4)_2(HPO_3)H_2O]H_2O$ is rather similar to that between anhydrous nitrate-selenite $Pb_2(NO_3)_2(SeO_3)$ (Meng *et* al., 2015) and nitrate-phosphite $Pb_2(NO_3)_2(HPO_3)$ (Ouarsal *et* al., 2009). As noted above, the nearly nonpolar P–H bond plays the same structural role as the lone pair of Se^{IV} providing the "one-sided" coordination of the dianion. It is important to note that such $SeEO_3^{2-}/HPO_3^{2}$ substitutions without changing the main structural motif are possible not only in divalent lead oxysalts with the very flexible and adaptive coordination of Pb^{2+}, but also in iron and copper compounds (Kovrugin *et* al., 2016).

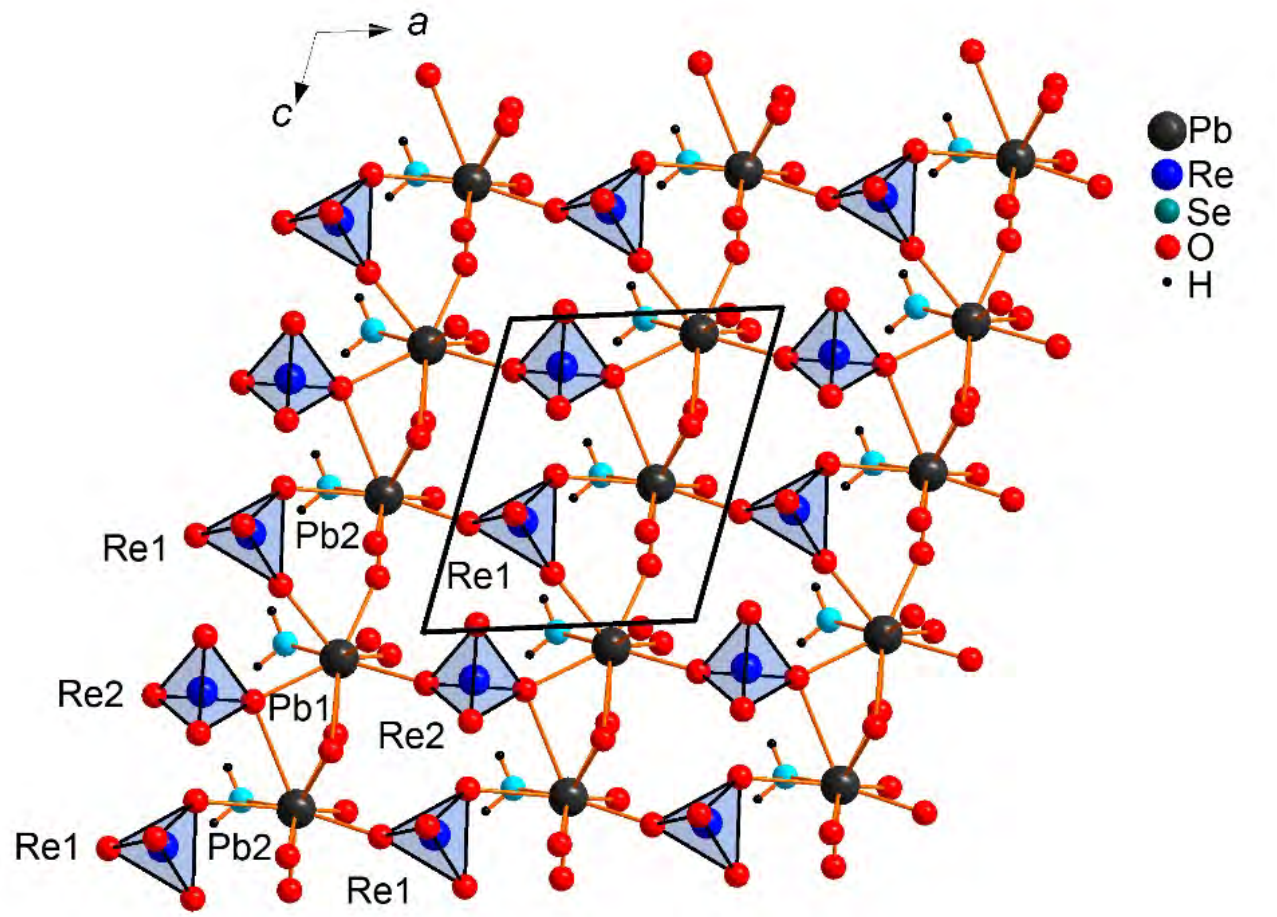

Fig. 3.3. The layer $Pb_2(ReO_4)_2H_2O]^{2+}$ in $Pb_2(ReO_4)_2(SeO_3)\cdot 2H_2O$ and $Pb_2(ReO_4)_2(HPO_3)\cdot 2H_2O$.

Incorporation of lone-pair anions into complex architectures containing also regular-shaped anions has been extensively investigated on both synthetic and mineral samples. Most common counterparts are the tetrahedral anions centered by the *p*-block (Si, P, As, S, Se, expected Ge) and *d*-block (Cr, Mo, W, expected V) elements (Sullens *et* al,. 2006, Lipp & Schleid, 2008, Zimmermann *et* al., 2014a,b, Xiao *et* al., 2015, Kong *et* al., 2018, Missen *et* al., 2020, Wu *et* al., 2021, Zhang *et* al., 2021). Hence, formation of $Pb_2(ReO_4)_2(SeO_3)H_2O]H_2O$ and $[Pb_2(ReO_4)_2(HPO_3)H_2O]H_2O$ involving tetrahedral perrhenate anions is not surprising. However, these seem to be the first examples based on single-charged tetrahedral oxyanions. It is also worth noting that even in the acidic medium formed, according to the proposed reaction $2Pb(ReO_4)_2 + H_3PO_3 + 2H_2O = Pb_2(ReO_4)_2(HPO_3)\cdot 2H_2O\downarrow + 2HReO_4$, the perrhenate anion is not reduced by the phosphorous acid. Proper chemical analogies can be observed to the formation of $Pb_2(NO_3)_2(HPO_3)$ when the phosphite anion is not oxidized by dilute nitric acid. It is thus possible that the HPO_3^{2-} anion can be introduced into a variety of other structures hitherto observed only with the "ψ-tetrahedral" sulfite, selenite, or tellurite anions. The most likely tetrahedral counterparts are hardly reducible (thermodynamically or kinetically) species like SiO_4^{4-}, GeO_4^{4-}, PO_4^{3-}, SO_4^{2-}, WO_4^{2-}, or ClO_4^{-}. As SeO_3^{2-} is relatively stable towards oxidation into SeO_4^{2-}, formation of pertechnate analog of $Pb_2(ReO_4)_2(SeO_3)H_2O]H_2O$ is also rather likely.

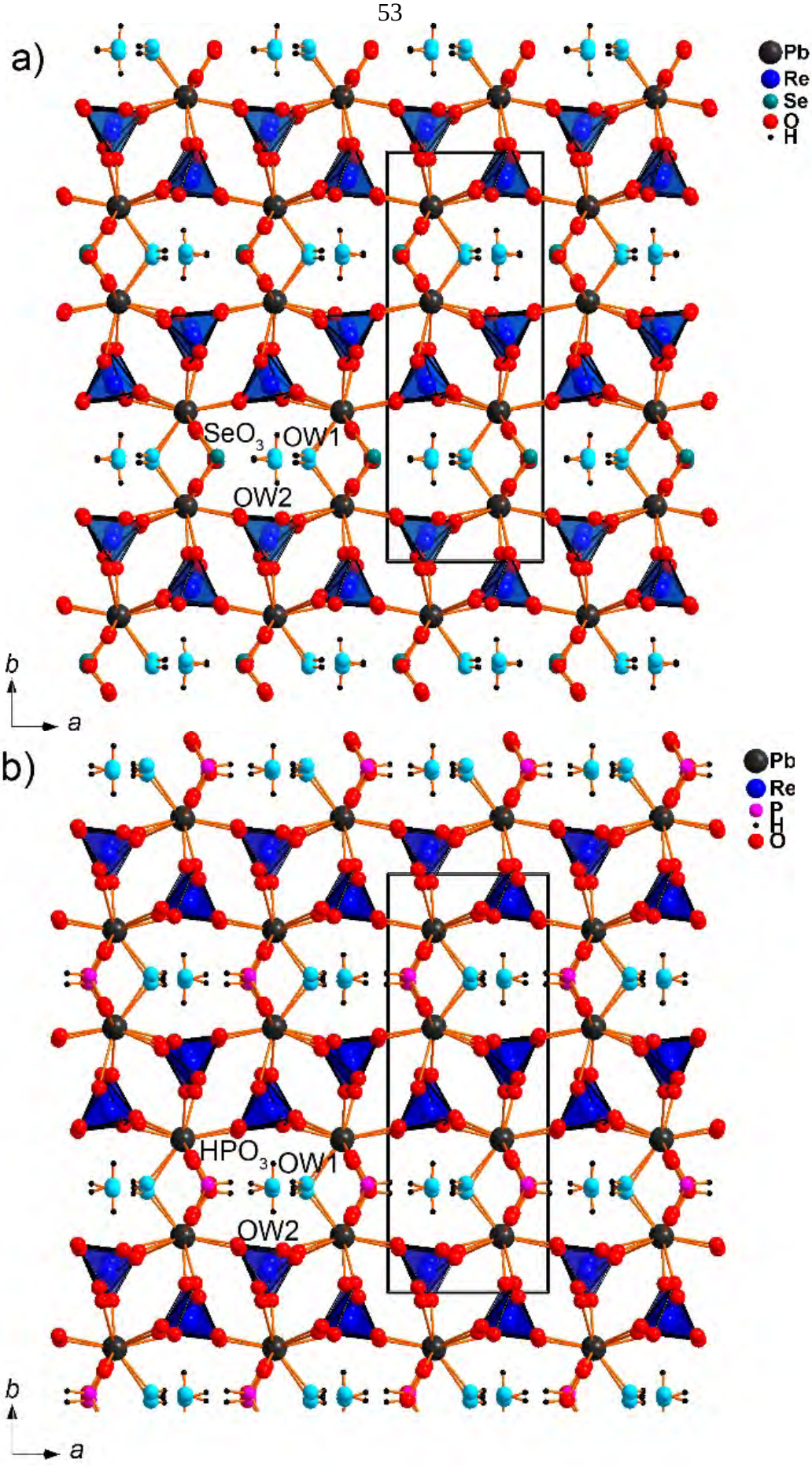

Fig. 3.4. General projections of structures $Pb_2(ReO_4)_2(SeO_3)\cdot 2H_2O$ (a) and $Pb_2(ReO_4)_2(HPO_3)\cdot 2H_2O$ (b)

The formation of complex polyanionic structures like Pb_2X_2Y (X = ReO_4^-, NO_3^-; Y = SeO_3^{2-}, HPO_3^{2-}) directly from aqueous solutions may seem surprising given the relatively low solubility $PbSeO_3$ and $PbHPO_3$. There is probably a rather delicate balance between the strength of the H_2Y diatomic acid and its high solubility and stability in aqueous solution. This may be the reason why the corresponding sulfite analog of $Pb_2(ReO_4)_2(SeO_3)H_2O]H_2O$ and $[Pb_2(ReO_4)_2(HPO_3)H_2O]H_2O$ could not be prepared. The sulfurous acid is unstable in aqueous solutions and decomposes into volatile SO_2 hardly soluble in acidic solutions; it is also readily oxidized into SO_4^{2-}. Preparation of lead perrhenate iodates has also been yet unsuccessful. Yet, one may suggest that at least some sulfite-, arsenite-, and iodate-bearing species could be prepared under mild hydrothermal conditions. It should however be borne in mind that both sulfite and arsenite species exhibit tautomerism with both lone-pair and hydride-bond configurations; the crystal chemistry of these species may be even more exciting.

It is also worth noting that despite similarities in chemical composition, there is nothing common between the structures of $Pb_2(NO_3)_2(TO_3)$ and $Pb_2(ReO_4)_2(TO_3)(H_2O)_2$ (T = Se or PH). Evidently, the reason lies in gross size and shape differences between ReO_4^- and NO_3^-, as well as possible bonding patterns. The only common feature is the presence of empty space around the lone pair of Se^{IV} or the P–H bond. With the smaller NO_3^-, it remains unoccupied while with larger ReO_4^-, there is enough room to accommodate water molecules attached to the framework via hydrogen bonds. Incorporation of species repelling ligands from one side (via lone pairs or nearly nonpolar bonds) results in the formation of low-dimensional or porous structures, those of $Pb_2(ReO_4)_2(SeO_3)H_2O]H_2O$ and $[Pb_2(ReO_4)_2(HPO_3)H_2O]H_2O$ being a new example for the latter case. By introducing some other species able to participate in hydrogen bonding, *e.g.* halides or organic species, one would probably be in position to prepare various templated structures; this intriguing area remains largely unexplored.

3.1.4 XRD and IR analysis

Powder X-ray studies of studied compounds were registered on a Rigaku MiniFlex II powder diffractometer (operating at 30 kV and 15 mA, Cu$K\alpha$ radiation). Samples were thoroughly ground, suspended in dry heptane, and transferred onto a silicon plate. Phase analysis was performed based on PDF-2 database (2020), PDXL (Rigaku, 2016), TOPAS V.5.0 (Bruker, 2014) suites. Both samples are pure and contain no admixtures of other phases (Fig. 3.5).

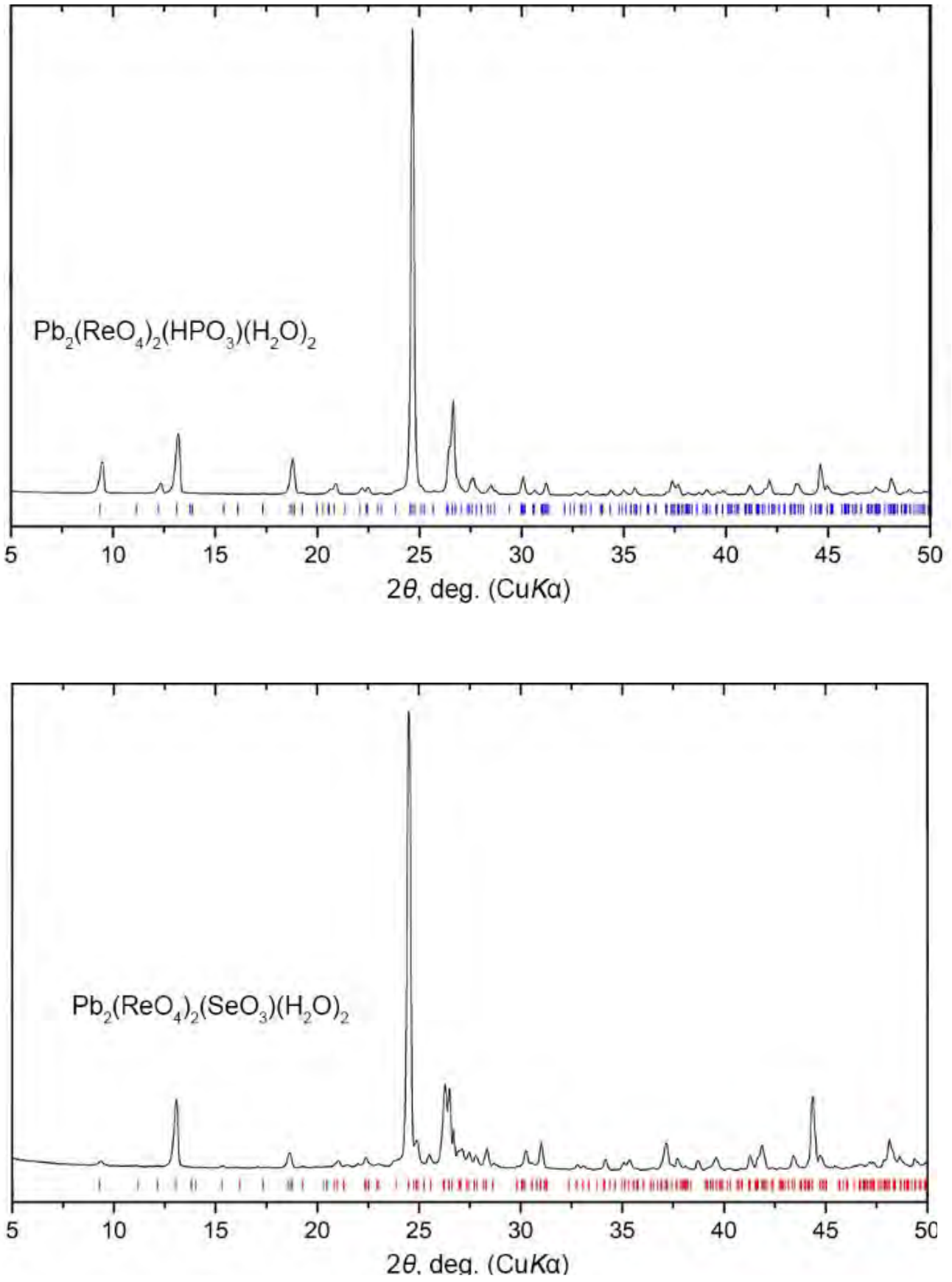

Fig. 3.5. Powder X-ray diffraction patterns of $[Pb_2(ReO_4)_2(SeO_3)H_2O]H_2O$ (above) and $[Pb_2(ReO_4)_2(HPO_3)H_2O]H_2O$ (below).

IR spectra of $Pb_2(ReO_4)_2(SeO_3)H_2O]H_2O$ and $[Pb_2(ReO_4)_2(HPO_3)H_2O]H_2O$ (Fig. 3.6) were acquired on a Bruker Vertex 70 FTIR spectrometer in the 4000–370 cm^{-1} wavelength range (4 cm^{-1}, 64 scans). The powdered sample was mixed with preheated potassium bromide (Sigma-Aldrich, > 99.0 %) and pressed into a pellet. A similar pellet of pure KBr was used as a reference. The spectra contain bands corresponding to the vibrations of perrhenate groups ReO_4^-, H_2O molecules and SeO_3^{2-} or HPO_3^{2-} species for $Pb_2(ReO_4)_2(SeO_3)H_2O]H_2O$ and $[Pb_2(ReO_4)_2(HPO_3)H_2O]H_2O$, respectively. The reference data were taken from (Tsuboi, 1957, Rees & Thod, 1966, Johnson *et* al., 1972, Range & Rögner, 1992, Seki *et* al., 2020)

For $Pb_2(ReO_4)_2(SeO_3)H_2O]H_2O$, positions (in cm^{-1}) and assignments of bands are the following: 374 (ν_4 doubly degenerate antisymmetric bending vibration of SeO_3^{2-}); 422, 455 (ν_2 symmetric bending vibrations of SeO_3^{2-}); 690 (ν_2 bending vibrations of ReO_4^-, also close to $2\nu_2$ SeO_3^{2-}); 744 (ν_3 doubly degenerate antisymmetric stretching vibration of SeO_3^{2-}); 800 (ν_1 symmetric stretching vibration of SeO_3^{2-}); 911 (ν_3 antisymmetric stretching vibration of ReO_4^-); 973 (ν_1 symmetric stretching vibration of ReO_4^-); 1596, 1622 (bending vibrations of H_2O molecules); 3210, 3460, 3558 (O–H stretching vibrations).

For $[Pb_2(ReO_4)_2(HPO_3)H_2O]H_2O$, these are: 448, 508 (antisymmetric deformation vibrations of HPO_3^{2-}); 573, 607 (δ symmetric deformation vibrations of HPO_3^{2-}); 727 (librational vibrations of H_2O molecules); 911 (ν_3 antisymmetric stretching vibration of ReO_4^-); 969 (ν_1 symmetric stretching vibration of ReO_4^-); 1055 (bending vibration of P–H bond); 1596, 1625 (bending vibrations of H_2O molecules); 2335, 2420 (stretching vibrations of P–H bond); 3470, 3550 (O–H stretching vibrations).

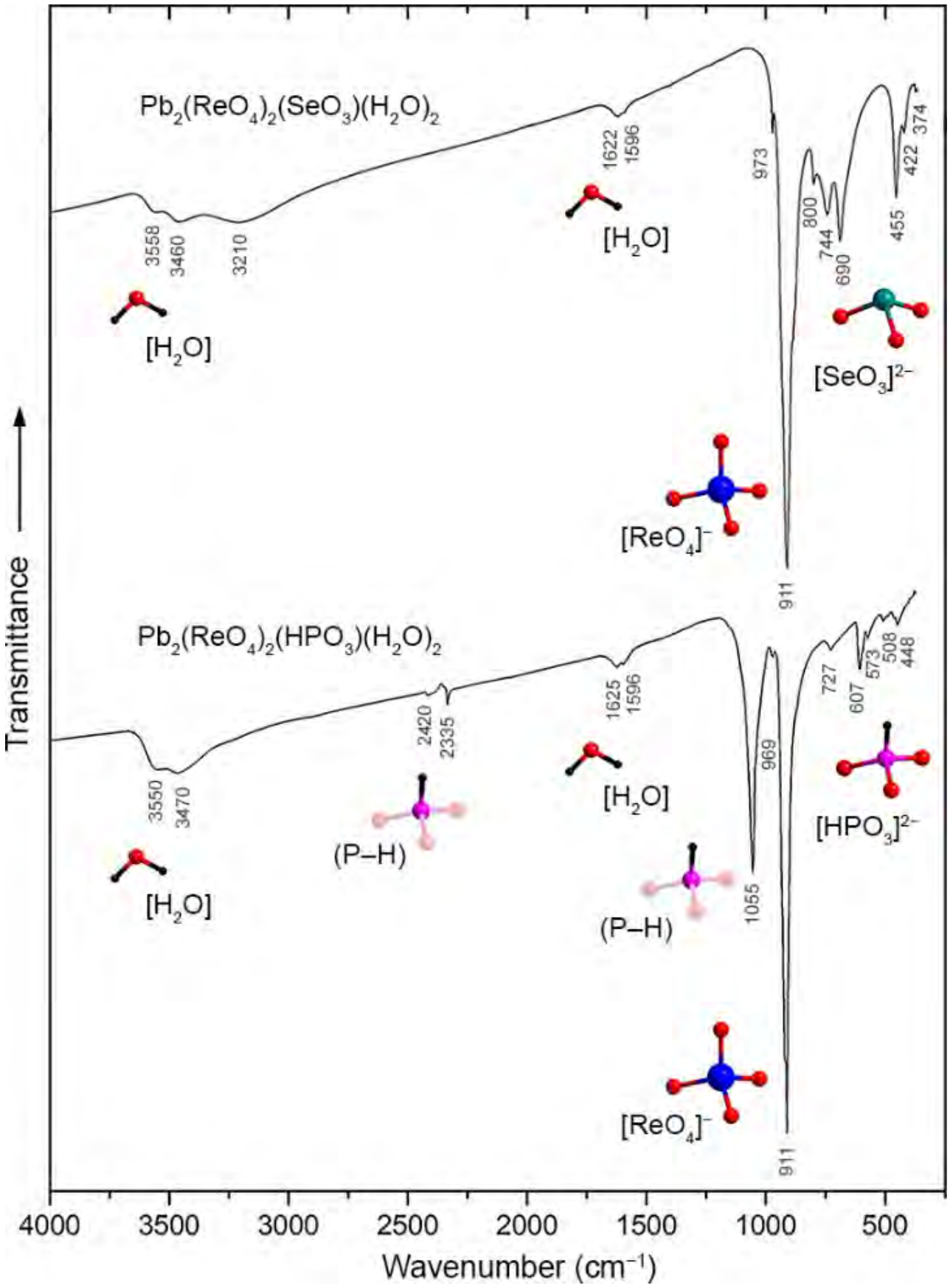

Fig. 3.6. IR spectra of $[Pb_2(ReO_4)_2(SeO_3)H_2O]H_2O$ (**1**) and $[Pb_2(ReO_4)_2(HPO_3)H_2O]H_2O$ (**2**) in the 4000–370 cm^{-1} region.

3.2. The new compound $Pb_4(SeO_3)_3(NO_3)_2•2H_2O$

3.2.1. Synthesis

The use of lone-pair cations often results in low-dimensional and porous structures. The probability of this is further increased when additional anions, primarily halogens, are introduced (Yu *et* al., 2018). Recent studies show that such unusual structures and promising properties can be observed when nitrate-anion is introduced into the structure (Reshak *et* al., 2016). In particular, nitrate-containing compounds such as $Pb_6O_5(NO_3)_2$ (Charkin *et* al., 2020) and $Pb_2(SeO_3)(NO_3)_2$ (Meng *et* al., 2015). Despite intensive studies, this class of compounds is yet sparsely studied and the general trends in structure formation are yet not formulated.

One of the advantages of selenites is the relative simplicity and softness of their synthesis, which is especially important for the preparation of compounds containing thermally unstable anions, particularly nitrate. For such syntheses, solution tecniques, including hydrothermal (Charkin *et* al., 2023a,b,c, Grishaev *et* al., 2023, Almond *et* al., 2002) are mostly employed.

The crystals of the new compound were obtained accidentally as a by-product during preparation oflead selenite. Initial solutions, containing 20 mmol of lead nitrate and 20 mmol of sodium selenite, respectively, were heated almost to boiling, after which the latter was poured into the latter. A heavy slightly yellowish precipitate was instantly formed, which was kept under the boiling mother liquor for approximately 30 minutes, to increase crystallity. After most of the mother liquor wasdecanted, a few needle crystals were found on the surface of the precipitate. This morphology is also characteristic of the second reaction product, sodium nitrate, but the crystals were not dissolved during repeated washing with distilled water. One of them was selected for X-ray studies.

Qualitative electron microprobe analysis (LINK AN-10000 EDS system) revealed no other elements, except Se and Pb with atomic number greater than 11 (Na).

3.2.2. Single crystal X-ray experiment

Single-crystal X-ray data of were collected using a Rigaku XtaLAB Synergy-S diffractometer equipped with a PhotonJet-S detector operating with Mo*K*α radiation at 50 kV and 1 mA. A single crystal was chosen and more than a hemisphere of data collected with a frame width of 0.5° in ω, and 10 s spent counting for each frame. The data were integrated and corrected for absorption applying a multi-scan

type model using the Rigaku Oxford Diffraction programs CrysAlis Pro. The structure was successfully refined with the use of SHELX software package (Sheldrick, 2015). The crystallographic and structure refinement parameters are shown in the Table 3.3. In the process of refining the structure it was found that oxygen atoms OW2, OW3 and OW4, The water molecules are half inhabited, while the OW1 position is fully populated. Calculated bond valence sums (BVS) are given in Table 5 in Appendix. Almost all calculated BVS values are well consistent with formal cations and anion valences in the structure $Pb_4(SeO_3)_3(NO_3)_2 \cdot 2H_2O$. The slightly underestimated sum for O9 may be due to the significant contribution of hydrogen bonds to the valence saturation of this oxygen atom, which cannot be accounted for at this stage.

Table 3.3. The crystallographic and structure refinement parameters of $Pb_4(SeO_3)_3(NO_3)_2 \cdot 2H_2O$

Crystal system	Triclinic
Space group	$P\bar{1}$
a, Å	7.2590(2)
b, Å	7.6454(2)
c, Å	14.7293(4)
α, °	84.386(2)
β, °	78.311(2)
γ, °	83.643(2)
V, Å^3	793.18 (4)
Radistion, λ, Å	Mo*K*α, 0.71073
Crystal size, mm	0.05×0.05×0.20
Total reflection number	13330
Number of unique reflections	3312
R_1	0.031
S	1.03
$\Delta\rho_{min}/\Delta\rho_{max}$, э/Å^3	-2.70/2.67
CCDC	2339041

3.2.3. Crystal structure of $Pb_4(SeO_3)_3(NO_3)_2 \cdot (H_2O)_2$

The crystal structure of $Pb_4(SeO_3)_3(NO_3)_2 \cdot 2H_2O$ refers to a new structural type. The compound crystallizes in the centrosymmetric group *P*-1. The structure contains four symmetrically independent positions of lead, three selenium, two nitrogen, and nineteen oxygen positions, four of which belong to water molecules. All lead atoms adopt irregular environment formed by oxygen atoms (Fig. 3.6). The environment of Pb1 consists of eleven oxygen atoms at 2.488(5) – 3.535(5) Å. Two oxygen positions OW2 and OW3 belong to water molecules and are half occupied. Pb2 is surrounded by ten oxygen atoms at 2.449(5) – 3.236(5) Å while Pb3, by eleven oxygen atoms at 2.508(5) – 3.473(5) Å, among which there are two positions of oxygen, OW2 and OW3, half occupied, making the Pb3 environment similar to that of Pb1. Pb4 is surrounded by ten oxygen atoms at 2.449(5) – 3.196(5) Å. In all coordination polyhedra it is possible to determine a "free" area which illustrates the stereochemical activity of the lone electron pairs. All four lead atoms show different coordination modes to the triangular nitrate groups (Fig. 3.6). Pb1 coordniates only $N1O_3$, Pb2 is coordinated by $N1O_3$ and $N2O_3$. Pb3 has both types of coordination to two nitrate groups, and the Pb4 atom is coordinated by three groups NO_3. The valence contribution of each of the two OW1-Pb1 links and the two OW1-Pb3 links is slightly more or equal to 0.03 *v.u.* (Table 5 in Appendix). The water molecule OW4 is not bound to cations and is held exclusively by hydrogen bonds.

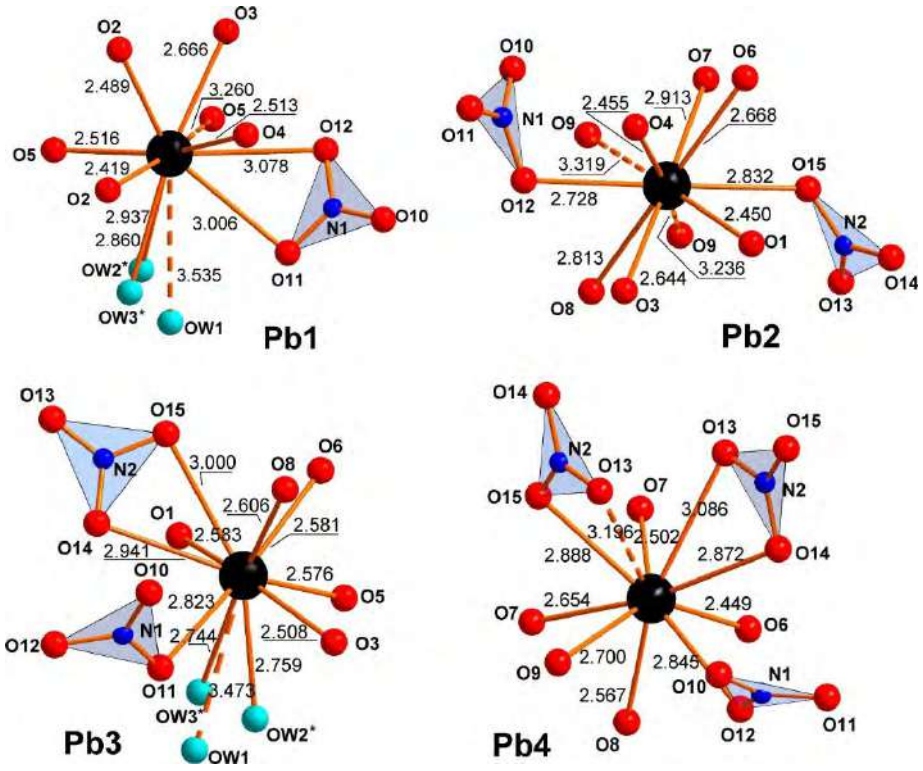

Fig. 3.6. Coordination environment of lead atoms Pb1, Pb2, Pb3 and Pb4 in $Pb_4(HSeO_3)_3(NO_3)_2 \cdot 2H_2O$. OW positions marked with an asterisk are half occupied. Pb-O links > 3.1 Å dotted. All links are shown Pb-O ≤ 3.55 Å.

The tetrarvalent selenium forms a classic "umbrella"-like group SeO_3E, (E is the stereochemically active lone pair). The Se–O distances are slightly non-equal (the difference in the length of the links is 0.02-0.03 Å), which is due to the different environments of the oxygens by lead cations. The SeO_3^{2-} sniond and Pb^{2+} cations form pseudo-layers of the composition $[Pb_4(SeO_3)_3]^{2+}$ which interleave with the layers formed by nitrate anions and water molecules (Fig. 3.7 and 3.8) which complete the coordination of lead cations located in the lead-selenite layer. The lone pairs of SeO3E groups look towards each other with the formation of channels, or the so-called "micelles" (Makovicky *et* al., 1997).

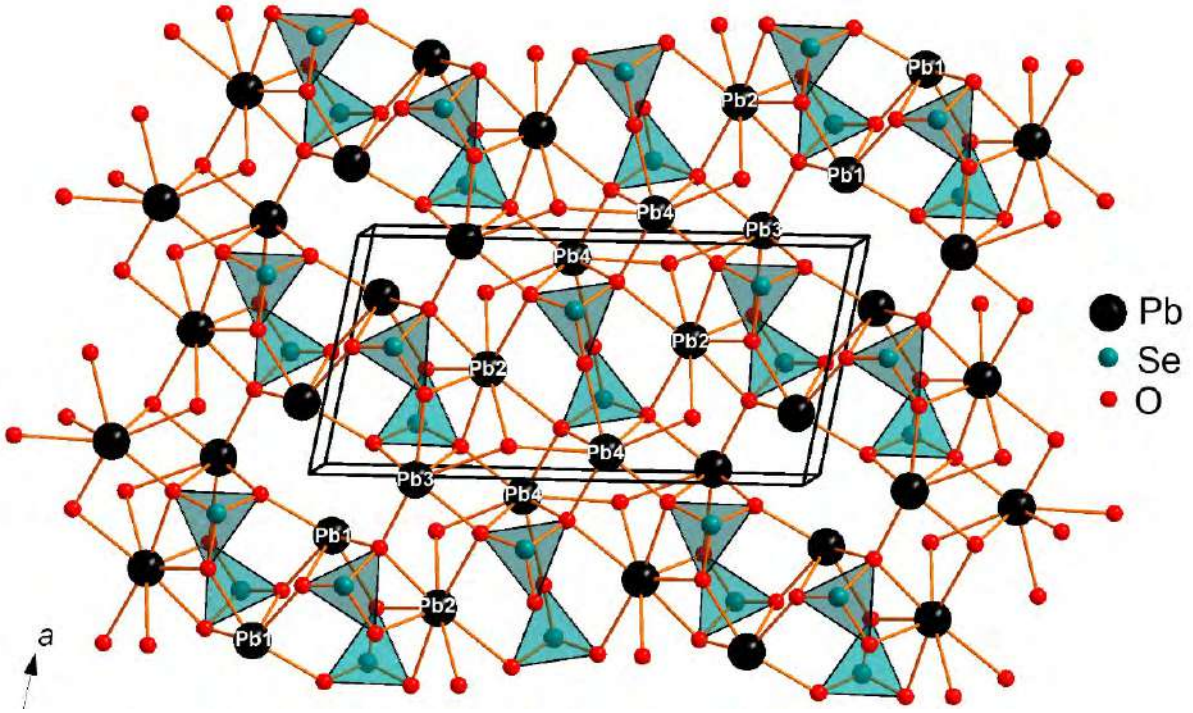

Fig. 3.7. Layers $[Pb_4(SeO_3)_3]^{2+}$ in $Pb_4(SeO_3)_3(NO_3)_2 \cdot 2H_2O$.

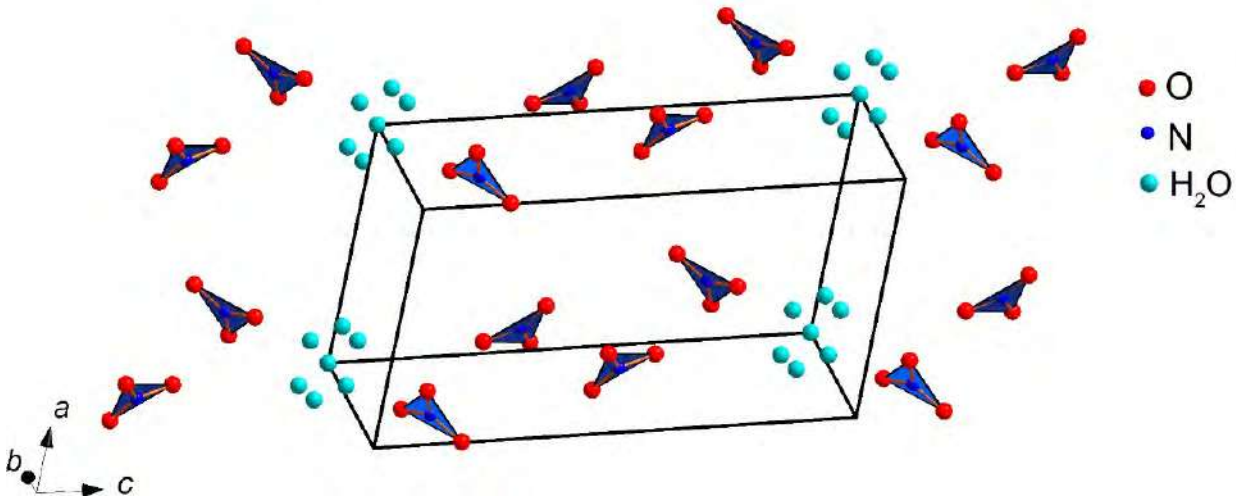

Fig. 3.8. Layers $\{(NO_3)_2(H_2O)_2\}^{2-}$ in $Pb_4(SeO_3)_3(NO_3)_2 \cdot 2H_2O$.

$Pb_4(SeO_3)_3(NO_3)_2 \cdot 2H_2O$ is the second lead selenite nitrate after that described in (Meng *et* al., 2015), the anhydrous $Pb_2(SeO_3)(NO_3)_2$. It is worth nothing that both selenite nitrates are obtained from aqueous solutions, yet under different conditions. $Pb_2(SeO_3)(NO_3)_2$ (like its phosphite analogue $Pb_2(HPO_3)(NO_3)_2$) is formed by adding selenious acid to the dilute solution of lead nitrate (wherein the medium is mildly acidic), while $Pb_4(SeO_3)_3(NO_3)_2 \cdot 2H_2O$ obtained by the interaction of solid lead selenite with excess $NaNO_3$ solution (possibly containing a small surplus of $Pb(NO_3)_2$, with the medium close to neutral). In our case, a hot solution containing high nitrate concentrations interacts with a solid phase containing selenite-anions. One can thus assume that due to the relatively high temperature and ionic force of the concentrated $NaNO_3$ solution, lead selenite partially dissolved and crystallized as $Pb_4(SeO_3)_3(NO_3)_2 \cdot 2H_2O$.

Both anhydrous $Pb_2(SeO_3)(NO_3)_2$ and $Pb_4(SeO_3)_3(NO_3)_2 \cdot 2H_2O$ can be described as porous architectures (Fig. 3.9). The main difference is due to both the presence of "additional" water molecules and the different Pb^{2+}: SeO_3^{2-} ratio. There exists an anhydrous selenite nitrate of a more complex composition, $Pb_2Cu_3O_2(NO_3)_2(SeO_3)_2$ (Effenberger *et* al., 1986), wherein the primary building blocks are CuO_4 squares which share vertices to form zigzag chains surrounded at both sides by the lead cations and selenite groups. In this case, the lone pairs of Se^{IV} and Pb^{II} are directed into the interlayer space, indicating the presence of the "chemical scissors" effect.

The structural similarity of nitrates to halogenides can be traced when comparing these compounds to $Pb_8Cu^{2+}(SeO_3)_4Br_{10}$ (Siidra *et* al., 2023) which obtained by a chemical gas transport reaction as a by-product in the synthesis of a bromide analogue of sarrabusite (Gemmi *et* al., 2012). Although this structure has a chain motif, it is formed in a similar way to $Pb_2Cu_3O_2(NO_3)_2(SeO_3)_2$ around the copper atoms and lined with unbound electron pairs, "pushing" halogen into the interlayer space. The role of water as a factor in reducing the dimension of the structure can be illustrated by the mineral faureauite $PbBiCu_6O_4(SeO_3)_4(OH)(H_2O)$ (Mills *et* al., 2014). The copper-selenite layers in this structure are strongly corrugated and their "lacunas" contain disordered water molecules, which are relatively loosely bound to the strong covalent layers and fill the free space.

To sum up, the combination of low-valence metal and non-metal cations in oxide environment results in formation of “boundaries” which are "lined" by the stereochemically active lone electron pairs. On the other side of these borders are the rigid anions which weakly interact with the low-valence cations, illustrating the effect of "chemical scissors". This effect seems to be amplified by water molecules, which only form relatively weak hydrogen bonds and also contribute to a reduction in the density and/or dimension of covalently coupled frameworks.

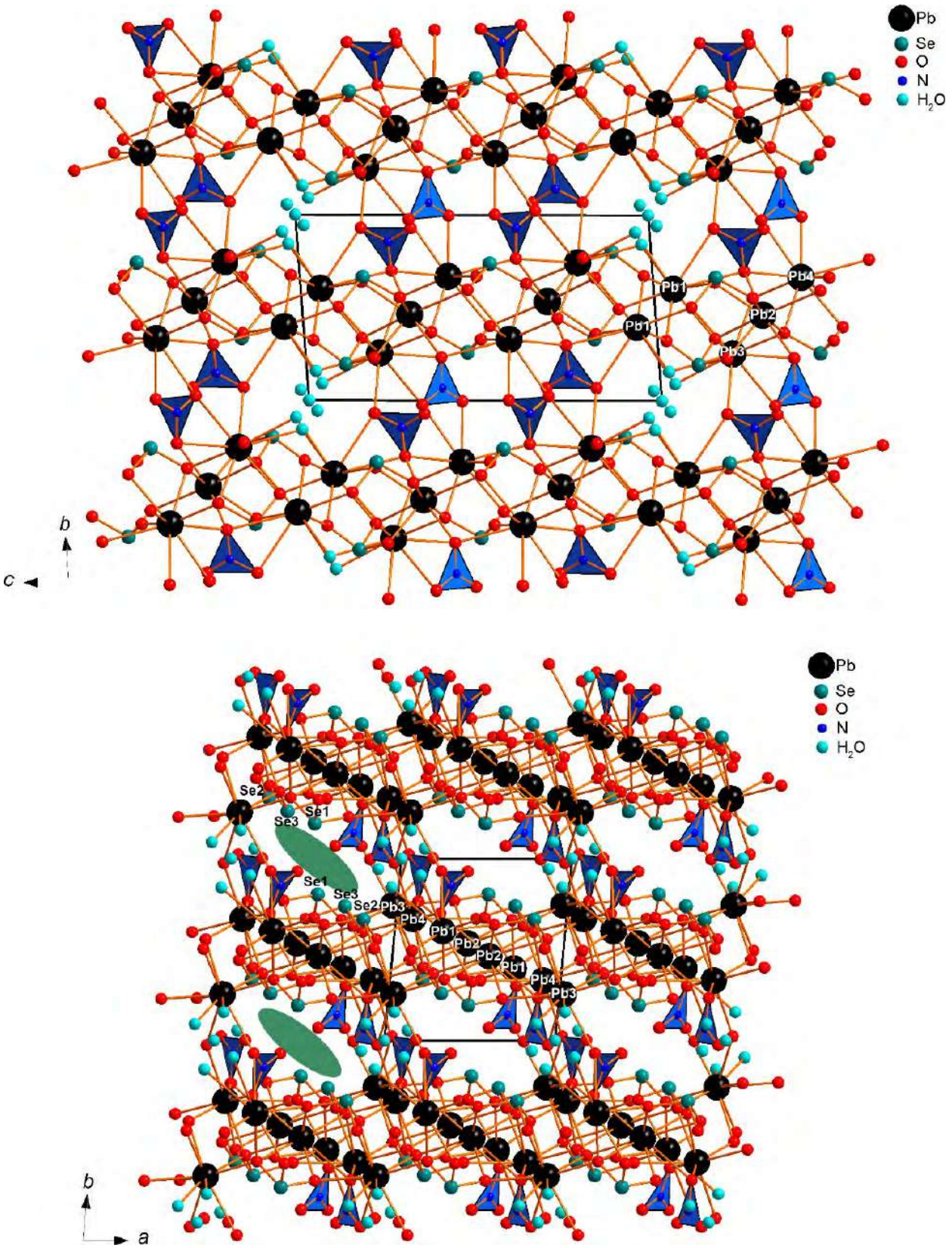

Fig. 3.9. General projection of structure of $Pb_4(SeO_3)_3(NO_3)_2 \cdot 2H_2O$

Chapter 4. New anhydrous selenites of heavy and transition metals

4.1. $Cd_7Cu_2(SeO_3)_8Br_2$

4.1.1. Synthesis

The combination of lone-pair electron cations and halogens results in a wide variety of structural motifs which ciontribute to a variety of physico-chemical properties. However, in addition to the variation of cations and anions, the choice of synthesis method has a profound effect on the outcome. In the previous chapters, the compounds obtained by solution methods and adopting layered (or pseudo-layered) structural motifs have been described, while the "host-guest" representation is often valid for the description of compounds obtained from vapor syntheses. In particular, the compounds containing Cu^{2+} with non-transition metal cations, such as yttrium, bismuth or lead, have been extensively investigated previously, while their analogs contain nonmagnetic *d*-metal cations (*e.g.* Zn^{2+}, Cd^{2+}, Sc^{3+}, Y^{3+}, Zr^{4+} *etc*) essentially less attention. The compounds $CdCu_2(SeO_3)_2Cl_2$ (Murtazoev *et* al., 2021) and $MCu_3(SeO_3)_2O_2X$ (*M* = Y, La; *X* = Cl, Br) (Zakharov *et* al., 2014; Markina *et* al., 2017) have been reported recently. The mineral structure prototype for the latter is francisite $BiCu_3(SeO_3)_2O_2Cl$ (Pring *et* al., 1990).

Crystals of $Cd_7Cu_2(SeO_3)_8Br_2$ were obtained by the chemical vapor transport (CVT) reactions of cadmium selenite $CdSeO_3$ and copper bromide $CuBr_2$ (Vekton, 99.5%) in sealed silica tubes. Cadmium selenite was obtained by adding selenous acid to a boiling solution of cadmium acetate, according to Gospodinov and Barkov (2002). The starting reagents were mixed in a molar ratio of 1:1 and placed in a 10 cm long silica tube, sealed under vacuum. The tube was placed in a Nabertherm furnace, with the cold end protruding 2-3 cm from the furnace. The tube was annealed at 400 °C for 48 hours. Green crystals of the new compound $Cd_7Cu_2(SeO_3)_8Br_2$ were found in the cold end of the tube. Qualitative electron microprobe analysis (Hitachi TM3000) of $Cd_7Cu_2(SeO_3)_8Br_2$ crystals revealed no other elements, except Cd, Cu, Se and Br with atomic number greater than 11 (Na).

4.1.2. Single crystal X-ray experiment

A prismatic crystal of $Cd_7Cu_2(SeO_3)_8Br_2$ was mounted on a glass fiber and studied on a Rigaku Synergy-S X-ray diffractometer equipped with a micro-focus X-ray tube operating with Mo*K*α radiation at 50 kV and 1 mA. More than a hemisphere of X-ray diffraction data was collected. The structure was solved by direct methods and refined using SHELX software package (Sheldrick, 2015). The new compound is triclinic, $P\bar{1}$, a = 5.3280(5) Å, b = 10.6190(12) Å, c = 11.4380(13) Å, α = 100.856(4) °, β = 93.321(4)°, γ = 91.021(4) °, V = 634.22(12) Å^3, R_1 = 0.027 (Table 4.1). Atom coordinates and bond-valence sums are given in Table 4.2 and selected interatomic distances are provided in Table 4.3. Bond-valence analysis was calculated using bond-valence parameters taken from Gagné and Hawthorne (2015) for the Cd-O, Cu^{2+}-O and Se^{4+}-O bonds and from Brese and O'Keeffe (1991) for the Cd-Br, Cu^{2+}-Br and Se^{4+}-Br bonds. All of the Cd-O and Cd-Br bonds ≤ 3.20 Å, Se-O bonds ≤ 3.65 Å, Se-Br bonds ≤ 3.75 Å, Cu^{2+}-O and Cu^{2+}-Br ≤ 3.00 Å were taken into consideration. All the calculated bond-valence sums agree well with expected oxidation states of all cations in $Cd_7Cu_2(SeO_3)_8Br_2$.

Table 4.1. Crystallographic data and refinement parameters for $Cd_7Cu_2(SeO_3)_8Br_2$

space group	$P\bar{1}$
a(Å)	5.3280(5)
b(Å)	10.6190(12)
c(Å)	11.4380(13)
α(°)	100.856(4)
β(°)	93.321(4)
γ(°)	91.021(4)
V(Å^3)	634.22(12)
D_x (g/cm^3)	5.471
crystal syze, mm^3	0.10×0.20×0.20
θ max (°)	28.774
total reflection number	4827
unique reflection number (R_{int})	3297(0.012)
unique reflection number F > 4σ(F)	3123
R_1	0.027
wR_1	0.066
S	1.037
CCDC	2339771

Table 4.2. Atomic coordinates, displacement parameters (Å^2) and bond-valence sums (in valence units (*vu*)) in $Cd_7Cu_2(SeO_3)_8Br_2$.

Atom	Wyck. site	B.V.S.	*x*	*y*	*z*	U_{eq}
Cd1	2*i*	2.08	0.45878(4)	0.38169(3)	0.17830(4)	0.01278(7)
Cd2	2*i*	1.90	0.05946(4)	0.83550(3)	-0.02125(4)	0.01411(8)
Cd3	1*c*	1.76	0	½	0	0.01663(11)
Cd4	2*i*	1.93	0.91543(5)	0.23887(3)	0.36109(4)	0.01256(7)
Cu1	1*h*	2.13	½	½	½	0.00927(15)
Cu2	1*b*	1.90	0	0	½	0.01086(16)
Se1	2*i*	4.07	0.99450(6)	0.52874(4)	0.33443(5)	0.00922(9)
Se2	2*i*	3.93	0.49925(6)	0.17655(4)	0.54795(5)	0.00988(9)
Se3	2*i*	4.10	0.53914(6)	0.71081(4)	0.10875(5)	0.00996(9)
Se4	2*i*	3.94	-0.38787(6)	0.91928(4)	-0.18600(5)	0.01115(10)
Br1	2*i*	0.50	0.99472(8)	0.12729(6)	0.74777(6)	0.02513(14)
O1	2*i*	2.10	0.0863(5)	0.4824(3)	0.1968(4)	0.0187(8)
O2	2*i*	2.05	0.1914(5)	0.4377(3)	0.4066(4)	0.0137(7)
O3	2*i*	2.12	0.7389(4)	0.4272(3)	0.3343(4)	0.0120(7)
O4	2*i*	2.01	0.5867(6)	0.3208(3)	0.5222(5)	0.0247(11)
O5	2*i*	2.03	0.2140(4)	0.1439(3)	0.4685(4)	0.0138(7)
O6	2*i*	1.98	0.6999(5)	0.0924(3)	0.4487(4)	0.0151(7)
O7	2*i*	1.98	0.5810(6)	0.5915(4)	0.1789(5)	0.0279(11)
O8	2*i*	2.18	0.7618(5)	0.6817(3)	0.0042(4)	0.0140(7)
O9	2*i*	1.99	0.2877(4)	0.6619(3)	0.0065(4)	0.0140(7)
O10	2*i*	2.00	-0.2634(5)	0.9724(3)	-0.0443(4)	0.0166(8)
O11	2*i*	2.08	-0.1862(5)	0.7947(3)	-0.2161(4)	0.0170(8)
O12	2*i*	1.99	-0.6450(5)	0.8239(3)	-0.1736(4)	0.0146(7)

Table 4.3. Selected interatomic distances (Å) in the structure of $Cd_7Cu_2(SeO_3)_8Br_2$

Cd1-O3	2.233(4)	Cu1-O2	1.943(3) ×2
Cd1-O1	2.273(3)	Cu1-O4	2.025(3) ×2
Cd1-O7	2.308(4)	Cu1-O3	2.360(3) ×2
Cd1-O8	2.313(4)		
Cd1-O12	2.407(3)	Cu2-O5	1.989(3) ×2
Cd1-O11	2.467(3)	Cu2-O6	2.007(3) ×2
Cd1-O9	2.548(4)	Cu2-Br1	2.9030(7) ×2

Cd1-O2	3.013(4)		
		Se1-O1	1.663(4)
Cd2-O10	2.271(3)	Se1-O2	1.718(3)
Cd2-O9	2.288(3)	Se1-O3	1.722(3)
Cd2-O10	2.307(3)	Se1-O7	2.916(4)
Cd2-O8	2.325(3)	Se1-O4	2.947(4)
Cd2-O12	2.403(4)	Se1-O2	3.137(4)
Cd2-O11	2.479(4)		
Cd2-Br1	3.1092(9)	Se2-O4	1.676(3)
		Se2-O5	1.720(3)
Cd3-O9	2.270(3) ×2	Se2-O6	1.739(3)
Cd3-O1	2.314(4) ×2	Se2-O6	3.037(3)
Cd3-O8	2.322(3) ×2	Se2-Br1	3.5024(8)
Cd3-O7	3.158(5) ×2	Se2-O7	3.648(5)
		Se2-Br1	3.7197(7)
		Se3-O7	1.635(4)
Cd4-O11	2.243(3)	Se3-O8	1.724(3)
Cd4-O3	2.290(3)	Se3-O9	1.731(3)
Cd4-O5	2.314(3)	Se3-Br1	3.1828(7)
Cd4-O6	2.324(3)	Se3-Br1	3.6595(7)
Cd4-O12	2.488(4)		
Cd4-O2	2.506(3)	Se4-O10	1.703(4)
Cd4-O4	2.654(4)	Se4-O11	1.716(3)
		Se4-O12	1.717(3)
		Se4-Br1	3.2026(7)
		Se4-O6	3.329(4)
		Se4-O10	3.349(4)

4.1.3. Crystal structure of $Cd_7Cu_2(SeO_3)_8Br_2$

The cadmium atoms adopt irregular coordination environments in which are consistent with the $4d^{10}$ configuration of Cd^{2+} (CFSE = 0). Cd1 is coordinated by eight oxygen atoms at ≤ 3 Å. The Cd2 coordination environment is strongly asymmetric with six oxygen atoms in one coordination hemisphere and one Br^- anion in the other (Fig. 4.1). The coordination of Cd3 can be described as close to octahedral with formation of two additional long Cd3-O7 bonds at 3.158(5) Å. Cd4 forms irregular $Cd4O_7$ polyhedra similar to those in the structure of monoclinic $CdSeO_3$ (Valkonen, 1994). Each of four Se atoms forms three nearly equal Se^{4+}-O bonds (Table 4.3) in the range 1.635(4) – 1.739(3) Å and occupies an apex of a SeO_3 pyramid. This one-sided pyramidal configuration is typical for Se^{IV}.

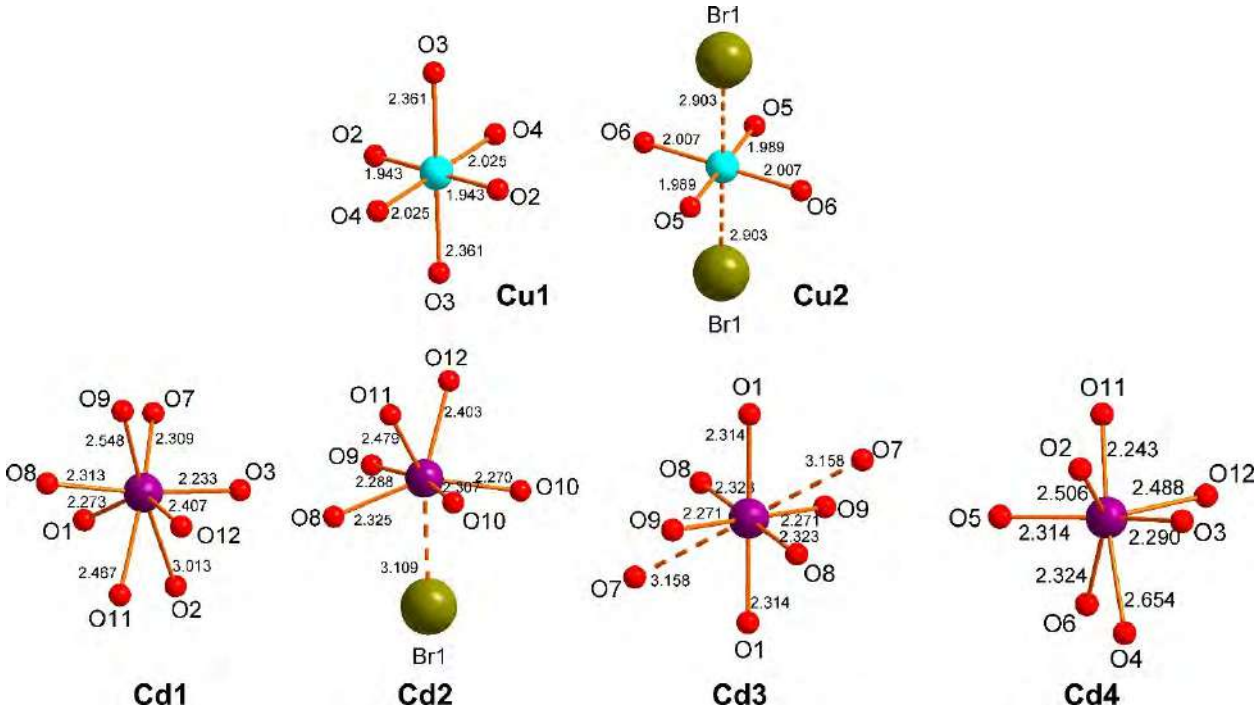

Fig. 4.1. Coordination of atoms in the structure of $Cd_7Cu_2(SeO_3)_8Br_2$.

The CdO_n polyhedra share vertices forming zigzag layers shown in Figure 4.2a. All oxygen atoms belong to the SeO_3 groups which "decorate" the layers. Compated to $CdSeO_3$, the layer contains Cd^{2+} vacancies (Figure 4.2b which are possibly necessary to reduce structural strain or are the cause of the strong corrugation of the layers. The $[Cd_7(SeO_3)_8]^{2-}$ layers are linked via Cu^{2+}-centered polyhedra (Figure 4.2a,c) into a $[Cd_7Cu_2(SeO_3)_8]^{2+}$ porous framework with channels running along *a* and occupied by Br^-. Smaller "empty" channels run along *c* (Figure 4.2d). The selenite groups are directed towards each other and towards the bromide anion, illustrating the halophilicity phenomenon. The Se3 and Se4 atoms form weakly interact with bromide anions, with bond valences of ~ 0.1 *v.u.* contrary to Se1 atom

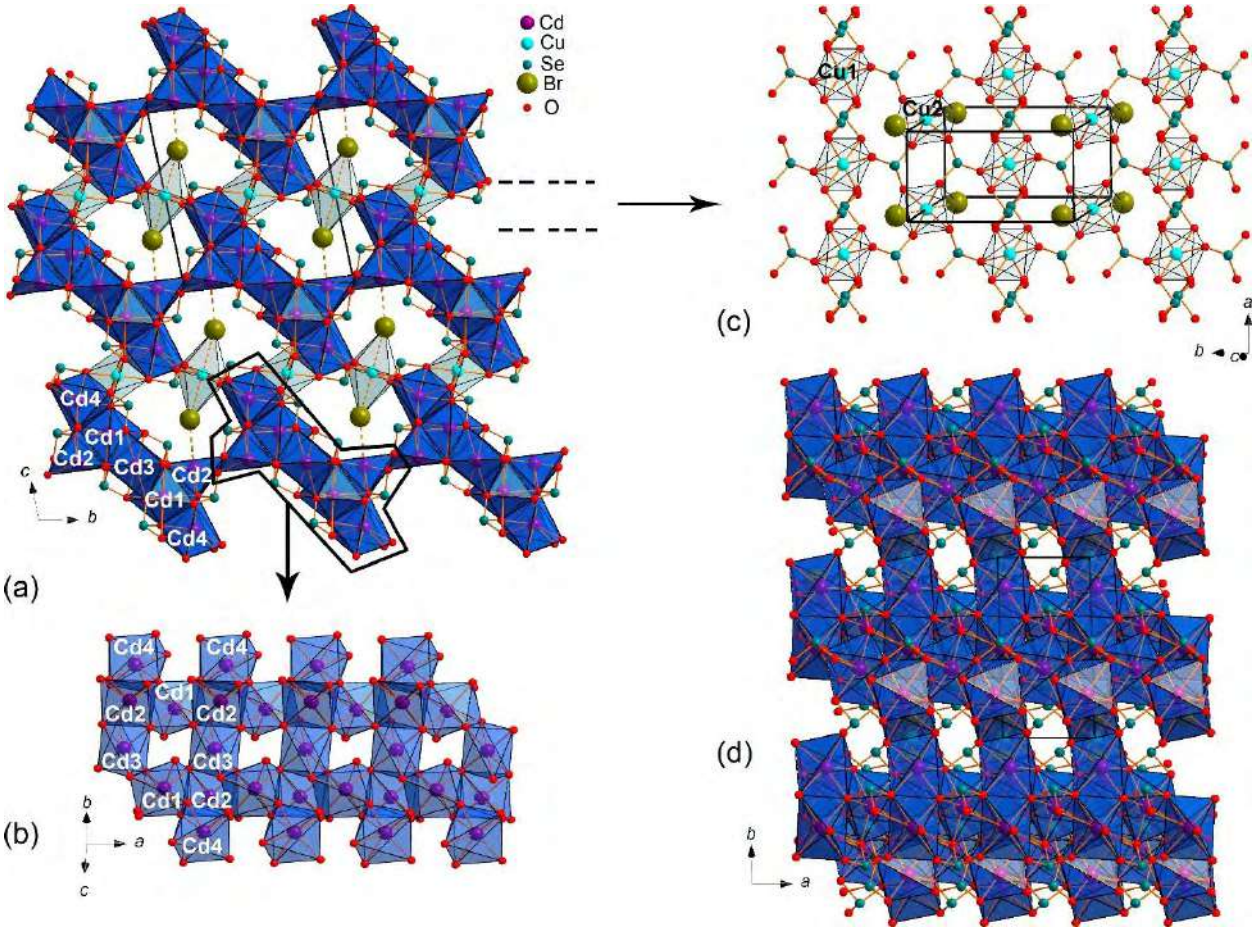

Fig. 4.2. General projection of the crystal structure of $Cd_7Cu_2(SeO_3)_8Br_2$ along the *a* axis (a). Fragment of the $[Cd_7(SeO_3)_8]^{2-}$ zigzag layer (b). Arrangement of Cu-centered polyhedra interconnected via SeO_3 groups (c). General projection of the crystal structure of $Cd_7Cu_2(SeO_3)_8Br_2$ along the *c* axis (d).

does not form bonds with Br^- (Table 4.2). The Se2-Br1 interactions are very weak. These Se-Br interactions might contribute to the stabilization of the structural architecture of $Cd_7Cu_2(SeO_3)_8Br_2$.

The structural architecture of $Cd_7Cu_2(SeO_3)_8Br_2$ is derived from that of monoclinic $CdSeO_3$ (β-$CdSeO_3$) (Valkonen, 1994). The latter is a three-dimensional framework containing cavities with a similar geometry and decorated with 'lone pair' Se^{4+} cations. The structure of $Cd_7Cu_2(SeO_3)_8Br_2$ is obtained from the ideal β-$CdSeO_3$ according to the following sequential transformations (Fig. 4.3): (1) incorporation of Br^- anions into the cavities in the β-$CdSeO_3$ framewok; (2) replacement of the part of Cd^{2+} cations in the β-$CdSeO_3$ framework by Cu^{2+} Jahn-Teller cations; (3) lowering of the symmetry to triclinic and strong distortion of cadmium coordination to reduce the stress induced by the insertion of Br^- anions and Cu^{2+} cations. The diversity of the Cd^{2+} coordination environments in $Cd_7Cu_2(SeO_3)_8Br_2$ is striking. There exist two coordinations, namely $Cd1O_8$ and $Cd4O_7$, which bear a resemblance to the structure of β-$CdSeO_3$, and a more symmetric counterpart, namely $Cd3O_6$, similar to those in the structure of orthorhombic α-$CdSeO_3$.

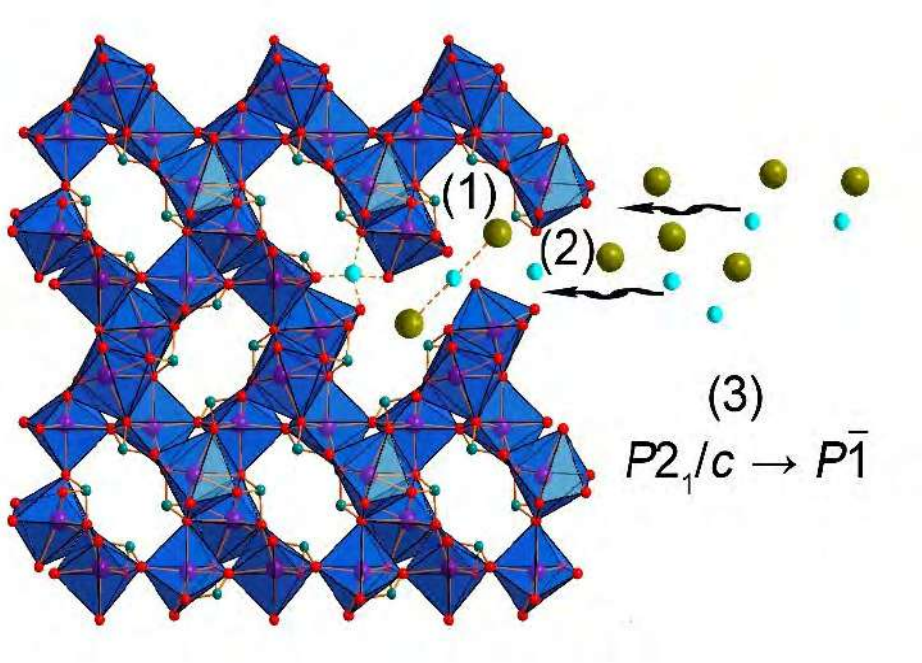

Fig. 4.3. Proposed scheme of the transformation from the ideal β-$CdSeO_3$ structure (CdO_7 = blue, SeO_3 = green) into $Cd_7Cu_2(SeO_3)_8Br_2$ via the following sequential transformations: (1) incorporation of Br atoms into the cavities in β-$CdSeO_3$; (2) replacement of the part of Cd^{2+} cations in the β-$CdSeO_3$ framework by the Cu^{2+} Jahn-Teller cations; (3) lowering of the symmetry to triclinic and strong distortion of cadmium coordination to reduce the stress induced by the insertion of Br^- anions and Cu^{2+} cations.

The structure of $Cd_7Cu_2(SeO_3)_8Br_2$ can be described as a host-guest architecture. The host is the cadmium-selenite interrupted framework, which consists of zigzag layers with a large aperture. The guests are divalent copper cations and $CuBr_2$ complexes. Thus, the formula can be written as $[Cd_7(SeO_3)_8]\{Cu_2Br_2\}$. Host-guest structures are characteristic of compounds crystallizing via CVT reactions (Siidra *et* al., 2018, 2023) and minerals formed from a gas in volcanic fumaroles (Siidra *et* al., 2018).

To date, just two cadmium-copper selenite halides are known: $CdCu_2(SeO_3)_2Cl_2$ (Murtazoev *et* al., 2021) and $Cd_7Cu_2(SeO_3)_8Br_2$ (this work). The cadmium atoms with an irregular and flexible environment in combination with SeO_3 groups results in the formation of large cavities and the inclusion of the guest Cu-Br complexes in $Cd_7Cu_2(SeO_3)_8Br_2$. Cadmium forms a CdO_2Cl_4 octahedron surrounded by eight copper-centered polyhedra in a perovskite-like fashion in $CdCu_2(SeO_3)_2Cl_2$ (Murtazoev *et* al., 2021). Both structures belong to the $xMSeO_3 \cdot yMX_2$ series. To date, the most common *x*:*y* ratios are 1:1, 2:1, and 4:1; the 8:1 ratio is observed for the first time. Further studies and CVT synthesis of cadmium selenite halides will significantly expand Cd(II) structural chemistry. The substitution of a Cd^{2+} cation with a magnetically active metal cation, such as Co^{2+}, can lead to the formation of compounds with unusual magnetic properties.

4.2. A new bismuth selenite chloride, $Bi_5(Se_2O_5)(SeO_3)_5Cl_3$

4.2.1. Synthesis

As already noted before, the combinations lone-pair cations and halogens can result in new low-dimensional and porous structures. The previous chapters described copper and lead compounds; in addition to those, the the lone pair of Bi^{3+} also commonly exhibits stereochemical activity. The introduction of magnetic cations in this case can lead to the formation of magnetic substructures with non-trivial architectures (Becker *et* al., 2007, Berdonosov *et* al., 2018). A variety of members of this group were found as minerals (Krivovichev *et* al., 2013, Kovrugin *et* al., 2015b, 2016a,b), and synthetic approaches to these analogs are relatively simple. Variations of synthesic protocols permit to achieve different structural motifs, including layered and pseudo-layered for solution methods and "host-guest-type" structures for compounds obtained via vapor transport. However, these compounds have been studied very selectively. In particular, compounds containing Cu^{2+} in combination with non-transition metal cations such as those of alkaline earth, bismuth or lead have been studied in relative detail (Siidra *et* al., 2018). To date, the structure of the mineral francisite $BiCu_3(SeO_3)_2O_2Cl$ (Pring *et* al., 1990), as well as a few bismuth selenite chlorides (Berdonosov *et* al., 2000, Ibragimov *et* al., 2002).

Crystals of the new compound were obtained by reactions of chemical vapor transport in the interaction of cesium hexachloroselenate Cs_2SeCl_6 and bismuth selenite $Bi_2(SeO_3)_3$ in sealed quartz ampoules. The starting reagents were mixed in molar ratio of 1:1, placed in a long quartz ampoule, which was evacuated to the residual pressure of ~ 50 Pa, placed in a programmable electric furnace so that the cold end protruded 2-3 cm out, and annealed at 400 °C for several days. A handful of colorless crystals was found in the cold end.

4.2.2. Single crystal X-ray experiment

The single crystal X-ray analysis was performed on the single-crystal diffractometer Rigaku XtaLAB Synergy-S, equipped with a PhotonJet-S detector. The data were collected with a frame width of 0.5° and an exposure time of 10 seconds per frame. The crystallographic data and refinement parameters are shown in Table 4.4.

Table 4.4. Crystallographic data and refinement parameters for $Bi_5(Se_2O_5)(SeO_3)_5Cl_3$

Crystal system	Monoclinic
Space group	$P2_1/c$
a (Å)	12.4229(3)
b (Å)	8.1467(2)
c (Å)	23.7991(6)
β (°)	103.827(1)
V (Å^3)	2338.81(10)
Radiation(Å)	Mo$K\alpha$, 0.71073
Total reflection number	19823
Unique reflection number $F > 4\sigma(F)$	5613
R_1	0.074
wR_2	0.199
Gof on F^2	1.04

Table 4.5. Selected interatomic distances (Å) in the structure of $Bi_5(Se_2O_5)(SeO_3)_5Cl_3$

Bi1—O17	2.236 (13)	Bi5—O1	2.240 (13)
Bi1—O11	2.364 (12)	Bi5—O18^{vi}	2.361 (14)
Bi1—O12	2.447 (12)	Bi5—O15^{xi}	2.379 (14)
Bi1—O20^{i}	2.492 (12)	Bi5—O16^{vi}	2.505 (14)
Bi1—O4^{ii}	2.517 (12)	Bi5—O5	2.631 (13)
Bi1—O8	2.695 (14)	Bi5—O13	2.703 (13)
Bi1—Cl2	2.822 (5)	Bi5—O15	2.761 (14)
Bi1—Cl1	2.840 (5)	Bi5—Cl3	2.769 (5)
Bi2—O8^{ii}	2.268 (14)	Se1—O7	1.681 (12)
Bi2—O9	2.300 (14)	Se1—O10	1.702 (13)
Bi2—O4^{ii}	2.454 (13)	Se1—O14	1.797 (13)
Bi2—O19^{iii}	2.455 (14)	Se2—O3	1.666 (14)
Bi2—O2^{iv}	2.495 (13)	Se2—O13	1.711 (12)
Bi2—O12	2.602 (12)	Se2—O5	1.727 (14)

Bi2—O18	2.637 (14)	Se2—Cl3	3.376 (5)
Bi2—Cl3^{iv}	2.979 (5)	Se3—O20	1.632 (14)
		Se3—O19	1.704 (14)
Bi3—O11	2.252 (12)	Se3—O14	1.840 (13)
Bi3—O5	2.323 (13)	Se3—Cl2	3.266 (5)
Bi3—O7	2.333 (13)	Se3—Cl1^{i}	3.560 (5)
Bi3—O3	2.377 (14)	Se4—O1	1.695 (12)
Bi3—O16^{vi}	2.426 (12)	Se4—O12	1.698 (12)
Bi3—Cl2	3.093 (5)	Se4—O11	1.759 (12)
Bi3—Cl1^{i}	3.130 (5)	Se4—Cl3^{iv}	3.051 (5)
Bi3—Cl2^{i}	3.331 (5)	Se5—O9	1.666 (13)
		Se5—O4	1.707 (13)
Bi4—O13^{vii}	2.237 (13)	Se5—O8	1.728 (13)
Bi4—O6	2.259 (14)	Se5—Cl1^{xii}	3.592 (5)
Bi4—O2^{vii}	2.460 (13)	Se6—O17	1.675 (13)
Bi4—O10	2.486 (13)	Se6—O16	1.719 (14)
Bi4—O3^{viii}	2.559 (13)	Se6—O18	1.727 (13)
Bi4—O19^{ix}	2.592 (13)	Se7—O15^{vii}	1.675 (15)
Bi4—O10^{ix}	2.649 (13)	Se7—O2^{vii}	1.712 (13)
Bi4—Cl1^{x}	3.057 (5)	Se7—O6	1.731 (14)
Bi4—O14^{ix}	3.083 (14)	Se7—Cl3	3.329 (5)

4.2.3. Crystal structure of $Bi_5(Se_2O_5)(SeO_3)_5Cl_3$

The crystal structure of $Bi_5(Se_2O_5)(SeO_3)_5Cl_3$ contains five crystallographically independent bismuth, seven selenium and three chlorine positions (Fig. 4.4). All bismuth atoms reside in asymmetric environment of oxygen and chlorine atoms. Bi1 is surrounded by six oxygen atoms at 2.236 – 2.695 Å and two chlorine atoms at nearly equal distances of *ca.* 2.8 Å. The coordination of the Bi2 atom consists of seven oxygen atoms at 2.299 – 2.637 Å and one chlorine atom at 2.979 Å. Bi3 has a coordination sphere of four oxygen at 2.252 – 2.426 Å and three chlorine atoms at 3.093 – 3.331 Å. Bi4 is coordinated by eight oxygen atoms at 2.237 – 3.082 Å and one chlorine atom at 3.057 Å. Bi5 is surrounded by seven oxygen atoms at 2.240 – 2.761 Å and one chlorine atom at 2.769 Å from the central atom. In all cases, the oxygen atoms are located in one half of the cation environment, while halogen atoms, in the other.

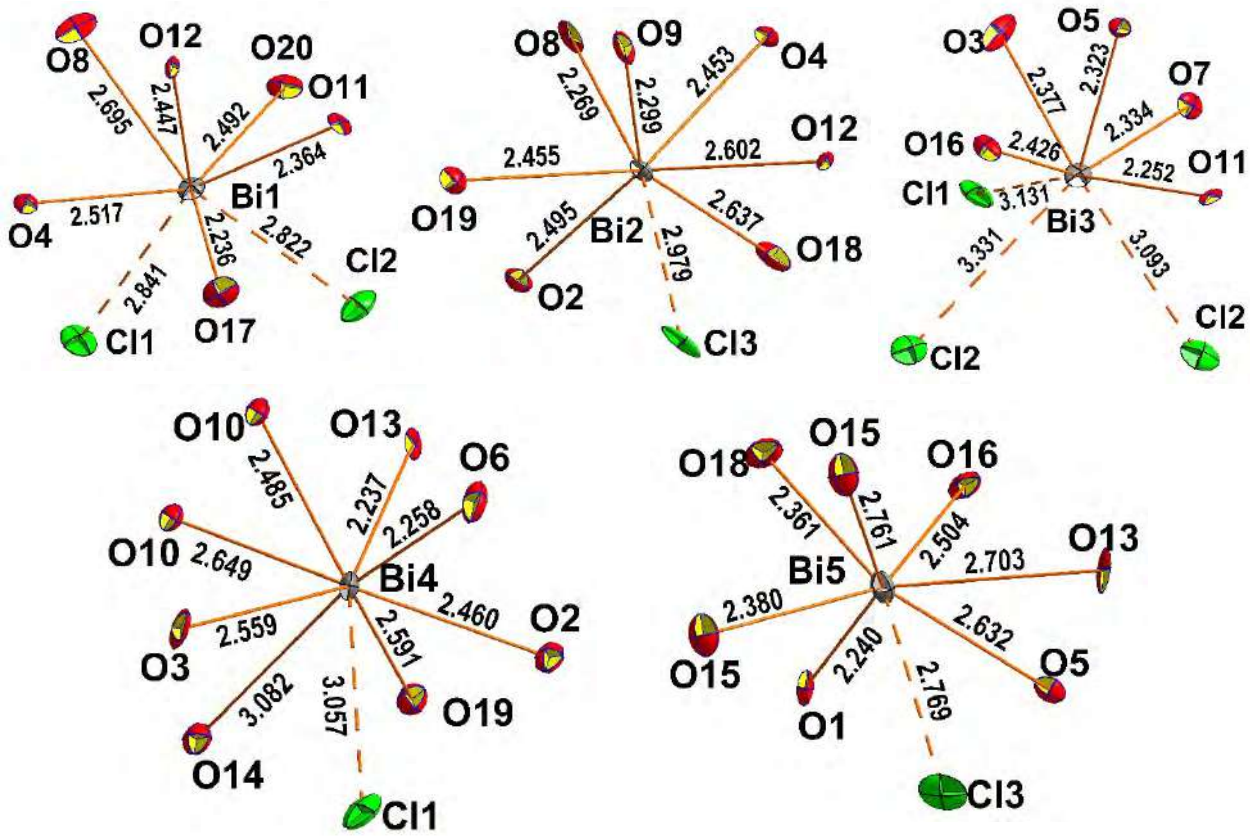

Fig. 4.4. Coordination of atoms Bi in the structure of $Bi_5(Se_2O_5)(SeO_3)_5Cl_3$

There are two kinds of Se^{IV}-based anoins: SeO_3^{2-} and $Se_2O_5^{2-}$ (Fig. 4.5), the latter comprising Se1 and Se3. In addition to oxygen at the common distances of 1.6 – 1.8 Å, these atoms are coordinated to chloride anions, illustrating the halophilicity of the lone pairs of selenium. This fact is proved by calculations of BVS (Table 6 in Appendix) and data from the work Krivovichev & Gorelova, 2018. All selenium atoms except Se1 and Se4 additionally include chlorine at 3 – 3,6 Å. These weak bonds are located at the side of the lone pair and do not affect the formation of an umbrella-line ψ-tetrahedron SeO_3E.

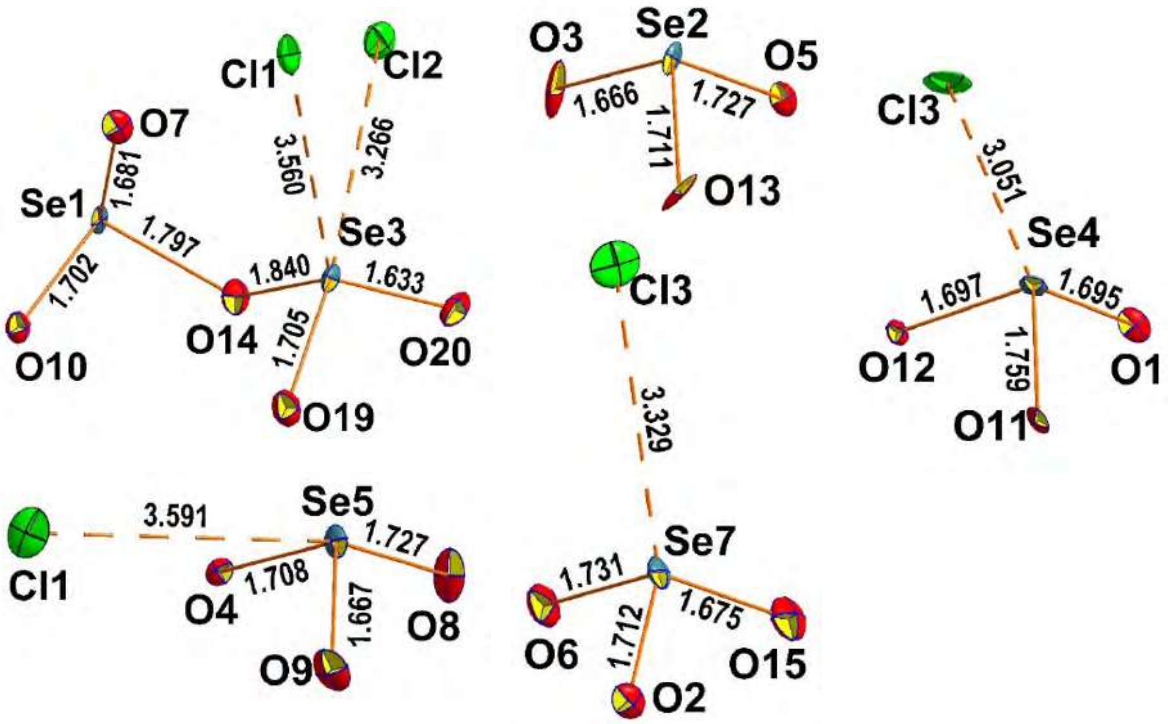

Fig. 4.5. Coordination of atoms Se in the structure of $Bi_5(Se_2O_5)(SeO_3)_5Cl_3$

The selenite groups and bismuth cations form layers (Fig. 4.6) containing voids hosting lone pairs of Se^{IV} and Bi^{III}. Groups $Se4O_3Cl$, $Se5O_3Cl$ and $Se7O_3Cl$ are "surface" at the boundary between the bismuth-selenite layer and the halogen-filled interlayer space. The $Se2O_3$ group occupies an "inner" position in the layer. The diselenite group «$Se1O_3Se3O_2Cl_2$» in this case performs a double role: while Se1 is entirely inside the layer and coordinates only the bismuth cations, Se3 resides in the interlayer space and coordinates two chlorine atoms acting as a bridge between the layers like a tetrahedron CuO_4X_2, (X = Cl, Br) in the structure of synthetic mixed chloride-bromide analogue of sarrabusite mineral (Siidra *et* al., 2023), connecting the structure into a framework (Fig. 4.7).

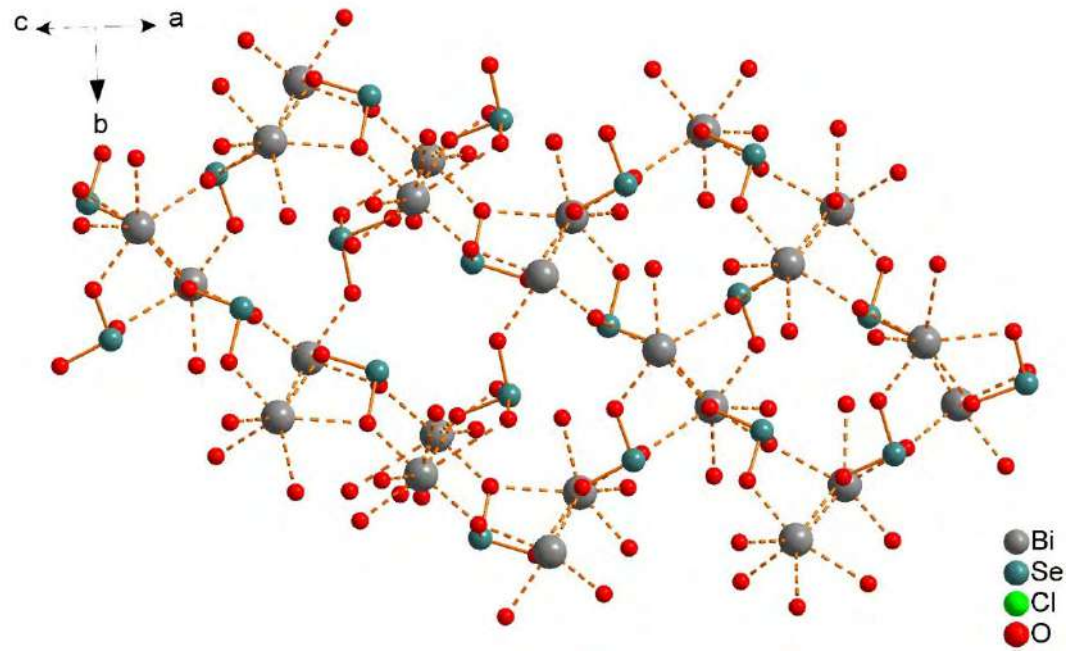

Fig. 4.6. The $[Bi_5(Se_2O_5)(SeO_3)_5]^{3+}$ layer in the structure of $Bi_5(Se_2O_5)(SeO_3)_5Cl_3$.

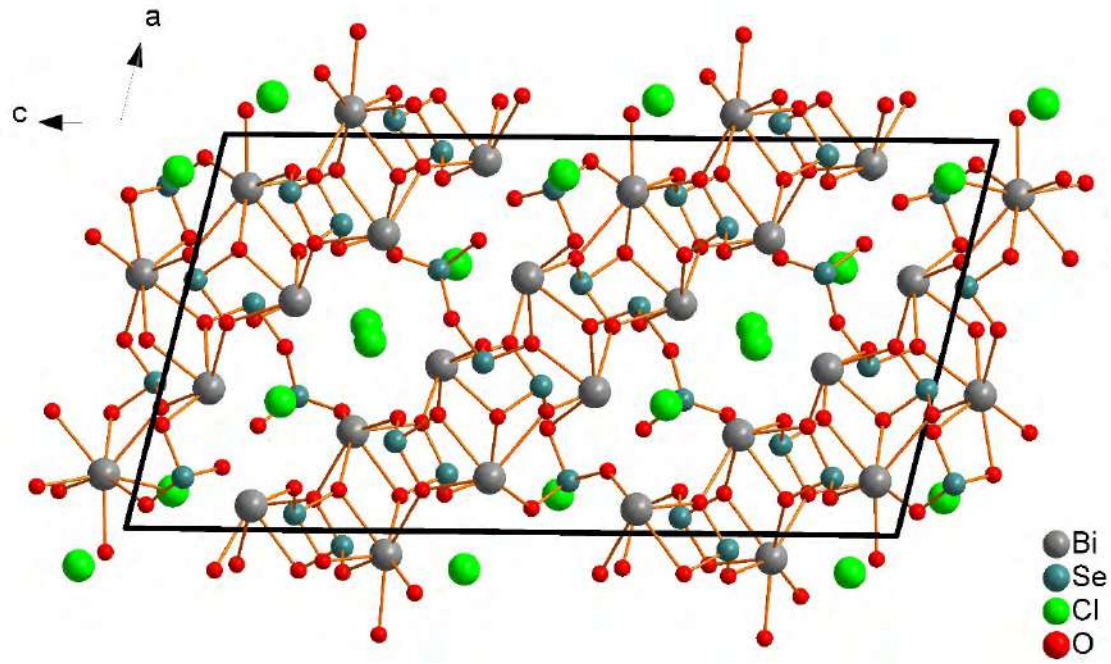

Fig. 4.7. General projection of the $Bi_5(Se_2O_5)(SeO_3)_5Cl_3$ structure

4.3. Crystal chemistry of new compounds in Pb-Cu-SeO_3-Cl/Br system

4.3.1. Sinthesis of new compounds

Until recently, copper-lead selenite bromides, which merge the properties of lone-pairs of selenium in combination with halogen, copper, which forms octahedral complexes with sreong Jahn-Teller distortion, as well as variable stereochemical activity of lead, described in previous chapters, were sparsely studied. In (Siidra *et* al., 2018) the number of its members was increased essentially by synthesis of new compounds in vacuum-sealed quartz ampules by means of chemical vapor transport reaction. Nine new compounds were described, most of which represented new structure types. Several copper-lead selenite chloride minerals are known from the fumaroles of Tolbachik volcano: prewittite, $KPb_{1.5}Cu_6Zn(SeO_3)_2O_2Cl_{10}$ (Shuvalov *et* al., 2013) and allochalcoselite, $Cu^{+}Cu^{2+}{}_5PbO_2(SeO_3)_2Cl_5$ (Krivovichev *et* al., 2005). Sarrabusite, $Pb_5Cu(SeO_3)_4Cl_4$ was described from an oxidation zone of the lead and arsenic mine at Baccu Locci, Sardinia, Italy (Campostrini *et* al., 1999). Selenite-bromides of lead and copper are not known in nature. In terrestrial rocks, Br minerals are extremely rare and only nine minerals known where Br is a dominant component (Karpenko *et* al., 2022). However, several bromides have recently been described from volcanic fumaroles (demicheleite-Br, BiSBr: Demartin *et* al., 2008) and natural coal fires (ermakovite, $(NH_4)(As_2O_3)_2Br$: Karpenko *et* al., 2022).

The interest in detailed study of copper selenites stems from the intriguing magnetic properties found for a number of representatives of this family (e.g. Zhang *et* al., 2010, Berdonosov *et* al., 2018, Badrtdinov *et* al., 2018). However, obtaining the single-phase polycrystalline samples of complex copper selenites remains a challenge.

Prof. Dr. Josef Zemann and his group at the University of Vienna made an outstanding contribution to the crystal chemistry of copper oxides and oxysalts, including selenites and especially tellurites. A large number of his works were devoted to the crystal chemistry of compounds with ‘lone-pair’ cations and features of their structural architectures. Three new copper-lead selenite bromides synthesized by the CVT method, and described herein in the special issue dedicated to Josef Zemann, further contribute to this field. In one of the compounds, a new type of Cu(II) mixed-ligand coordination was revealed. All three new compounds demonstrate the use of ‘lone-pair’ cations as ‘chemical scissors’ and the segregation of the structure into regions with different types of chemical bonding.

Syntheses were performed according to the protocols published in Siidra *et* al., 2018. The starting materials used in this study were $PbSeO_3$, CuBr, $CuBr_2$ and $CuCl_2$ (all from Vekton, analytical or extra pure grade, purity ≥ 99.5%). For the synthesis of $Pb_5Cu^{+}{}_4(SeO_3)_4Br_6$, $PbSeO_3$ and CuBr were mixed in

a 1:1 molar ratio and thoroughly ground and placed in thin-walled silica ampoules (inner diameter 5 mm, length 150 mm), sealed under vacuum, and placed in a furnace. The furnace was heated to and held at 400 °C for two weeks, after which it was switched off to reach an ambient temperature. The temperature gradient between the hot and cold ends of the tube was ~ 50 °C. Two other new compounds were synthesized in similar fashion. For the synthesis of $Pb_8Cu^{2+}(SeO_3)_4Br_{10}$, a ratio of $PbSeO_3$:$CuBr_2$ 2:1 was used, and for the synthesis of $Pb_5Cu^{2+}(SeO_3)_4(Br,Cl)_4$, a ratio of $PbSeO_3$, $CuBr_2$ and $CuCl_2$ 2:1:1.

Crystals of the new compounds were found in the cold zones of the tubes. Crystals of $Pb_5Cu^{+}_4(SeO_3)_4Br_6$ are light-brown, whereas crystals of $Pb_8Cu^{2+}(SeO_3)_4Br_{10}$ and $Pb_5Cu^{2+}(SeO_3)_4(Br,Cl)_4$ are green. Many other differently coloured crystals, including those reported in Siidra *et* al., 2018, were found in the different zones of the tubes. Most of them were grown in overlapping areas and in close proximity to each other; neither their colour nor their habit made it possible to distinguish clearly between the different species. Because of this, studies other than crystallographic ones have not been performed.

Qualitative electron microprobe analysis (Hitachi TM3000) revealed no other elements in all studied compounds, except the Cu, Br, Se, Pb, and Cl (in $Pb_5Cu^{2+}(SeO_3)_4(Br,Cl)_4$ only) with an atomic number greater than 11 (Na).

4.3.2. Single crystal X-ray experiment

Single crystals of all compounds were selected under the microscope and mounted on thin glass fibers for X-ray diffraction analysis using Bruker APEX II DUO X-ray diffractometer with a micro-focus X-ray tube operated with MoKα radiation at 50 kV and 0.6 mA. The data were integrated and corrected for absorption using a multi scan type model using the Bruker programs *APEX* and *SADABS*. More than a hemisphere of X-ray diffraction data was collected for each crystal. The structure refinements were performed using SHELXL software. Occupancies of partially occupied Cu sites in $Pb_5Cu^{+}_4(SeO_3)_4Br_6$ were first refined and later fixed in the final stages of the crystal structure refinement constrained to keep the electroneutrality of the formula. Crystallographic information for the new compounds is summarized in Table 4.6. Selected interatomic distances are given in Tables 4.7-4.9 and atomic coordinates, displacement parameters and valence-sums are provided in Tables 7-9 in Appendix.

Bond valence analysis was done using bond-valence parameters taken from Gagné and Hawthorne (2015) for the Pb^{2+}-O, Se^{4+}-O, and Cu^{2+}-O bonds, from Brese and O'Keeffe (1991) for the Cu^{2+}-Cl, Cu^{2+}-Br, Pb^{2+}-Cl, Se^{4+}-Cl, and Se^{4+}-Br bonds and from Hu (2007) for the Pb^{2+}-Br bonds. Bond valences were not calculated for Cu^{+}-Br bonds in the crystal structure of $Pb_5Cu^{+}_4(SeO_3)_4Br_6$ due to the

disorder of Cu^{+} cations. All of the Pb-O and Pb-*X* bonds ≤ 3.55 Å, Se-O bonds ≤ 2.00 Å, Se-*X* bonds ≤ 3.75 Å, Cu^{2+}-O and Cu^{2+}-*X* ≤ 3.00 Å were taken into account.

Table 4.6. Crystallographic data and refinement parameters for $Pb_5Cu^{+}_4(SeO_3)_4Br_6$, $Pb_8Cu^{2+}(SeO_3)_4Br_{10}$ and $Pb_5Cu^{2+}(SeO_3)_4(Br,Cl)_4$.

	$Pb_5Cu^{+}_4(SeO_3)_4Br_6$	$Pb_8Cu^{2+}(SeO_3)_4Br_{10}$	$Pb_5Cu^{2+}(SeO_3)_4(Br,Cl)_4$
Crystal system	monoclinic	orthorhombic	monoclinic
Space group	*C*2/*m*	*I*222	*C*2/*c*
a (Å)	17.7248(14)	9.5893(5)	24.590(6)
b (Å)	5.5484(5)	12.4484(9)	5.5786(14)
c (Å)	12.7010(10)	12.7927(6)	14.248(4)
β (°)	103.398(2)		102.883(7)
V ($Å^3$)	1215.08(17)	1527.08(15)	1905.3(9)
Radiation (Å)	Mo*K*α, 0.71073	Mo*K*α, 0.71073	Mo*K*α, 0.71073
Total reflections number	3911	7859	9259
Unique reflections number	1448	1808	1976
$F > 4\sigma(F)$			
R_1	0.024	0.027	0.026
wR_2	0.055	0.065	0.063
Gof on F^2	1.079	1.078	1.074

Table 4.7. Selected interatomic distances ((in Å) in crystal structure of $Pb_5Cu^{+}_4(SeO_3)_4Br_6$

Pb1-O4	2.481(4) ×2	Cu2A…Cu2B	0.32(3)
Pb1-O2	2.532(5) ×2	Cu2A-Br1	2.416(11)
Pb1-Br2	3.3023(6) ×2	Cu2A-Br2	2.498(9)
Pb1-Br3	3.3954(10)	Cu2A-Br3	2.505(12)
Pb1-Br1	3.4085(11)	Cu2A-Br2	2.652(11)
		Cu2B-Br3	2.401(15)
Pb2-O1	2.433(7)	Cu2B-Br2	2.458(14)
Pb2-O2	2.663(4) ×2	Cu2B-Br1	2.479(18)
Pb2-O4	2.710(4) ×2	Cu2B-Br2	2.751(16)

Pb2-O4	2.721(4) ×2		
Pb2-O3	2.897(2) ×2	Se1-O1	1.656(7)
		Se1-O2	1.717(5) ×2
Pb3-O3	2.557(6) ×2	Se1-Br2	3.5199(12)
Pb3-O2	2.666(5) ×4	Se1-Br3	3.6063(8) ×2
Pb3-O1	3.212(4) ×4		
		Se2-O3	1.699(7)
Cu1A…Cu1B	0.390(12)	Se2-O4	1.707(5) ×2
Cu1A-Br3	2.414(6) ×2	Se2-Br2	3.6493(13)
Cu1A-Br1	2.615(7) ×2	Se2-Br1	3.7477(9) ×2
Cu1B-Br1	2.322(7)		
Cu1B-Br1	2.623(5)		
Cu1B-Br3	2.414(6)		
Cu1B-Br3	2.731(7)		

Таõle 4.8. Selected interatomic distances (in Å) in crystal structure of $Pb_8Cu^{2+}(SeO_3)_4Br_{10}$.

Pb1-O2	2.422(10) ×2	Cu-O1	1.990(9) ×4
Pb1-Br1	3.1001(15) ×2	Cu-O2	2.967(11) ×4
Pb1-Br3	3.2906(16) ×2		
Pb1-Br3	3.4631(16) ×2	Se-O2	1.702(11)
		Se-O1	1.720(9)
Pb2-O3	2.562(10)	Se-O3	1.723(10)
Pb2-O2	2.573(11)	Se-Br1	3.2264(19)
Pb2-O3	2.608(10)	Se-Br1	3.3730(18)
Pb2-O3	2.641(10)	Se-Br3	3.449(2)
Pb2-O1	2.730(9)		
Pb2-Br3	3.2830(17)		
Pb2-Br1	3.3442(15)		
Pb2-Br2	3.3537(16)		
Pb2-Br1	3.4172(15)		
Pb3-O1	2.890(10) ×2		
Pb3-Br3	3.0231(14) ×2		
Pb3-Br2	3.0951(14) ×2		
Pb3-Br1	3.1587(14) ×2		

Table 4.9. Selected interatomic distances (in Å) in crystal structures of $Pb_5Cu^{2+}(SeO_3)_4(Br,Cl)_4$ and sarrabusite, $Pb_5Cu(SeO_3)_4Cl_4$ (Gemmi *et* al. 2012).

	$Pb_5Cu^{2+}(SeO_3)_4(Br,Cl)_4$ this study	Sarrabusite $Pb_5Cu(SeO_3)_4Cl_4$ Gemmi M. et al. 2012 Manual refined model	Sarrabusite $Pb_5Cu(SeO_3)_4Cl_4$ Gemmi M. et al. 2012 Automated refined model
Pb1-O2	2.413(6)	2.47(5)	2.50(3)
Pb1-O6	2.441(6)	2.32(4)	2.38(3)
Pb1-O4	2.635(6)	2.96(4)	2.89(3)
Pb1-O3	2.732(6)	2.54(3)	2.54(3)
Pb1-O1	2.733(6)	2.77(4)	2.79(3)
Pb1-O5	2.891(6)	2.67(4)	2.85(3)
Pb1-*X*2	3.2424(17)	3.16(3)	3.122(19)
Pb1-*X*1	3.5321(12)	3.36(4)	3.42(3)
Pb2-O3	2.405(6)	2.48(4)	2.45(3)
Pb2-O3	2.662(6)	3.04(5)	2.75(3)
Pb2-O1	2.686(6)	2.48(4)	2.45(3)
Pb2-O1	2.766(6)	3.04(5)	2.75(3)
Pb2-*X*1	3.1396(12)	2.91(3)	2.980(17)
Pb2-*X*1	3.1591(12)	3.21(4)	3.14(2)
Pb2-*X*2	3.1961(18)	2.82(3)	3.27(2)
Pb2-*X*1	3.2280(12)	3.14(3)	3.134(17)
Pb3-O6	2.526(5) ×2	2.67(4)	2.52(3)
Pb3-O4	2.532(6) ×2	2.48(5)	2.49(3)
Pb3-O5	2.652(6) ×2	2.69(5)	2.69(3)
Pb3-O2	2.690(6) ×2	2.62(4)	2.52(3)
Cu-O5	1.952(5) ×2	2.16(4)	2.03(3)
Cu-O4	2.370(6) ×2	2.17(5)	2.17(3)
Cu-*X*2	2.4376(17) ×2	2.94(3)	2.48(2)
Se1-O6	1.686(5)	1.69(4)	1.74(3)

Se1-O1	1.706(6)	1.61(5)	1.68(3)
Se1-O3	1.741(6)	1.74(4)	1.80(3)
Se1-*X*1	3.4818(15)	-	-
Se1-*X*2	3.6323(19)	-	-
Se2-O2	1.681(6)	1.70(6)	1.82(3)
Se2-O4	1.709(6)	1.75(4)	1.71(3)
Se2-O5	1.735(5)	1.89(4)	1.88(3)
Se2-*X*2	3.2992(18)	-	-
Se2-*X*2	3.5361(18)	-	-

*X*1 = $Br_{0.823(8)}Cl_{0.177(8)}$; *X*2 = $Br_{0.281(7)}Cl_{0.719(7)}$.

4.3.3. Crystal structures of new compounds

The crystal structure of $Pb_5Cu^+_4(SeO_3)_4Br_6$ contains three symmetrically unique Pb and two Se sites. In order to determine the coordination of Pb^{2+} cations, all bonds below 3.5 Å were taken into account. An environment of the Pb^{2+} cation is variable (Fig. 4.8). Pb1 atom is coordinated by the four O and four Br atoms thus forming a distorted PbO_4Br_4 square antiprism. This type of coordination is typical for Pb^{2+} cations in Pb oxyhalides and is usually explained in terms of stereoactive behaviour of the $6s^2$ lone electron pair. Pb2 and Pb3 atoms are coordinated exclusively by oxygen atoms. The Pb2 is coordinated by nine O atoms in a modestly one-sided fashion. The Pb3 atom forms an irregular PbO_{10} polyhedron.

Each of two symmetrically independent Se^{4+} cations forms three nearly equal Se^{4+}-O bonds (Table 4.7) in the range 1.656(7) – 1.717(5) Å. This one-sided pyramidal configuration is typical for $Se(IV)O_3$ groups.

Two Cu sites were refined each as a split atom model, thus being disordered over several neighbouring positions with very short Cu··Cu distances and low occupancies indicated in Table 7 in Appendix. The Cu^+ cations are located in Cu1 and Cu2 sites. Each environment can be described as a distorted Cu^+Br_4 tetrahedron, the individual values of the Cu^+-Br distances are somewhat longer compared to those in CuBr (<Cu^+-Br> = 2.46 Å) (Vegard & Skofteland, 1942) due to the disorder. The latter is a typical feature of Cu^+ ion in oxyhalides obtained by the CVT.

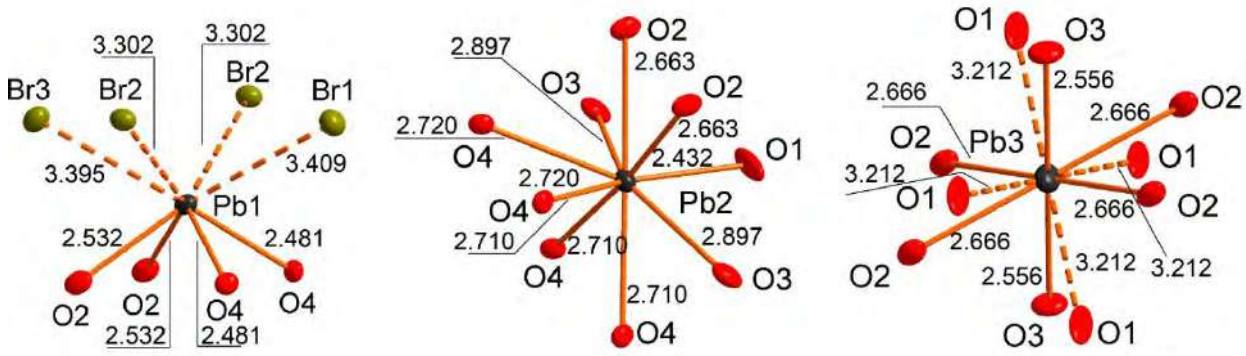

Fig. 4.8 Coodination environment of cations Pb^{2+} and Cu^{+} in $Pb_5Cu^{+}_4(SeO_3)_4Br_6$

The new compound $Pb_5Cu^{+}_4(SeO_3)_4Br_6$ belongs to a new structure type. The crystal structure consists of two distinct parts: corner- and edge-sharing $CuBr_4$ tetrahedra that form unique infinite $[Cu^{+}_4Br_6]^{2-}$ layers and $[Pb(SeO_3)_4]^{2+}$ cationic layers (Fig. 4.9). The $[Cu^{+}_4Br_6]^{2-}$ layers have a topology of [PbO] layers in litharge (α-PbO). The anionic and cationic layers, are separated one from each other by an interface composed of the lone pairs associated with both Se(IV) and Pb(II). The lone pairs act as chemical scissors for the lead selenite blocks by creating nonbonding interleafs separating them from anionic copper-bromide units. Similar examples of the segregation of structural parts of different kinds of chemical interaction have been previously reported in several lone-pair oxyhalide systems (Becker *et* al., 2003, Mayerová *et* al., 2006).

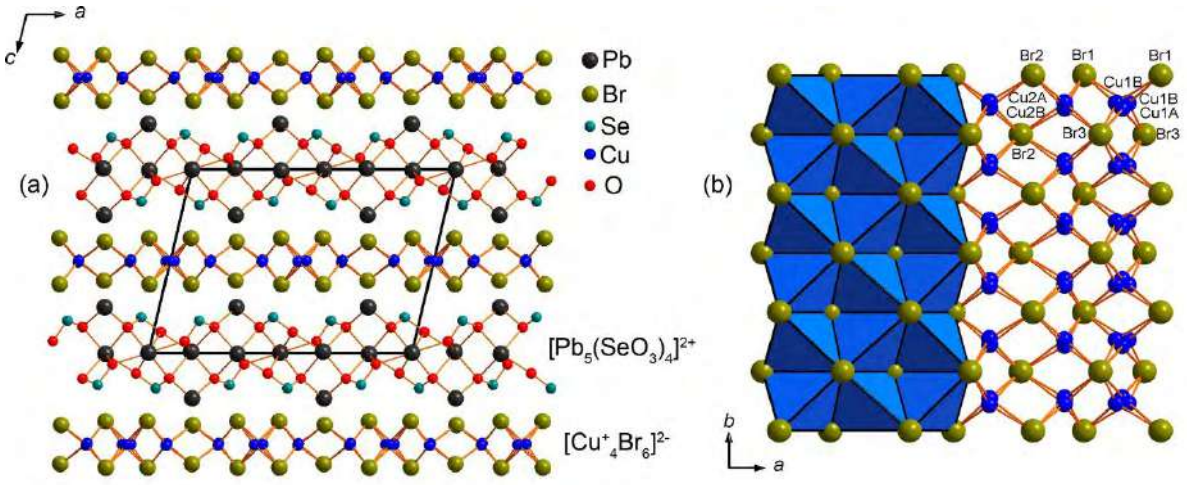

Fig. 4.9. General projection of the crystal structure of $Pb_5Cu^{+}_4(SeO_3)_4Br_6$ (a). The layer $[Cu^{+}_4Br_6]^{2-}$ in $Pb_5Cu^{+}_4(SeO_3)_4Br_6$ (b)

There are three sites occupied by Pb atoms (Table 7 in Appendix) in the crystal structure of $Pb_8Cu^{2+}(SeO_3)_4Br_{10}$. The coordination of the Pb1 atom is asymmetric with two strong Pb1-O2 bonds located in one side of the hemisphere and six Pb1-Br bonds distributed uniformly over the coordination sphere (Fig. 4.9). Pb3 atom has the same CN (coordination number) and similar geometry of coordination environments, whereas Pb2 atom has a typical for Pb^{2+} cation coordination with five

relatively short and strong Pb2-O bonds located in one coordination hemisphere and four long and weak Pb2-Br bonds in the other.

The crystal structure of $Pb_8Cu^{2+}(SeO_3)_4Br_{10}$ contains one symmetrically independent Cu atom (Fig. 4.10). All Cu^{2+}-O bonds ≤3.0 Å were taken into consideration. Cu1 atom forms four very strong Cu-O_{eq} bonds (≤ 2 Å) resulting in a CuO_4 square which is complemented by four very long Cu-O_{ap} bonds of 2.967(11) Å each. These four Cu1-O2 bonds contribute 0.12 *v.u.* to the bond-valence sum of Cu1. Taking Cu1-O2 bonds into account, the overall coordination polyhedron of Cu^{2+} can be considered as "an octahedron with two split vertices". A similar [4+4] coordination mode was observed in several copper phosphates (Anderson *et* al., 1981, Escobal *et* al., 2006, Senga & Kawahara, 1980, Yakubovich *et* al., 2008). Cu^{2+} coordination environments with CN >6 in minerals and synthetic compounds with TO_4 anions were recently reviewed in Siidra *et* al., 2021.

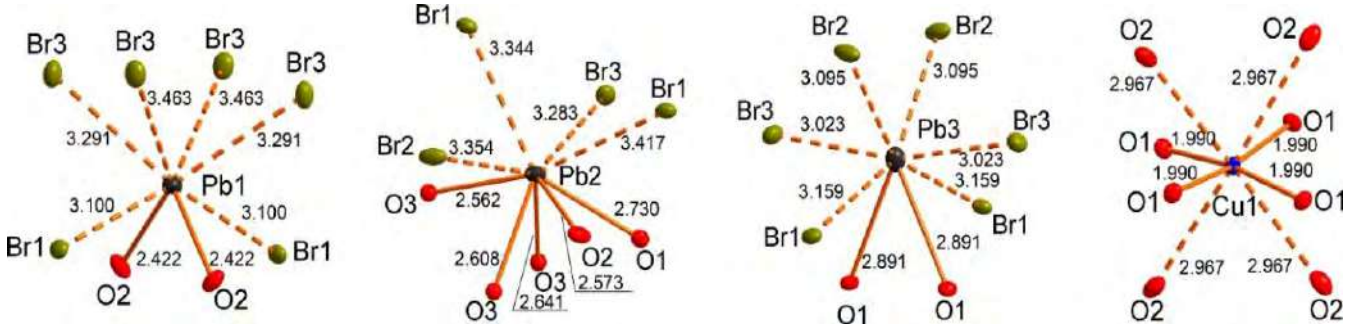

Fig. 4.10. Coordination of Pb^{2+} and Cu^{2+} in $Pb_8Cu^{2+}(SeO_3)_4Br_{10}$

There is one symmetrically independent selenium site in the crystal structure of $Pb_8Cu^{2+}(SeO_3)_4Br_{10}$. The Se^{4+} cation has a typical oxygen coordination of triangular pyramid.

Due to the variability of Pb^{2+} coordination, it is necessary to determine strongly bonded structural units in terms of bond-valence considerations. The selenite groups are isolated from each other and linked through Pb-O bonds. The crystal structure of $Pb_8Cu^{2+}(SeO_3)_4Br_{10}$ exhibits a 1*D* structure, consisting of positively charged unique $[Pb_8Cu^{2+}(SeO_3)_4]^{10+}$ rod-like chains (Fig. 4.11) with Cu^{2+} cations in the core. The chains extend along the *a* axis and they are mutually held together by the Br^- anions.

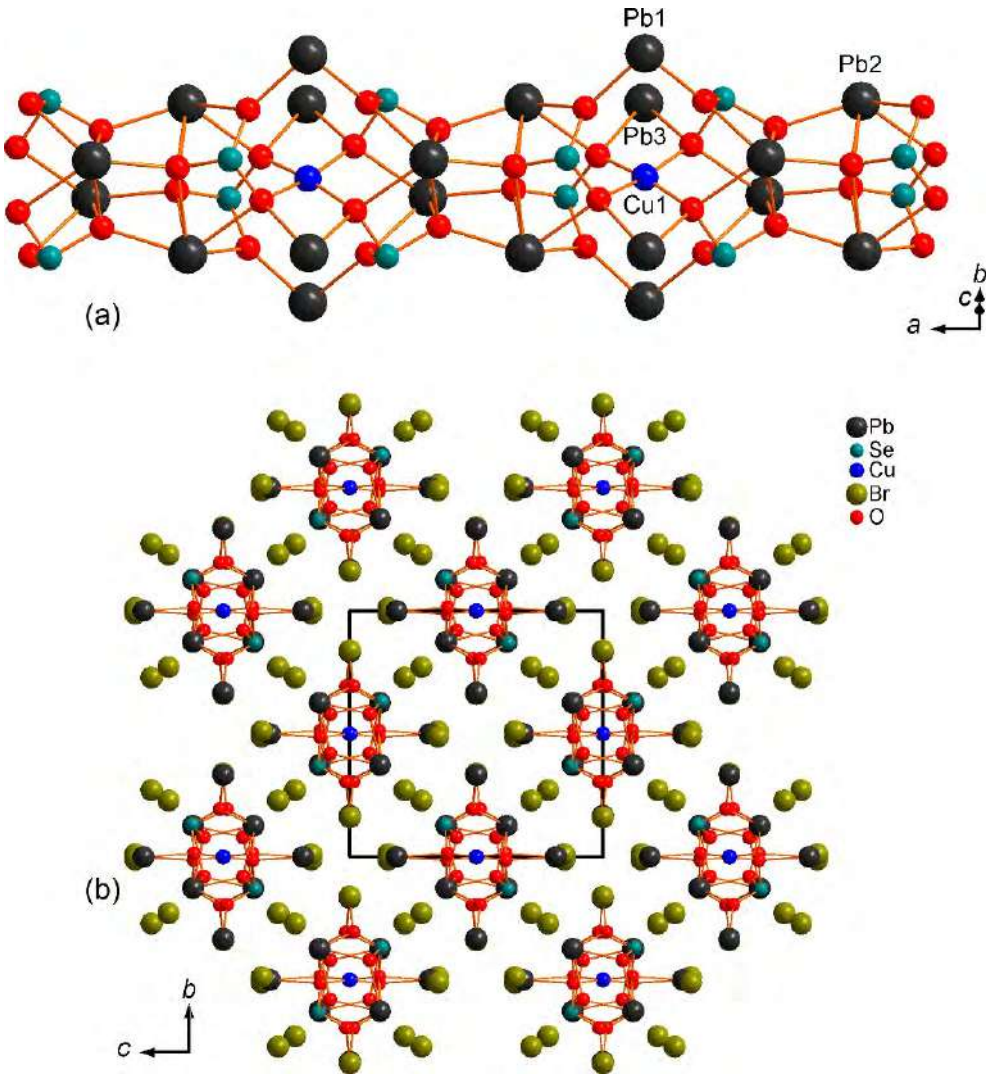

Fig. 4.11. Chain $[Pb_5Cu^{2+}_4(SeO_3)_4]^{6+}$ in $Pb_8Cu^{2+}(SeO_3)_4Br_{10}$ (a). General projection of the crystal structure of $Pb_8Cu^{2+}(SeO_3)_4Br_{10}$ (b)

The chemical formula and general crystallographic data of the new compound $Pb_5Cu^{2+}(SeO_3)_4(Br,Cl)_4$ are similar to the mineral sarrabusite $Pb_5Cu(SeO_3)_4Cl_4$ (Gemmi *et* al., 2011). The crystal structure of sarrabusite has been determined using an electron diffraction tomography technique. Some of the reported cation-anion distances calculated on the basis of the refined models (manual or automated) show significant differences depending on the model (Table 4.11). Therefore, the determination of the structure of the synthetic sarrabusite by conventional single-crystal X-ray diffraction is important for clarifying the coordination of cations and revealing features of the crystal structure. The coordinates from Gemmi *et* al., 2011, were taken as a starting model for the structure refinement.

The crystal structure of the synthetic $Pb_5Cu^{2+}(SeO_3)_4(Br,Cl)_4$ contains three symmetrically independent Pb sites occupied by Pb atoms, one Cu site occupied by Cu atoms and two Se sites (Table 7 in Appendix). The crystal structure also contains two *X* halide sites. *X*1 site is predominantly occupied

by bromine ($Br_{0.823(8)}Cl_{0.177(8)}$), whereas position *X*2 is predominantly occupied by chlorine (**(**$Br_{0.281(7)}Cl_{0.719(7)}$).

The two independent SeO_3 groups show the usual triangular pyramidal shape with Se-O bond lengths varying from 1.681(6) to 1.741(6) Å depending on their bonding to Pb and Cu. No significant elongations of the Se-O bonds like Se2-O5 = 1.89(4) Å (Table 4.8) reported by Gemmi *et* al., 2011, were found in the crystal structure of the synthetic $Pb_5Cu^{2+}(SeO_3)_4(Br,Cl)_4$.

Pb1 adopts a mixed ligand coordination of six oxygen anions in the range 2.413(6)-2.891(6) Å and two *X* anions at much longer distances 3.2424(17)-3.5321(12) Å. The Pb2 site is coordinated by four O and four *X* atoms (Fig. 4.12). The resulting PbO_4X_4 polyhedron is a square antiprism very similar in geometry to Pb1 atom in $Pb_5Cu^{+}_4(SeO_3)_4Br_6$ and to the mixed ligand coordination of Pb^{2+} cations in Pb oxyhalides in general. Pb3 atom is coordinated by eight oxygen atoms thus forming relatively symmetrical coordination environments similar to Pb2 atom in $Pb_5Cu^{+}_4(SeO_3)_4Br_6$ described above.

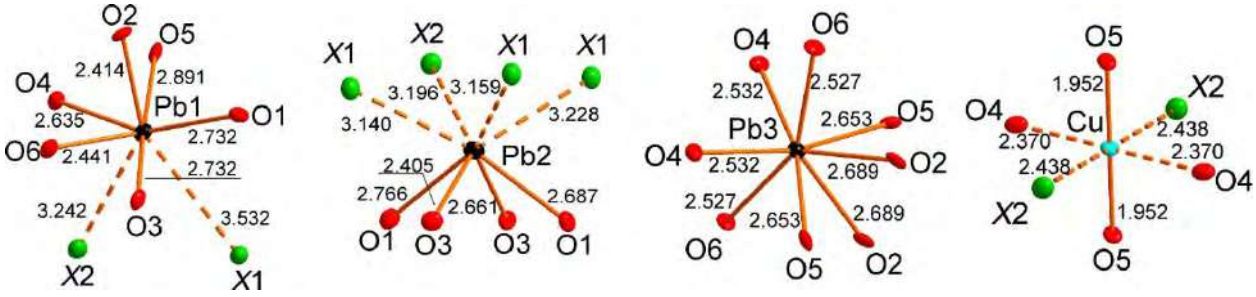

Fig. 4.12. Coordination environment of Pb^{2+} and Cu^{2+} in the structure of synthetic sarrabusite $Pb_5Cu^{2+}(SeO_3)_4(Br,Cl)_4$

The Cu^{2+} cation coordination is well-defined in $Pb_5Cu^{2+}(SeO_3)_4(Br,Cl)_4$ and differs notably from the Cu [4O+2Cl] coordination reported by Gemmi et al. (2011). All Cu-O and Cu-*X* bonds shorter than 3.2 Å are included into the Cu coordination sphere. Cu forms two strong Cu-O bonds 1.952(5) Å each with O5 atoms (Fig. 4.13). Two Cu1-O4 bonds are significantly elongated up to 2.370(6) Å each. The coordination is complemented by two Cu-*X*2 bonds of 2.4376(17) Å each. Thus, Cu has [2O+(2O+2*X*)] strongly distorted octahedral coordination. To the best of our knowledge, this type of Cu^{2+} mixed-ligand coordination has never been described in divalent copper oxyhalide synthetic compounds and minerals. However, similar in geometry [2OH+4O] octahedral coordination by O/OH is well-known e.g. for volborthite $Cu_3V_2O_7(OH)_2{\cdot}2H_2O$ (Ginga *et* al., 2021). This type of coordination in volborthite was explained by Burns & Hawthorne, 1996, by the dynamic Jahn-Teller effect.

Note, *X*1 site predominantly occupied by Br is bonded to Pb atoms only, whereas *X*2 site mostly occupied by Cl is bonded to both Pb and Cu.

Because of the large size and variability of coordination polyhedra around Pb^{2+} cations and the strength of the Pb-O and Se-O bonds in comparison to the Pb-*X* bonds, it is convenient to describe the substructure of $Pb_5Cu^{2+}(SeO_3)_4(Br,Cl)_4$ in PbO_n and SeO_3 polyhedra. The latter interconnect via common oxygen atoms into $[Pb_5(SeO_3)_4]^{2+}$ layers parallel to the *a* axis (Fig. 4.13). Cu^{2+} cations

interconnect the layers into the framework shown in Fig. 4.13. The large cavities are filled by halide *X* anions.

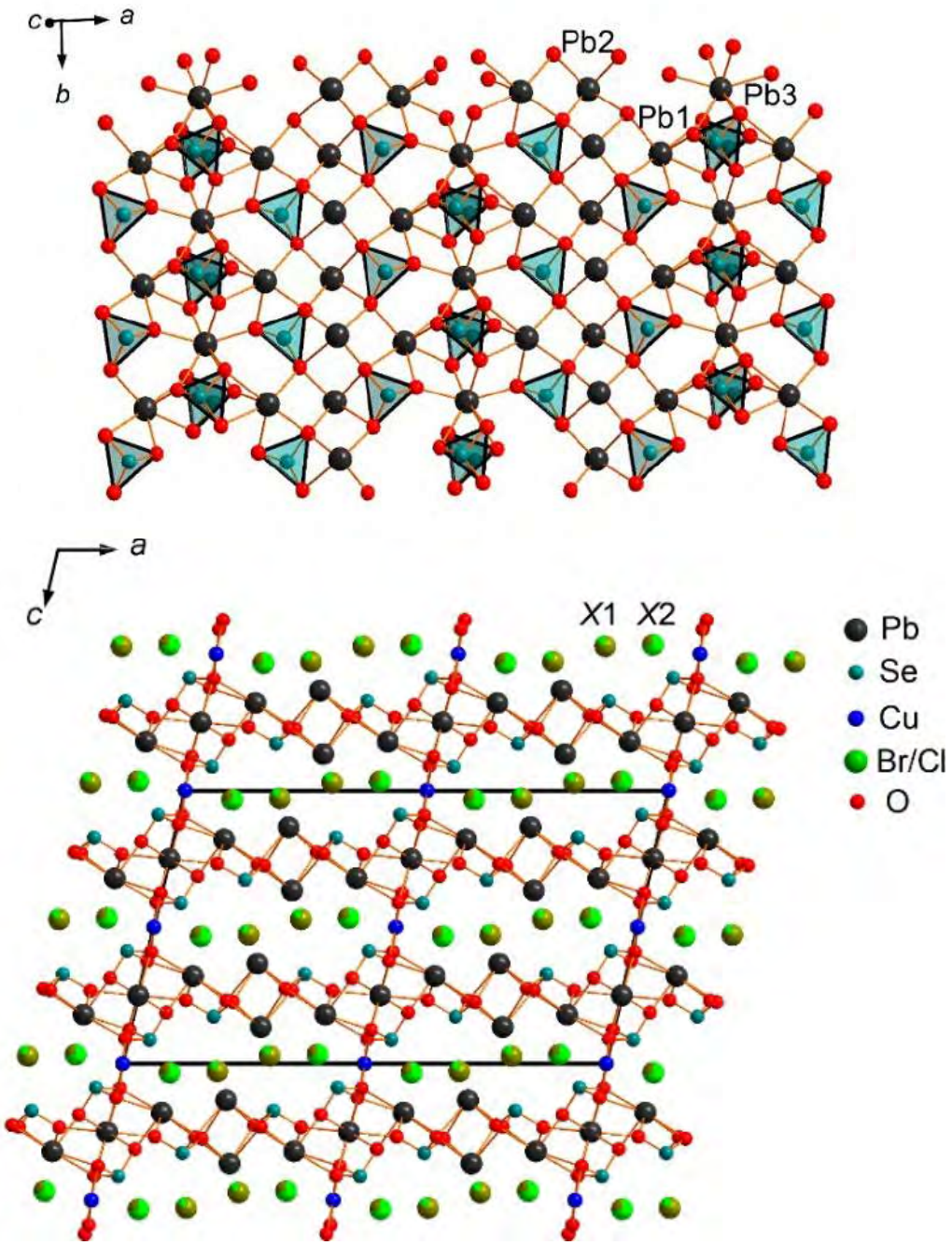

Fig. 4.13. The layer $[Pb_5(SeO_3)_4]^{2+}$ (above). General projection of the crystal structure of synthetic sarrabusite $Pb_5Cu^{2+}(SeO_3)_4(Br,Cl)_4$ (below).

Conclusion

As a result, 24 new compounds with Se^{4+} cations were synthesized, of which one is a synthetic analogue of the mineral; all crystal structures were solved and 12 new structure types were identified.

The family of layered copper halides forms more polymorphic modifications than originally thought. This may be due to the diffusion of ions in the crystal lattice and the changing energy of polymorphs over time. New polymorphic modifications $NaCl•Cu(HSeO_3)_2$ apart from the isostructural compound of the family (namely $KCl•Cu(HSeO_3)_2$) produced a completely new structure type with a different layer topology, which indicates the importance of the order of dimers of the hydroselenite groups in the layer relative to the polyhedra of the bivalent metals.

When the halogen ion was substituted by nitrate in the only known member of the family, the disappearance of the inversion centre and the folding of the layers of selenic acid into channels were revealed due to the appearance of a large amount of hydrogen bonds, which allows us to predict the structures of new members of the family, as well as other compounds with similar compositions. The results are of both fundamental and practical interest for further research in the field of crystal chemistry, mineralogy and structural chemistry of Se in low oxidation states.

Studies of the $M^INO_3 \cdot nH_2SeO_3$ (M^I = NH_4, Na, K, Rb, Cs, n = 1-3) family demonstrate that selenic acid can form molecular salt crystals not only with halides (Markovski *et* al., 2020, Wang *et* al., 2022) and selenates (Baran, 1991), but at least with some other inorganic compounds containing oxyanions. In all these cases, anions serve as hydrogen bond acceptors, resulting in the formation of cationic frameworks. This pattern can be regarded as "inverse" to the numerous families containing anionic frameworks formed by organic compounds or hydrated metal cations that are donors of hydrogen bonds (see. selenite review Rao *et* al., 2006). The crystallochemical prerequisites for the formation of such matrix structures are, firstly, that the matrix components must form hydrogen bonds from medium to high, but with low proton affinity, that is, formed from relatively strong acid; Secondly, in the case of oxoanions, there should be a significant difference in the nature of the central atom-oxygen bond compared to the main component of the framework (selenic acid), which is not the case for hydroselenites; Third, the framework must be a relatively strong donor of hydrogen bond. Our attempts to obtain similar compounds using phosphoric acid have been unsuccessful, despite significant similarities between the phosphate and selenite structures. However, the H_2SeO_3 family of molecular crystals seems to be of interest as a possible source of new compounds with attractive optical properties.

The selenite halide family of divalent metals and organic cations is a logical extension of the series of selenite halides of copper and alkali metals. In addition to steric factors (namely, the size of organic cation above the size of alkali metal cations) and the study of hydrogen bond systems, organo-

inorganic compounds of this family have interesting principles of structure construction. The layer $M^{II}(HSeO_3)_2Cl_2]^{2-}$ inherits its topology from the polymorph III copper and sodium hydroselenite chloride described in this work. Changing the organic cation to a larger (ethylenediamine - piperazine - methylpiperazine) allows not only to "push" the layers, but also to shift them relative to each other, which allows a finer structural design. Successful synthesis of compounds without divalent metal cations, as well as their nitrate analogues, allows structural analogies between the $MX•Cu(HSeO_3)_2$ and $MX•nH_2SeO_3$ families (Charkin *et* al., 2019, Markovski *et* al., 2020b)

Complete structural analogy between $Pb_2(ReO_4)_2(SeO_3)·2H_2O$ and $Pb_2(ReO_4)_2(HPO_3)·2H_2O$ is rather similar to the analogy between anhydrous nitrate selenite $Pb_2(NO_3)_2(SeO_3)$ (Meng *et* al., 2015) and nitrate phosphite $Pb_2(NO_3)_2(HPO_3)$ (Ouarsal *et* al., 2009). As noted above, the almost non-polar P-H bond plays the same structural role as the lone-pair of Se^{IV}, providing a "one-way" coordination of the dianion. It is important to note that such variation $SeEO_3^{2-}/HPO_3^{2-}$ without altering the main structural motif is possible not only in oxysalts of divalent lead with very flexible and adaptive Pb^{2+} coordination, but also in iron and copper compounds (Kovrugin *et* al. 2016). Formation of complex polyanionic structures such as Pb_2X_2Y ($X = ReO_4^-$, NO_3^-; $Y = SeO_3^{2-}$, HPO_3^{2-}) directly from aqueous solutions is quite unlikely given the relatively low solubility $PbSeO_3$ and $PbHPO_3$. Perhaps there is a delicate balance between the strength of the diatomic acid H_2Y and its high solubility and stability in aqueous solution. This may be the reason that the suggested sulfite analog $Pb_2(ReO_4)_2(SeO_3)·2H_2O$ and $Pb_2(ReO_4)_2(HPO_3)·2H_2O$ was not obtained. Sulfurous acid is unstable in aqueous solutions and decomposes into volatile SO_2 weakly soluble in acidic solutions; it is also easily oxidized to SO_4^{2-}. Lead iodate perrenate is also not yet available. However, it can be assumed that at least some sulfite-, arsenite- and iodate-containing compounds could be produced under mild hydrothermal conditions. However, it should be borne in mind that both sulfite and arsenite exhibit tautomerism with both lone-pairs and hydrogen bond configurations; the crystal chemistry of these compounds may be even more unusual.

It is also worth noting that despite the similarity in chemical composition, there is nothing in common between the structures $Pb_2(NO_3)_2(TO_3)$ and $Pb_2(ReO_4)_2(TO_3)(H_2O)_2$ (T = Se or PH). Obviously, the reason lies in the large differences in size and shape between ReO_4^- and NO_3^- as well as possible communication systems. The only common feature is the presence of an empty space around a lone-pare of Se^{IV} or a P-H bond. At a smaller size NO_3^- it remains unoccupied, while more ReO_4^- there is enough space for the water molecules connected to the framework by hydrogen bonds. Inclusion of ligands repulsive particles on the one hand (through lone-pairs or almost non-polar bonds) leads to low-dimensional or porous structures and structures $Pb_2(ReO_4)_2(SeO_3)·2H_2O$ and $Pb_2(ReO_4)_2(HPO_3)·2H_2O$ are a new example for the latter case. By introducing some other complexes capable of participating in the formation of hydrogen bonds, such as halides or organic compounds, different template structures could probably be obtained.

Five new compounds have been produced by chemical vapor transport reactions, of which three are anhydrous lead selenite halides and copper with a low-dimensional structure. This is due to the influence of stereochemically active lone-pairs on Se^{4+} cations, which in all structures are oriented towards halogen anions, which indicates the halophilic nature of interactions. Two other compounds, namely $Bi_5(Se_2O_5)(SeO_3)_5Cl_3$ and $Cd_7Cu_2(SeO_3)_8Br_2$, are of the "host-guest" type, which is typical for minerals and compounds produced by CVT.

Three new compounds were obtained in the system Cu–Pb–Se–O–Br/Cl. The method of chemical vapor transport reactions has been successfully applied for the synthesis of single crystals of copper oxysalts demonstrating magnetic properties (Han *et* al., 2011, Siidra *et* al., 2020, Ginga *et* al., 2022). One of the new compounds, $Pb_5Cu^{2+}(SeO_3)_4(Br,Cl)_4$, is an analogue of sarrabusite mineral. Refinement of the crystal structure based on X-ray data provided a more accurate understanding of the mineral crystal structure. Successful synthesis of $Pb_5Cu^{2+}(SeO_3)_4(Br,Cl)_4$ by CVT method shows the possibility of sarrabusite formation not only in oxidation zones (Campostrini *et* al., 1999), but also from a gas in volcanic fumaroles. It has not yet been possible to obtain a pure bromide analogue of sarrabusite, which may be caused by the stabilizing role of chlorine. Chloride analogues are also unknown today for most of the bromide compounds previously described in the system Cu-Pb-Se-O-Br by Siidra *et* al. (2018).

In most new compounds described herein, a common feature is the formation of a seleniophilic substructure, which ends with a shell of a lone-pair facing the bromide complexes, thus forming a halophilic layer surface. Interactions Se-*X* (*X* = Br, Cl) also seem to be important for stabilizing the obtained structural architectures. Se-Br distances in the structures of new compounds vary from 3.226(2) Å to 3.7477(9) Å. Importance of Se^{4+}-Cl interactions was recently analyzed by Krivovichev S.V. and Gorelova L.A. (Krivovichev & Gorelova, 2018). These interactions were classified into two types: interactions with significant covalent contributions and interactions with electronic clouds. Similar interactions seem to occur in the selenite bromide family.

Two new compounds obtained by CVT are: $Bi_5(Se_2O_5)(SeO_3)_5Cl_3$ and $Cd_7Cu_2(SeO_3)_8Br_2$. The former is the only known to date mixed bismuth selenite-diselenite halide. Isostructural compounds may form in fumaroles of oxidizing type at Tolbachik volcano.

References

1. Almond P.M., Albrecht-Schmitt T.E. Hydrothermal syntheses, structures, and properties of the new uranyl selenites $Ag_2(UO_2)(SeO_3)_2$, $M[(UO_2)(HSeO_3)(SeO_3)]$ (M = K, Rb, Cs, Tl), and $Pb(UO_2)(SeO_3)_2$.// *Inorg. Chem.* – 2002. - Vol. 41. – P. 1177-1183.
2. Anderson J.B., Kostiner E., Ruszala F.A. The crystal structure of $Ca_3Cu_3(PO_4)_4$ // *J. Solid State Chem.* – 1981. – Vol. 39. – P. 29-34
3. Asai T., Kiriyama R., Optical and magnetic studies of $CuSeO_3(H_2O)_2$ based on the refined crystal structure. // *Bull. Chem. Soc. Jpn.* - 1973. – Vol. 46. – P. 2395.
4. Badrtdinov D.I., Kuznetsova E.S., Verchenko V.Y., Berdonosov P.S., Dolgikh V.A., Mazurenko V, Tsirlin A.A. Magnetism of coupled spin tetrahedra in ilinskite-type $KCu_5O_2(SeO_3)_2Cl_3$. // *Sci Rep*. – 2018. - Vol. 8. – P. 2379
5. Baran J., Lis T., Marchewka M., Ratajczak H. Structure and polarized IR and Raman spectra of $Na_2SeO_4 \cdot H_2SeO_3 \cdot H_2O$ crystal. // *J. Mol. Struct*. – 1991. – Vol. 250. – P. 13-45.
6. Becker R, Johnsson M, Kremer R., Lemmens P. Crystal structure, magnetic properties and conductivity of $CuSbTeO_3Cl_2$. // *Solid State Sci*. – 2003. – Vol. 5. – P.1411-1416
7. Berdonosov P.S., Janson O., Olenev A.V., Krivovichev S.V., Rosner H., Dolgikh V.A., Tsirlin A.A. Crystal structures and variable magnetism of $PbCu_2(XO_3)_2Cl_2$ with X = Se, Te. *Dalton T*.- 2013. – Vol. 42. – P. 9547-9554.
8. Berdonosov P.S, Kuznetsova E.S., Dolgikh V.A. Transition metal selenite halides: a fascinating family of magnetic compounds. // *Crystals*. – 2018. Vol. 8. – P. 159
9. Berdonosov P.S., Stefanovich S.Yu., Dolgikh V.A. A new bismuth-selenium oxychloride, $BiSeO_3Cl$: crystal structure and dielectric and nonlinear optical properties. // *J. Solid State Chem.* – 2000. – Vol. 149. – P. 236-241.
10. Berger J. Infrared and Raman spectra of $CuSO_4$, $5H_2O$; $CuSO_4$, $5D_2O$; and $CuSeO_4$, $5H_2O$. // *J. Raman Spectrosc.* – 1976. – Vol. 5. – P. 103-114.
11. Brammer L. Developments in inorganic crystal engineering. // *Chem. Soc. Rev.* – 2004. – Vol. 33, - P. 476-489.
12. Brese N.E., O'Keeffe M. Bond-valence parameters for solids. // *Acta Crystallogr B.* – 1991. – Vol. 47. – P. 192-197
13. Bruker AXS. Topas V5.0. Karlsruhe, Germany. - 2014
14. Boldt K., Engelen B., Panthöfer M., Unterderweide K. Stereochemical Equivalence of P^{III}-Bonded Hydrogen Atoms and Se^{IV} Lone Electron Pairs in $Sr(H_2PO_3)_2$ and $Sr(HSeO_3)_2$. // *Eur. J. Inorg. Chem.* – 2000. – N. 2071-2075.

15. Burns P.C., Hawthorne F.C. Static and dynamic Jahn-Teller effects in Cu^{2+} oxysalt minerals. // *Can Mineral.* – 1996. – Vol. 34. – P. 1089-1105

16. Campostrini I, Gramaccioli CM, Demartin F. Orlandiite, $Pb_3Cl_4(SeO_3)_3{\cdot}H_2O$, a new mineral species, and an associated lead-copper selenite chloride from the Baccu Locci mine, Sardinia, Italy. // *Can Mineral.* – 1999. – Vol. 37. – P. 1493-1498

17. Chakraborty J., Ganguli N., Saha-Dasgupta T., Dasgupta I. of Te in the low-dimensional multiferroic material $FeTe_2O_5Br$. // *Phys. Rev. B.* – 2013. – Vol. 88. – P. 094409.

18. Charykova M. V., Krivovichev V. G. Mineral systems and the thermodynamics of selenites and selenates in the oxidation zone of sulfide ores - a review // *Miner. Petrol.* - 2017. - Vol. 111. - P. 121-134.

19. Charkin D.O., Grishaev V.Yu., Borisov A.S., Chachin P.A., Nazarchuk E.V., Siidra O.I. A nonpolar bond to hydrogen vs. lone pair: Incorporation of HPO_3^{2-} and $SeEO_3^{2-}$ into a lead perrhenate framework. // *Solid State Sci*. – 2023c. – Vol. 318. – P. 123706.

20. Charkin, D.O.; Grishaev, V.Y.; Markovski, M.R.; Nekrasova, D.O.; Siidra, O.I. Influence of the alkali cation size on the Cu^{2+}coordination environments in $(AX)[Cu(HSeO_3)_2]$ (A = Na, K, NH_4, Rb, Cs; X = Cl, Br) layered copper hydrogen selenite halides. // *Z. Krist.*–*Cryst. Mat*. – 2019. – Vol. 234. – P. 739–747.

21. Charkin D.O., Grishaev V.Yu., Omelchenko T.A., Nazarchuk E.V., Stefanovich S.Yu., Siidra O.I. $KNO_3{\cdot}3H_2SeO_3$ and $NaHSeO_3{\cdot}3H_2SeO_3$: Two non-centrosymmetric co-crystals. // *Solid State Sci*. – 2023a. – Vol. 137. – P. 107116.

22. Charkin D.O., Borisov A.S., Plokhikh I.V., Stefanovich S.Yu., Zadoya A.I., Zaloga A.N., Semenova T.F., Siidra O.I. $Pb_6O_5(NO_3)_2$: A nonlinear optical oxynitrate structurally based on lead oxide framework. // *Inorg. Chem.* – 2020. – Vol. 59. – P. 3523-03526.

23. Charkin D.O., Nazarchuk E.V., Dmitriev D.N., Grishaev V.Yu., Omelchenko T.A., Spiridonova D.V., Siidra O.I. Protonated organic diamines as templates for layered and microporous structures: synthesis, crystal chemistry, and structural trends among the compounds formed in aqueous systems transition metal halide or nitrate-diamine-selenious acid. // *Int. J. Mol. Sci.* – 2023b. - Vol. 24. – P. 14202.

24. Charkin D.O., Volkov S.N., Dolgikh V.A., Aksenov S.M. Potassium rare-earth tellurite chlorides: a new branch from the old root. // *Solid State Sci.* – 2022. – Vol. 129. – P. 106895.

25. Chilas G.I., Lalioti N., Vaimakis T., Kubicki M., Kabanos N. Hydrothermal syntheses, crystal structures and physicochemical properties of 2-D and 3-D inorganic coordination cobalt(II)-sulfite polymers. // *Dalton T.* – 2010. – Vol. 39. – P. 8296-8305.

26. Chisholm C.R.I., Haile S.M. Structure and thermal behavior of the new superprotonic conductor $Cs_2(HSO_4)(H_2PO_4)$. // *Acta Crystallogr.* – 1999. – B. 55. – P. 937-946.
27. Chomniplan S., Tellgren R., Liminga R. The structure of paraelectric $NaH_3(SeO_3)_2$. // *Acta Crystallogr.* – 1977. – B. 33. – P. 2108-2112
28. Colodero R.M.P., Olivera-Pastor P., Cabeza A., Bazaga-García M. Properties and applications of metal phosphates and pyrophosphates as proton conductors. // *Mater.* – 2022. – Vol. 15. – P. 1292.
29. Dai Z., Chen Y.-G., Guo Y., Wang F., Yang Y.-Y., Zhang X.-M. $Sr_2Pb(BeB_5O_{10})(BO_3)$: An excellent ultraviolet nonlinear-optical beryllium borate by the Pb-modified construction of a conjugated system and lone-pair effect. // *Inorg. Chem.* – 2021. – Vol. 60. – P. 11214–11221.
30. Demartin F, Gramaccioli CM, Campostrini I, Orlandi P. Demicheleite, BiSBr, a new mineral from La Fossa crater, Vulcano, Aeolian Islands, Italy. // *Am Mineral.* – 2008. – Vol. 93. – P. 1603-1607
31. Dolomanov, O.V.; Bourhis, L.J.; Gildea, R.J.; Howard, J.A.K.; Puschmann, H. OLEX2: A complete structure solution, refinement and analysis program. // *J. Appl. Crystallogr*. – 2009. – Vol. 42. – P. 339–341.
32. Effenberger H. $PbCu_3(OH)(NO_3)(SeO_3)_3 \cdot 0.5H_2O$ and $Pb_2Cu_3O_2(NO_3)_2(SeO_3)_2$: Synthesis and crystal structure. // *Monatsh. Chem.* – 1986. – Vol. 117. – P. 1099-1106.
33. Effenberger H., Miletich R., Pertlik F. Structure of dilead(II) hydrogenarsenate(III) dichloride. // *Acta Crystallogr.* - 1990. – Vol. 46. – P. 541-543.
34. Escobal J, Pizarro JL, Mesa JL, Larranaga A, Fernandez JR, Arriortua MI, Rojo T Neutron diffraction, specific heat and magnetic susceptibility of $Ni_3(PO_4)_2$. // *J. Solid State Chem.* – 2006. – Vol. 179. – P. 3052-3058
35. Farrugia, L.J. WinGX suite for small-molecule single-crystal crystallography. // *J. Appl. Crystallogr*. – 1999. – Vol. 32. – P. 837–838.
36. Feng, M.-L., Prosvirin, A.V., Mao, J.-G., Dunbar, K.R. Syntheses, structural studies, and magnetic properties of divalent Cu and Co selenites with organic constituents. // *Chem. Eur. J.* – 2006. – N. 8312-8323.
37. Fischer R., Zemann J., Leutwein F. Selenium. In Handbook of Geochemistry (Edited by Wedepohl K. H.). // *Springer, New York*. - 1978. - Vol. 2(3). - P. 34-34.
38. Furberg S, Landmark S. The crystal structure of phosphorous acid. // *Acta Chem. Scand.* – 1957. – Vol. 11. – P. 1505-1511.
39. Gagné O.C., Hawthorne F.C. Comprehensive derivation of bond-valence parameters for ion pairs involving oxygen. // *Acta Crystallogr.* – 2015. – Vol. 71. – P. 562-578.

40. Gemmi M., Campostrini I., Demartin F., Gorelik T.E., Gramaccioli C.M. Structure of the new mineral sarrabusite, $Pb_5CuCl_4(SeO_3)_4$, solved by manual electron-diffraction tomography. // *Acta Crystallogr B.* – 2012. – Vol. 68. – P. 15-23.

41. Ginga V.A., Siidra O.I., Ugolkov V.L., Bubnova R.S. Refinement of the crystal structure and features of the thermal behavior of volborthite $Cu_3V_2O_7(OH)_2·2H_2O$ from the Tyuya-Muyun deposit, Kyrgyzstan. // *Zapiski Rossiyskogo Mineralogicheskogo Obshchestva.* – 2021. – Vol. 150. – P. 115-133 (In Russian)

42. Ginga V.A., Siidra O.I., Breitner F., Jesche A., Tsirlin A.A. Chemical vapor transport synthesis of $Cu(VO)_2(AsO_4)_2$ with two distinct spin-1/2 magnetic ions. // *Inorg. Chem.* – 2022. – Vol. 61. – P. 16539-16548

43. Goerigk F.C., Schander S., Ben Hamida M., Kang D.-H., Ledderboge F., Wickleder M.S., Schleid T. Die monoklinen Seltenerdmetall(III)-Chlorid-Oxidoarsenate(III) mit der Zusammensetzung $SE_5Cl_3[AsO_3]_4$ (*SE*=La–Nd, Sm). // *Z. Naturforsch. B.* – 2019. – Vol. 74. – P. 497-506.

44. Gospodinov G., Barkov D. A study of the system $CdO–SeO_2–H_2O$ *et* 25 and 100°C. // *J. Therm. Anal. Cal*. – 2002. – Vol. 70. – P. 615-620.

45. Grishaev, V.Y.; Siidra, O.I.; Markovski, M.R.; Charkin, D.O.; Omelchenko, T.A.; Nazarchuk, E.V. Synthesis and crystal structure of two novel polymorphs of $(NaCl)[Cu(HSeO_3)_2]$: A further contribution to the family of layered copper hydrogen selenites. // *Z. Krist.–Cryst. Mater*. – 2023. – Vol. 238. – P. 177–185.

46. Grundmann G., Förster H.-J. Origin of the El Dragón Selenium Mineralization, Quijarro Province, Potosí, Bolivia // *Miner.* - 2017. - Vol. 7(5). - P. 68

47. Halasyamani P.S., Poeppelmeier K.R. Noncentrosymmetric oxides. // *Chem. Mater*. - 1998. - Vol. 10. - P. 2753-2769.

48. Handlovic M. The crystal structure of $CuHPO_3·2H_2O$. // *Acta Crystallogr.* B. – 1969. – Vol. 25. – P. 227-231.

49. Han T.H., Helton J.S., Chu S., Prodi A., Singh D.K., Mazzoli C., Müller P., Nocera D.G., Lee Y.S. Synthesis and characterization of single crystals of the spin-1/2 kagome-lattice antiferromagnets $Zn_xCu_{4-x}(OH)_6Cl_2$. // *Phys Rev.* – 2011. - Vol. 83. – P. 100402

50. He F., Wang Q., Hu C., He W., Luo X., Huang L., Gao D., Bi X., Wang X., Zou G. Centrosymmetric $(NH_4)_2SbCl(SO_4)_2$ and non-centrosymmetric $(NH_4)SbCl_2(SO_4)$: synergistic effect of hydrogen-bonding interactions and lone-pair cations on the framework structures and macroscopic centricities. // *Cryst. Growth Des.* – 2018. – Vol. 18. – P. 6239–6247.

51. Hiltunen L., Hölsä J., Mička Z. Crystal structure, thermal behavior, and infrared absorption spectrum of cesium hydrogen selenite – selenious acid (l/2) $CsHSeO_3 \cdot 2H_2SeO_3$. // *J. Solid State Chem.* – 1987. – Vol. 68. – P. 397-313.

52. Hoffmann J. E. Recovering selenium and tellurium from copper refinery slimes // *J. Miner.* - 1989. - Vol. 41(7). - P. 33-38.

53. Ibragimov S.A., Berdonosov P.S., Dolgikh V.A., Huong, D.Q., Oppermann, H. Crystal structure and SHG characterization of γ-$BiSeO_3Cl$ // *Inorg. Mat.* – 2002. – Vol. 38 (12). - P. 1291-1296

54. Jahn H.A., Teller E. Stability of polyatomic molecules in degenerate electronic states. // *Proc. R. Soc. London, Ser.* – 1937. – Vol. A161. – P. 220.

55. Jiang H.-G., Mao J.-G. Syntheses, crystal structures and optical properties of the first strontium selenium(IV) and tellurium(IV) oxychlorides: $Sr_3(SeO_3)(Se_2O_5)Cl_2$ and $Sr_4(Te_3O_8)Cl_4$. // *J. Solid State Chem*. – 2008. – V. 181. – P. 345–354.

56. Johnson R.A., Rogers M.T., Leroi G.E. Vibrational spectra of ammonium and other scheelite-type perrhenates. // *J. Chem. Phys*. – 1972. – Vol. 56. – P. 789–792.

57. Jo V., Kim M.K., Lee D.W., Shim I.-W., Ok K.M. Lone pairs as chemical scissors in new antimony oxychlorides, $Sb_2ZnO_3Cl_2$ and $Sb_{16}Cd_8O_{25}Cl_{14}$. // *Inorg. Chem.* – 2010. – Vol. 49. – P. 2990–2995.

58. Jones, P.G.; Schwartzmann, E.; Sheldrick, G.M.; Timpe, H. Preparation and crystal structure of di-gold(III)bis(selenite) diselenite, $Au_2(SeO_3)_2(Se_2O_5)$. // *Z. Natuforsch*. – 1981. – Vol. 36. – P. 1050–1052.

59. Karpenko V.Yu., Pautov L.P., Siidra O.I., Mirakov M., Zaitsev A.N., Plechov P.Yu., Makhmadsharif S. Ermakovite $(NH_4)(As_2O_3)_2Br$, a new exhalative arsenite bromide mineral from the Fan-Yagnob coal deposit, Tajikistan. // *Mineral. Mag.* – 2022. – Vol. 87 (1). – P. 67-78.

60. Krivovichev S.V., Gorelova L.A. Se-Cl interactions in selenite chlorides: a theoretical study. // *Crystals* – 2018. – Vol. 8. – P. 193.

61. Krivovichev S. V., Filatov S. K., Burns P. C., Vergasova L. P. The crystal structure of allochalcoselite, $Cu^+Cu_5^{2+}PbO_2(SeO_3)_2Cl_5$, a mineral with well-defined Cu^+ and Cu^{2+} positions // *Can. Mineral.* - 2006. - Vol. 44. - P. 507-514.

62. Krivovichev S. V., Filatov S. K., Semenova T. F., Rozhdestvenskaya I. V. Crystal chemistry of inorganic compounds based on chains ofoxocenterd tetrahdera. I. Crystal structure of chloromenite, $Cu_9O_2(SeO_3)_4Cl_6$ // *Z. Krist. – Cryst. Mater.* - 1998. - Vol. 213. - P. 645-649.

63. Krivovichev S.V., Filatov S.K., Vergasova L.P. The crystal structure of ilinskite, $NaCu_5O_2(SeO_3)_2Cl_3$, and review of mixed-ligand CuO_mCl_n coordination geometries in minerals and inorganic compounds. // *Miner Petrol.* – 2013. – Vol. 107. – P. 235-242

64. Krivovichev V. G., Charykova M. V., Vishnevsky A. V. The thermodynamics of selenium minerals in near-surface environments // *Miner.* - 2017. - Vol. 7. - P. 188.

65. Krivovichev V. G., Krivovichev S. V., Charykova M. V. Selenium Minerals: Structural and Chemical Diversity and Complexity // *Miner.* - 2019. - Vol. 9(7). - P. 455.

66. Krivovichev V. G., Krivovichev S. V., Charykova M. V. Tellurium Minerals: Structural and Chemical Diversity and Complexity // *Miner.* - 2020. - Vol. 10(7). - P. 623

67. Krivovichev S. V., Shuvalov R. R., Semenova T. F., Filatov S. K. Crystal chemistry of inorganic compounds based on chains ofoxocentered tetrahedra. III. Crystal structure of georgbokiite, $Cu_5O_2(SeO_3)_2Cl_2$ // *Z. Krist. – Cryst. Mater.* - 1999. - Vol. 214. - P. 135-138.

68. Krivovichev S. V., Vergasova L. P., Starova G. L., Filatov S. K., Britvin S. N., Roberts A. C., Steele I. M. Burnsite, $KCdCu_7O_2(SeO_3)_2Cl_9$, a new mineral species from the Tolbachik Volcano, Kamchatka Peninsula, Russia // *The Can. Mineral.* - 2002. - Vol. 40. - P. 1171-1175

69. Kong F., Ma Y., Mao J. Lanthanide inorganic solids based on main group borates and oxyanions of lone pair cations. // *Chin. J. Chem.* – 2018. – Vol. 36. – P. 63-72.

70. Koskenlinna, M.; Valkonen, J. The crystal structure of $PrH_3(SeO_3)_2(Se_2O_5)$, a compound with selenite and diselenite groups. // *Acta Chem. Scand*. – 1977a. – Vol. 31a. – P. 457–460.

71. Koskenlinna, M., Valkonen. J. Crystal structure of manganese(III) hydrogen selenite diselenite, $MnH(SeO_3)(Se_2O_5)$. // *Acta Chem. Scand*. - 1977b. – Vol. 31a. – P. 638–640.

72. Kovrugin V. M., Colmont M., Siidra O. I., Gurzhiy V. V., Krivovichev S. V., Mentré O. Pathways for synthesis of new selenium-containing oxo-compounds: Chemical vapor transport reactions, hydrothermal techniques and evaporation method // *J. of Cryst. Growth.* - 2017a. - Vol. 457. - P. 307-313.

73. Kovrugin V. M., Colmont M., Terryn C., Colis S., Siidra O. I., Krivovichev S. V., Mentré O. pH-Controlled pathway and systematic hydrothermal phase diagram for elaboration of synthetic lead nickel selenites // *Inorg. Chem.* - 2015a. - Vol. 54(5). - P. 2425-2434.

74. Kovrugin V. M., Colmont M., Mentré O., Siidra O. I., Krivovichev S. V. Dimers of oxocentred $[OCu_4]^{6+}$ tetrahedra in two novel copper selenite chlorides, $K[Cu_3O](SeO_3)_2Cl$ and $Na_2[Cu_7O_2](SeO_3)_4Cl_4$, and related minerals and inorganic compounds // *Miner. Mag.* – 2016a. - Vol. 80. - P. 227-238.

75. Kovrugin V. M., Colmont M., Siidra O. I., Mentré O., Al-Shuray A., Gurzhiy V. V., Krivovichev S. V. Oxocentered Cu(II) lead selenite honeycomb lattices hosting Cu(I)Cl2 groups obtained by chemical vapor transport reactions // *Chem. Commun.* - 2015b. - Vol. 51. - P. 9563- 9566.

76. Kovrugin V.M., Gordon E.E., Kasapbasi E.E., Whangbo M.-H., Colmont M., Siidra O.I., Colis S., Krivovichev S.V., Mentré O. Bonding scheme, hydride character, and magnetic paths of $(HPO_3)^{2-}$ versus $(SeO_3)^{2-}$ building units in solids. // *J. Phys. Chem. C.* – 2016b. – Vol. 120. – P. 1650–1656.

77. Kovrugin V. M., Krivovichev S. V., Mentré O., Colmont M. $[NaCl][Cu(HSeO_3)_2]$, NaCl intercalated Cu(HSeO3)2: synthesis, crystal structure and comparison with related compounds // *Z. Krist. – Cryst. Mater.* - 2015c. - Vol. 230. - P. 573-577.

78. Kretzschmar J., Jordan N., Brendler E., Tsushima S., Franzen C., Foerstendorf H., Brendler V. Spectroscopic evidence for selenium (IV) dimerization in aqueous solution. // *Dalton T.* – 2015. – Vol. 44. – P. 10508–10515.

79. Kurtz S.K., Perry T.T. A powder technique for the evaluation of nonlinear optical materials. // *J. Appl. Phys.* – 1968. – Vol. 39. – P. 3798-3813.

80. Lafront, A.M., Trombe, J.C. 'Layered hydrogenselenite'. I. Synthesis, structure redetermination of $[Cu(HSeO_3)_2(H_2O)_2]$ and determination of $[Cu(HSeO_3)_2(NO_3)_2]^{2-}\cdot 2NH_4^+$,$NH_4NO_3$. Structural relationships of these complexes with $[Cu(HSeO_3)_2]$. // *Inorg. Chim. Acta*. -1995. – Vol. 234. – P. 19-25.

81. Lehmann M.S., Larsen F.K. The hydrogen bond system in potassium trihydrogen bis-selenite, $KH_3(SeO_3)_2$, and in potassium trideuterio bis-selenite $KD_3(SeO_3)_2$, as determined by neutron diffraction. // *Acta Chem. Scand.* – 1971. - Vol 25. – P. 3859-3871.

82. Levanov A.V., Isaikina O.Y., Lunin V.V. Dissociation constant of nitric acid. // *Russ. J. Phys. Chem.* – 2017. – Vol. 91. – P. 1221–1228

83. Lin K., Cross J.N., Diwu J., Meredith N.A., Albrecht-Schmitt T.E. Comparisons of plutonium, thorium, and cerium tellurite sulfates. // *Inorg. Chem.* – 2013. – Vol. 52. – P. 4277–4281.

84. Li, P.-F., Gong, Y.-P., Hu, C.-L., Zhang, B., Mao, J.-G., Kong., F. Four UV Transparent Linear and Nonlinear Optical Materials Explored from Pure Selenite Compounds. // *Adv. Optical Mater*. – 2024. – Vol. 12. – №2301426.

85. Lipp C., Schleid T. $Er_3F[SiO_4][SeO_3]_2$: An ErF_3-derivative with two different kinds of complex oxoanions. // *Z. Anorg. Allg. Chem.* – 2008. – Vol. 634. – P. 1025-1029.

86. Liu X., Li G., Hu Y., Yang M., Kong X., Shi Z., Feng S. Hydrothermal synthesis and crystal structure of polar and nonpolar compounds in indium iodate family. // *Cryst. Growth Des.* – 2008. – Vol. 8. – P. 2453–2457.

87. Loub J., Mička Z., Podlahová J., Malý K. Kopf J. Structure of sodium hydrogen selenite-selenious acid adduct (1:3), $NaHSeO_3 \cdot 3H_2SeO_3$. *// Collect. Czech. Chem. Commun.* – 1992. – Vol. 57. – P. 2309-2314.

88. Makovicky E.. Modular and crystal chemistry of sulfosalts and other complex sulfides. In: S. Merlino (ed). Modular Aspects of Minerals // *EMU Notes in Mineralogy Eotvos Univesity Press, Budapest.* – 1997. – Vol. 1. – P. 237-271.

89. Markina M.M., Zakharov K.V., Zvereva E.A., Denisov R.S., Berdonosov P.S., Dolgikh V.A., Kuznetsova E.S., Olenev A.V., Vasiliev A.N. Static and dynamic magnetic properties of two synthetic francisites $Cu_3La(SeO_3)_2O_2X$ (X = Br and Cl). // *Phys. Chem. Miner*. – 2017. – Vol. 44. – P. 277-285.

90. Markovski M. R., Charkin D. O., Siidra O. I., Nekrasova D. O., Grishaev V. Yu. Copper hydroselenite nitrates $(A^+NO_3)_n[Cu(HSeO_3)_2]$ (A = Rb^+, Cs^+ and Tl^+, n = 1, 2) related to Ruddlesden - Popper phases // *Z. Krist. – Cryst. Mater*. – 2019. - Vol. 234. - P. 749-756.

91. Markovski M. R., Siidra O. I., Charkin D. O., Grishaev V. Yu. Layered calcium hydrogen selenite chlorides $Ca(HSeO_3)Cl$ and $Ca(HSeO_3)Cl(H_2O)$, the first halides obtained in $CaCl_2$-H_2SeO_3-H_2O system // *Z. Krist. – Cryst. Mater* - 2020a. - Vol. 235(10). - P. 439-443.

92. Markovski M. R., Siidra O. I., Charkin D. O., Nazarchuk E. V., Grishaev V. Yu. Molecular inorganic polymers: synthesis and crystal structures of $KCl.2H_2SeO_3$ and $CsCl.H_2SeO_3$ // *Z. Krist. – Cryst. Mater*. - 2020b. - Vol. 235(11). - P. 553-557.

93. Markovski M. R., Siidra O. I., Charkin D. O., Vladimirova V. A., Tsirlin A. A., Grishaev V. Yu. $Li_2(Se_2O_5)(H_2O)_{1.5} \cdot CuCl_2$, a salt-inclusion diselenite structurally based on tetranuclear Li4 complexes // *Dalton T.* - 2020c. - Vol. 49. - P. 7790-7795.

94. Mayerová Z, Johnsson M, Lidin S. Lone-pair interfaces that divide inorganic materials into ionic and covalent parts. // *Angew Chem Int Edit* - 2006. – V. 45. – P. 5602-5606

95. Meng C.-Y., Geng L., Chen W.-T., Wei M.-F., Dai K., Lu H.-Y., Cheng W.-D. Syntheses, structures, and characterizations of a new second-order nonlinear optical material: $Pb_2(SeO_3)(NO_3)_2$. // *J. Alloys Compd.* – 2015. – Vol. 640. – P. 39-44.

96. Mills S.J., Kampf A.R., Housley R.M., Christy A.G., Thorne B., Chen Y.-S., Steele I.M. Favreauite, a new selenite mineral from the El Dragón mine, Bolivia. // *Eur. J. Miner*. – 2014. – Vol. 26. – P. 771-781.

97. Missen O.P., Weil M., Mills S.J., Libowitzky E. The crystal structure of the first synthetic copper(II) tellurite arsenate, $Cu^{II}_5(Te^{IV}O_3)_2(As^{V}O_4)_2$. // *Acta Crystallogr. B.* – 2020. – Vol. 76. – P. 1-6.

98. Missen O. P., Rama R., Mills S. J. Etschmanna B. Reithcd F., Shustercd J., Smithe D. J. Brugger. J. Love is in the Earth: A review of tellurium (bio)geochemistry in surface environments // *Earth- Sci. Rev.* - 2020. - Vol. 204. - P. 103150.

99. Momma, K.; Izumi, F. VESTA 3 for three-dimensional visualization of crystal, volumetric and morphology data. // *J. Appl. Crystallogr*. – 2011. – Vol. 44. – P. 1272–1276.

100. Mudring, A.-V. Thallium Halides – New Aspects of the Stereochemical Activity of Electron Lone Pairs of Heavier Main-Group Elements. // *Eur. J. Inorg. Chem*. – 2006. – Vol. 6. – P. 882-890.

101. Murtazoev A.F., Berdonosov P.S., Tafeenko V.A., Dolgikh V.A., Danilovich I.L., Pchelkina Z.V., Vasiliev A.N. Cadmium copper selenite chloride, $CdCu_2(SeO_3)_2Cl_2$, an insulating spin gap system. // *J Solid State Chem*. – 2021. – Vol. 303. – P. 122518.

102. Nabi, S.A., Bushra, R., Al-Othman, Z.A., Naushad, Mu. Synthesis, Characterization, and Analytical Applications of a New Composite Cation Exchange Material Acetonitrile Stannic(IV) Selenite: Adsorption Behavior of Toxic Metal Ions in Nonionic Surfactant Medium. // *Sep. Sci. Technol.* – 2011. – Vol. 46. - № 5. – P. 847–857

103. Nakamoto K. Infrared and Raman Spectra of Inorganic and Coordination Compounds, Part B, Applications in Coordination, Organometallic, and Bioinorganic Chemistry. // *John Wiley and Sons, Hoboken.* - 2009. - P. 54,

104. Nelmes R.J. Recent structural studies of the KDP-type transition: A review. // *Ferroelectrics.* – 1984. – Vol. 53. – P. 207-214

105. Ouarsal R., Lachkar M., Dusek M., Feifarová K., El Bali B. Dilead(II) hydrogenphosphite dinitrate. // *Acta Cryst.* – 2009. – Vol. E65. – P. i35.

106. Pasha, I.; Choudhury, A.; Rao, C.N.R. An organically templated open-framework cadmium selenite. // *Solid State Sci*. – 2003. – Vol. 5. – P. 257–262.

107. Pring A., Gatehouse B. M., Birch W. D. Francisite, $Cu_3Bi(SeO_3)_2O_2Cl$, new mineral from Iron Monarch, South Australia: Description and crystal structure // *Am Mineral.* - 1990. - Vol. 75. - P. 1421-1425.

108. Range K.-J., Rögner P. An X-ray, Raman and IR study of α-$CsReO_4$, the high-temperature modification of cesium perrhenate. // *Z. Naturforsch.* – 1992. – Vol. 47b. – P. 1513–1520.

109. Rao C.N.R., Behera J.N., Dan M. Organically-templated metal sulfates, selenites and selenates. // *Chem. Soc. Rev.* – 2006. – Vol. 35. – P. 375-387.

110. Rees C.E., Thod H.G. Selenium isotope effects in the reduction of sodium selenite and of sodium selenate. // *Can. J. Chem.* – 1966. – Vol. 44. – P. 419–427.

111. Reshak A.H. Lead nitrate hydroxide: A strong second-order optical nonlinearity acentric crystal with high laser damage thresholds. // *J. Appl. Phys*. – 2016. – Vol. 119. – P. 105706.

112. Rigaku PDXL: Integrated X-ray powder diffraction software. // *Rigaku Corporation, Oxford, U.K.* – 2016.

113. Robinson P.D., Sen Gupta P.K., Swihart G.H., Houk L. Crystal structure, H positions, and the Se lone pair of synthetic chalcomenite, $Cu(H_2O)_2[SeO_3]$. // *Am. Miner.* – 1992. – Vol. 77. – P. 834–838.

114. Séby F., Potin-Gautier M., Giffaut E., Borge, G., Donard O. F. A critical review of thermodynamic data for selenium species *et* 25°C // *Chem. Geol.* - 2001. - Vol. 171. - P. 173-194.

115. Seki T., Chiang K.-Y., Yu C.-C., Yu X., Okuno M., Hunger J., Nagata Y., Bonn M. The bending mode of water: a powerful probe for hydrogen bond structure of aqueous systems. // *Phys. Chem. Lett.* – 2020. – Vol. 11. – P. 8459–8469.

116. Semenova T. F., Rozhdestvenskaya I. V., Filatov S. K., Vergasova L. P. Crystal structure and physical properties of sophiite $Zn_2(SeO_3)Cl_2$, a new mineral. // *Miner. Mag.* - 1992. - Vol. 56. - P. 241-245.

117. Senga Y, Kawahara A The structure of synthetic copper sodium phosphate: $Cu_9Na_6(PO_4)_8$. // *Acta Crystallogr B.* - 1980. – Vol. 36. – P. 2555-2558

118. Sheldrick G.M. Crystal structure refinement with SHELXL. // *Acta Crystallogr.* - 2015. – Vol. A71. – P. 3.

119. Sheldrick W.S., Häusler H.-J. Das Hydrogendiarsenit-Anion $HAs_2O_5^{3-}$. Darstellung und Struktur von $K_3HAs_2O_5{\cdot}6H_2O$. // *Z. Naturforsch.* – 1985. – Vol. B40. – P. 1622-1625.

120. Sheldrick W.S., Häusler H.-J. Zur Kenntnis von Natriumarseniten im Dreistoffsystem $Na_2O – As_2O_3 – H_2O$ bei 6°C. // *Z. Anorg. Allg. Chem.* – 1987. – Vol. 549. – P. 177-186.

121. Shen Y.-L., Mao J.-G., Jiang H.-L. Synthesis, crystal structure and magnetic property of a new nickel selenite chloride: $Ni_5(SeO_3)_4Cl_2$. // *J. Solid State Chem.* - 2005. – Vol. 178. – P. 2942-2946.

122. Shuvalov L.A., Bondarenko V.V., Varikash V.M., Gridnev S.A., Makarova I.P., Simonov V.I. Thallium-tri-hydrogen selenite, $TlH_3(SeO_3)_2$ – a new member of alkaline tri-hydrogen selenite crystal family. // *Ferroelectrics Lett.* – 1984. – Vol. 2. – P. 143-146.

123. Shuvalov R. R., Vegasova L. P., Semenova T. F., Filatov S. K., Krivovichev S. V., Siidra O. I., Rudashevsky M. S. Prewittite, $KPb_{1.5}Cu_6Zn(SeO_3)_2O_2Cl_{10}$, a new mineral from

Tolbachik fumaroles, Kamchatka peninsula, Russia: Description and crystal structure // *Am. Miner.* - 2013. - Vol. 98. - P. 463-469.

124. Shannon R. D, Prewitt C. T. Revised values of effective ionic radii // *Acta Crystallogr.* - 1970. - Vol. B26. - P. 1046-1048.
125. Siidra O.I., Charkin D.O., Kovrugin V.M., Borisov A.S. K(Na,K)$Na_2[Cu_2(SO_4)_4]$: a new highly porous anhydrous sulfate and evaluation of possible ion migration pathways. // *Acta Crystallogr B.* – 2021. – Vol. 77. – P. 1003-1011
126. Siidra O. I., Chukanov N. V., Pekov I. V., Krivovichev S. V., Magganas A., Katerinopoulos A., Voudouris P.; $Pb_2(AsO_2OH)Cl_2$, a new phase from the Lavrion ancient slags, Greece: occurrence and characterization. // *Miner. Mag.* – 2012. – Vol. 76 (3). – P. 597–602.
127. Siidra O.I., Grishaev V.Yu., Nazarchuk E.V., Kayukov R.A. Three new copper-lead selenite bromides obtained by chemical vapor transport: $Pb_5Cu^{+}_4(SeO_3)_4Br_6$, $Pb_8Cu^{2+}(SeO_3)_4Br_{10}$, and the synthetic analogue of the mineral sarrabusite, $Pb_5Cu^{2+}(SeO_3)_4(Br,Cl)_4$. // *Miner. Petrol*. – 2023. – Vol. 1. – P. 11.
128. Siidra, O.I., Grishaev V.Yu. $[Cd_7(SeO_3)_8]\{Cu_2Br_2\}$, a host-guest structure derived from β-$CdSeO_3$. // *Z. Kristallogr.* – 2024a. (published online) https://doi.org/10.1515/zkri-2024-0072
129. Siidra, O.I., Grishaev V.Yu. Synthesis and crystal structure of new hydrated lead selenite nitrate $Pb_4(SeO_3)_3(NO_3)_2•2H_2O$. // *J. Struct. Chem.* – 2024b. – Vol. 65. – №7. – P. 1432-1438
130. Siidra O.I., Kozin M.S., Depmeier W., Kayukov R.A., Kovrugin V.M. Copper-lead selenite bromides: A new large family of compounds partly having Cu^{2+} substructures derivable from Kagome-nets. // *Acta Crystallogr.* – 2018. – Vol. 74. – P. 712-724
131. Siidra O.I., Vladimirova V.A., Tsirlin A.A., Chukanov N.V., Ugolkov V.L. $Cu_9O_2(VO_4)_4Cl_2$, the first copper oxychloride vanadate: mineralogically inspired synthesis and magnetic behavior. // *Inorg Chem.* – 2020. – Vol. 59. – P. 2136-2143
132. Siidra O.I., Zinyakhina D.O., Zadoya A.I., Krivovichev S.V., Turner R.W. Synthesis and modular structural architectures of mineralogically inspired novel complex Pb oxyhalides. // *Inorg. Chem.* – 2013. – Vol. 52. – P. 12799-12805.
133. Soda G., Chiba T. Hydrogen-bond network in ferroelectric lithium trihydrogen selenite, $LiD_3(SeO_3)_2$ by deuteron magnetic resonance. // *J. Phys. Soc. Jpn*. – 1969. – Vol. 26. – P. 717-722.
134. Spirovski F., Wagener M., Stefov V., Engelen B., Crystal structures of rubidium zinc bis (hydrogenselenate (IV)) chloride $RbZn(HSeO_3)_2Cl$, and rubidium zinc bis

(hydrogenselenate (IV)) bromide $RbZn(HSeO_3)_2Br$. // *Z. Kristallogr. NCS.* - 2007. – Vol. 222. – P. 91.

135. Sullens T.A., Almond P.M., Byrd J.A., Beitz J.V., Bray T.H., Albrecht-Schmitt T.E. Extended networks, porous sheets, and chiral frameworks. Thorium materials containing mixed geometry anions: Structures and properties of $Th(SeO_3)(SeO_4)$, $Th(IO_3)_2(SeO_4)(H_2O)_3{\cdot}H_2O$, and $Th(CrO_4)(IO_3)_2$. // *J. Solid State Chem.* – 2006. – Vol. 179. – P. 1192-1201.

136. Shuvalov L.A., Bondarenko V.V., Varikash V.M., Gridnev S.A., Makarova I.P., Simonov V. I. Thallium-tri-hydrogen selenite, $TlH_3(SeO_3)_2$ – a new member of alkaline tri-hydrogen selenite crystal family. // *Ferroelectrics Lett.* -1984. – Vol. 2. – P. 143–146

137. Tanini D., Dalia C., Capperucci A. The polyhedral nature of selenium-catalysed reactions: Se (iv) species instead of Se (vi) species make the difference in the on water selenium-mediated oxidation of arylamines // *Green Chem.* – 2021. – Vol. 23. – № 15. – P. 5680-5686

138. Tellgren R., Ahmad D., Liminga R., Hydrogen bond studies: the crystal structure of rubidium trihydrogen selenite, $RbH_3(SeO_3)_2$. // *J. Solid State Chem.* – 1973. – Vol. 6. – P. 250–257

139. Tellgren R., Liminga R. Hydrogen bond studies. LXXXVII. A neutron diffraction study of ammonium trihydrogen selenite. // *Acta Crystallogr.* – 1973. – Vol. 30. – P. 2497–2499,

140. Trombe J.C., Lafront A.M., Bonvoisin J. Synthesis, structure and magnetic measurement of a new layered copper hydrogenselenite: $(Cu(HSeO_3)_2){\cdot}((NH_4)Cl)$. // *Inorg. Chim. Acta* – 1997. – Vol. 262. – P. 47.

141. Tsuboi M. Vibrational spectra of phosphite and hypophosphite anions, and the characteristic frequencies of PO_3^- and PO_2^- groups. // *J. Am. Chem. Soc.* – 1957. – Vol. 79. – P. 1351–1354.

142. Udayakumar D., Rao C.N.R. Organically templated three-dimensional open-framework metal selenites with a diamondoid network. // *J. Mater Chem.* – 2003. – Vol. 13. – P. 1635–1638.

143. Valkonen J. Cadmium selenite-water (4/3) and two polymorphic forms of cadmium selenite. // *Acta Crystallogr.* – 1994. – V. 50. – P. 991-994.

144. Valkonen J. Crystal structures, infrared-spectra, and thermal behavior of calcium hydrogenselenite monohydrate $Ca(HSeO_3)_2H_2O$, and dicalcium diselenite bis(hydrogenselenite) $Ca_2(HSeO_3)_2(Se_2O_5)$. // *J. Solid State Chem.* – 1986. – Vol. 65. – P. 363-369.

145. Vergasova L. P., Krivovichev S. V., Britvin S. N., Filatov S. K., Burns P. C., Ananyev V. V. Allochalcoselite, $Cu^{+}Cu_5^{2+}PbO_2(SeO_3)_2Cl_5$ - A new mineral from volcanic exhalations (Kamchatka, Russia) // *Zapiskiy Rossiyskogo Mineralogicheskogo Obshestva*. - 2005. - Vol. 134.- P. 70-74. (in Russian)

146. Vergasova L. P., Semenova T. F., Krivovichev S. V., Filatov S. K., Zolotarev A. A., Ananiev V. V. Nicksobolevite, $Cu_7(SeO_3)_2O_2Cl_6$, a new complex copper oxoselenite chloride from Tolbachik fumaroles, Kamchatka peninsula, Russia // *Eur. J. of Mineral.* - 2014. - Vol. 26(3). -P. 439-449.

147. Vinorgadova I.S. 2D and ^{133}Cs NMR study of the hydrogen bond network and antiferroelectric phase transition of cesium trihydrogen selenite. // *J. Solid State Chem.* – 1981. – Vol. 40. – P. 361–368,

148. Walsh A., Payne D.J., Egdell R.G., Watson G.W. Stereochemistry of post-transition metal oxides: revision of the classical lone pair model. // *Chem. Soc. Rev*. – 2011. – Vol. 40. – P. 4455-4463.

149. Wang H., Liu L., Hu Z., Wang J., Zhu M., Meng Y., Xu J. RbCl_$(H_2SeO_3)_2$: A salt-inclusion selenite featuring short UV cut-off edge and large birefringence. // *Inorg. Chem*. – 2023. – Vol. 62. – P. 557–564.

150. Wickleder M.S. $Sm_2Se_5O^{13}$: A selenite–diselenite according to $Sm_2(SeO_3)(Se_2O_5)_2$. // *Z. Anorg. Allg. Chem*. – 2006. – Vol. 632. – P. 2377–2379.

151. Wilcox J.S., Prideaux E.B.R. The dissociation constants of selenious acid. // *J. Chem. Soc. Trans*. – 1925. – Vol. 127. – P. 1543-1546.

152. Wu Q., Zhou J., Liu X., Jiang X., Zhang Q., Lin Z., Xia M. $Ca_3(TeO_3)_2(MO_4)$ (M = Mo, W): mid-infrared nonlinear optical tellurates with ultrawide transparency ranges and superhigh laser-induced damage thresholds. // *Inorg. Chem.* - 2021. – Vol. 60. – P. 18512−18520.

153. Xiao B., Klinkenberg M., Bosbach D., Suleimanov E.V., Alekseev E.V. Effects of Te(IV) oxo-anion incorporation into thorium molybdates and tungstates. // *Inorg. Chem*. – 2015. – Vol. 54. – P. 5981−5990.

154. Xiao D., An H., Wang E., Sun C., Xu L. Structural effects of lone-pair electrons: a novel three-dimensional, open-framework metal selenite constructed from $\{CoSeO_3\}_n$ double helical chains linked via ethylenediamine pillars. // *J. Coord. Chem.* – 2006. – Vol. 59. – P. 395-402.

155. Xiao F., Lei C., Dong Z., Martínez C., Martínez-Triguero J., Chen W., Corma A. Cationic Oligomer as an Organic Template for Direct Synthesis of Aluminosilicate ITH Zeolite. // *Ang. Chem. Int. Ed.* - 2020. - Vol. 59. - P. 15649-15655

156. Yakubovich O.V., Steele I.M., Dimitrova O.V. A new type of mixed anionic framework in microporous rubidium copper vanadyl(V) phosphate, $Rb_2Cu(VO_2)_2(PO_4)_2$. // *Acta Crystallogr*. – 2008. – Vol. C64. – P. i62-i65

157. Yu H., Koocher N., Rondinelli J.M., Halasyamani P.S. Pb_2BO_3I: a borate iodide with the largest second-harmonic generation (SHG) response in the $KBe_2BO_3F_2$ (KBBF) family of nonlinear optical (NLO) materials. // *Angew. Chem. Int. Ed.* – 2018. – Vol. 57. – P. 6100−6103.

158. Zakharov K.V., Zvereva E.A., Berdonosov P.S., Kuznetsova E.S., Dolgikh V.A., Clark L., Black C., Lightfoot P., Kockelmann W., Pchelkina Z.V., Streltsov S.V., Volkova O.S., Vasiliev A.N. Thermodynamic properties, electron spin resonance, and underlying spin model in $Cu_3Y(SeO_3)_2O_2Cl$. // *Phys. Rev*. - 2014, – B90. – Vol. 21. – P. 214417.

159. Zhang D, Berger H, Kremer RK, Wulferding D, Lemmens P, Johnsson M. Synthesis, crystal structure and magnetic properties of the copper selenite chloride: $Cu_5(SeO_3)_4Cl_2$. // *Inorg Chem*. – 2010. – Vol. 49. – P. 9683-9688

160. Zhang J., Zhao X., Wu Y., Mei D., Wen S., Doert T. Synthesis, crystal structures, and thermal analyses of two new antimony tellurite sulfates: $[Sb_2(TeO_4)](SO_4)$ and $[Sb_2(TeO_3)_2](SO_4)$. // *Z. Anorg. Allg. Chem*. – 2021. – Vol. 647. – P. 1269–1276

Illustrative materials

Appendix

Table 1. Bond-valence sums (in valence units, *vu*) in $KNO_3 \cdot 3H_2SeO_3$.

	O1	O2	O3	O4	O5	O6	O7	O8	O9	O10	O11	O12	∑va
K1	0.18	0.15	0.07	0.17	0.15		0.14	0.18	0.08				1.12
Se1	1.58	1.26	1.17										4.01
Se2				1.5	1.22	1.15							3.87
Se3							1.58	1.19	1.14				3.91
N1										1.69	1.67	1.66	5.02
H1	0.2	0.8											1.00
H2			0.68							0.06	0.26		1.00
H3				0.26	0.74								1.00
H4						0.71				0.22		0.07	1.00
H5							0.12	0.81	0.05				1.00
H6									0.73		0.08	0.19	1.00
∑vc	1.96	2.21	1.92	1.93	2.11	1.86	1.84	2.18	2.00	1.97	1.95	1.92	

Table 2. Bond-valence sums (in valence units, *vu*) in $NaHSeO_3 \cdot 3H_2SeO_3$.

	O1	O2	O3	O4	O5	O6	O7	O8	O9	O10	O11	O12	∑va
Na1		0.2	0.16	0.15	0.17		0.19				0.19		1.06
Se1	1.38	1.39		1.06									3.83
Se2			1.17			1.13				1.5			3.80
Se3							1.5	1.13				1.2	3.83
Se4					1.52				1.18		1.13		3.83
H1									0.73	0.21		0.06	1.00
H2								0.84	0.08				1.00
H3							0.29				0.71		1.00
H4	0.32											0.68	1.00
H5		0.29	0.71										1.00
H6				0.8	0.2								1.00
H7	0.08					0.86				0.08		0.06	1.00
∑vc	1.78	1.88	2.04	2.01	1.89	1.99	1.98	1.97	1.99	1.78	2.03	2.00	

Table 3. Bond-valence sums (in valence units, *vu*) in $Pb_2(ReO_4)_2(SeO_3)(H_2O)_2$.

	O1	O2	O3	O4	O5	O6	O7	O8	O9	O10	O11	OW1	OW2	$\sum_v a$
Pb1	0.31	0.24	0.47	0.18				0.27	0.18		0.14	0.27		2.06
Pb2	0.23	0.41	0.32		0.32	0.13	0.14			0.27		0.17		1.99
Re1					1.71	1.76	1.73		1.76					6.96
Re2				1.68				1.71		1.79	1.76			6.94
Se1	1.25	1.33	1.33											3.91
H1A												0.79	0.21	1.0
H1B												0.82	0.18	1.0
H2A				0.09									0.91	1.0
H2B	0.15												0.85	1.0
$\sum_v c$	1.94	1.98	2.12	1.95	2.03	1.89	1.87	1.98	1.94	2.06	1.90	2.05	2.15	

Table 4. Bond-valence sums (in valence units, *vu*) in $Pb_2(ReO_4)_2(HPO_3)(H_2O)_2$.

	O1	O2	O3	O4	O5	O6	O7	O8	O9	O10	O11	OW1	OW2	$\sum_v a$
Pb1	0.36	0.16	0.51	0.18		0.06		0.28	0.17		0.13	0.26		2.12
Pb2	0.23	0.46	0.25	0.05	0.33	0.12	0.16			0.29		0.15		2.06
Re1					1.70	1.72	1.73		1.78					6.93
Re2				1.74				1.70		1.80	1.73			6.97
P1*	1.31	1.42	1.42											4.14
H1A												0.79	0.21	1.0
H1B												0.83	0.17	1.0
H2A				0.08									0.83	1.0
H2B	0.14												0.86	1.0
$\sum_v c$	2.04	2.04	2.18	2.05	2.03	1.90	1.89	1.98	1.95	2.09	1.86	2.03	2.07	

Table 5. Bond-valence sums (in valence units, *vu*) in $Pb_4(HSeO_3)_3(NO_3)_2 \cdot 2H_2O$

	O1	O2	O3	O4	O5	O6	O7	O8	O9	O10	O11	O12	O13	O14	O15	OW1	OW2*	OW3*	OW4*	$\sum_v c$
Pb1		0.78	0.24	0.34	0.40						0.11	0.09				0.03↓→ 0.03↓	0.07	0.08		2.14
Pb2	0.39		0.25	0.38		0.24	0.14	0.17	0.13			0.21			0.16					2.07
Pb3	0.29		0.34		0.29	0.29		0.27			0.17			0.13	0.11	0.04↓→ 0.04↓	0.10	0.10		2.15
Pb4						0.39	0.60	0.30	0.22			0.16	0.16	0.15	0.14					2.12
Se1	1.32	1.28	1.27																	3.87
Se2				1.31	1.31	1.20														3.82
Se3							1.32	1.31	1.20											3.83
N1										1.80	1.63	1.55								4.98
N2													1.83	1.63	1.59					5.05
$\sum_v a$	2.00	2.06	2.10	2.03	2.00	2.12	2.06	2.05	1.55	1.80	1.91	2.01	1.99	1.91	2.00	0.14	0.17	0.18	0	

Table 6. Bond-valence sums (in valence units, *vu*) in $Bi_5(Se_2O_5)(SeO_3)_5Cl_3$

	O1	O2	O3	O4	O5	O6	O7	O8	O9	O10	O11	O12	O13	O14	O15	O16	O17	O18	O19	O20	Cl1	Cl2	Cl3	$\sum_v c$
Bi1				0.33				0.23	0.23		0.46	0.39					0.65		0.02	0.35	0.17	0.18		2,73
Bi2		0,35		0.38				0.56	0.56			0.28						0.26	0.38				0.13	2,86
Bi3	0,02		0,45		0,50		0.49			0.05	0.58					0.40				0.05	0.09	0.06 + 0.06		2,80
Bi4		0,38	0,31			0,57				0.25 +0.36			0.60	0.10					0.29		0.11			2,96
Bi5	0,59				0,26	0,02							0.23		0.20 + 0.44	0.34		0.46					0.20	2,75
Se1						0.08	1.36			1.29	0.02		0.01	1.02		0.02	0.03		0.01			0.01		3,84
Se2			1.41		1.21		0.03 + 0.01			0.10 + 0.01			1.26			0.01			0.01				0.02	4,08
Se3							0.05	0.01	0.05	0.01				0.92					1.29	1.54	0.01	0.03		3,90
Se4	1.32				0.09	0.01					1.12	1.31			0.01	0.01	0.02	0.01					0.04 + 0.01	3,93
Se5	0.01	0.01		1.28 + 0.01				1.21 + 0.01	1.41			0.09									0.01			4,05
Se6	0.02			0.10					0.01			0.01				1.24	1.38	1.21		0.03		0.01		4,02
Se7	0.07	1.26				1.20							0.01		1.38			0.01			0.01		0.02	3,97
$\sum_v a$	2,03	1,99	2,17	2.10	2,07	1,87	1.94	2.02	2.02	2.07	2.18	2.07	2.11	2.04	2.03	2.02	2.09	1.96	1.99	1.98	0.40	0.38	0.42	sum

Table 7. Atomic coordinates, displacement parameters ($Å^2$) and bond-valence sums (in valence units, *vu*) in $Pb_5Cu^{+}_4(SeO_3)_4Br_6$.

Atom	B.V.S.	x/a	y/b	z/c	Ueq	U11	U22	U33	U23	U13	U12
Pb1	1.98	0.20736(2)	0	0.24894(3)	0.01785(11)	0.02264(19)	0.0159(2)	0.01605(17)	0	0.00672(13)	0
Pb2	2.02	0.16141(2)	½	-0.00600(3)	0.01814(11)	0.01362(17)	0.0240(2)	0.01667(17)	0	0.00321(12)	0
Pb3	1.84	½	½	0	0.02900(15)	0.0163(3)	0.0468(4)	0.0229(3)	0	0.00256(19)	0
Br1	n/a	0.39943(6)	0	0.37459(8)	0.0276(2)	0.0227(5)	0.0316(7)	0.0267(5)	0	0.0020(4)	0
Br2	n/a	0.23400(6)	-½	0.39389(7)	0.0216(2)	0.0264(5)	0.0186(5)	0.0187(4)	0	0.0028(3)	0
Br3	n/a	0.05759(6)	0	0.37408(8)	0.0263(2)	0.0283(5)	0.0276(6)	0.0259(5)	0	0.0123(4)	0
Se1	4.08	0.05965(5)	-½	0.19334(6)	0.01231(18)	0.0127(4)	0.0141(5)	0.0102(3)	0	0.0027(3)	0
Se2	3.95	0.33617(5)	½	0.17530(6)	0.01321(19)	0.0131(4)	0.0121(5)	0.0135(4)	0	0.0011(3)	0
Cu1A1	n/a	½	0.281(2)	½	0.051(3)						
Cu1B2	n/a	0.4845(3)	0.2322(12)	0.5011(5)	0.050*						
Cu2A3	n/a	0.3480(6)	-0.227(2)	0.5045(7)	0.054(3)	0.064(4)	0.063(6)	0.043(3)	0.011(3)	0.028(3)	0.015(4)
Cu2B4	n/a	0.1512(7)	0.220(4)	0.5061(11)	0.065(4)	0.047(6)	0.069(9)	0.060(6)	-0.024(5)	-0.026(4)	0.029(5)
O1	2.13	-0.0283(4)	-0.500000	0.1124(6)	0.065(4)	0.012(4)	0.147(12)	0.031(4)	0	-0.005(3)	0
O2	1.81	0.1020(3)	-0.2667(9)	0.1393(3)	0.0213(10)	0.035(3)	0.009(2)	0.022(2)	0.0004(19)	0.0109(19)	0.000(2)
O3	2.10	0.3732(4)	0.500000	0.0633(6)	0.0295(17)	0.024(4)	0.034(5)	0.037(4)	0	0.020(3)	0
O4	1.95	0.2733(2)	0.2647(9)	0.1408(3)	0.0172(9)	0.020(2)	0.013(3)	0.019(2)	-0.0007(18)	0.0057(17)	-0.0048(19)

Table 8. Atomic coordinates, displacement parameters (Å^2) and bond-valence sums (in valence units, *vu*) in $Pb_8Cu^{2+}(SeO_3)_4Br_{10}$

Atom	*B.V.S.*	*x*/*a*	*y*/*b*	*z*/*c*	U_{eq}	U_{11}	U_{22}	U_{33}	U_{23}	U_{13}	U_{12}
Pb1	1.98	½	0.83257(5)	0	0.01835(17)	0.0219(3)	0.0123(3)	0.0208(4)	0	0.0025(3)	0
Pb2	1.94	0.35743(5)	0.87374(4)	0.38065(4)	0.01907(15)	0.0226(2)	0.0205(2)	0.0141(3)	-0.0033(2)	0.0016(2)	-0.0008(2)
Pb3	2.05	½	½	0.31521(7)	0.02170(18)	0.0185(3)	0.0189(3)	0.0277(4)	0	0	0.0023(3)
Se1	4.01	0.26743(12)	0.63118(10)	0.12424(10)	0.0111(2)	0.0118(5)	0.0129(5)	0.0085(6)	-0.0019(5)	0.0008(4)	-0.0001(4)
Cu1	1.84	½	½	0	0.0097(5)	0.0110(11)	0.014(1)	0.0039(13)	0	0	0
Br1	1.02	0.55355(15)	0.72899(10)	0.21669(11)	0.0169(3)	0.0239(6)	0.0151(6)	0.0117(6)	-0.0020(4)	-0.0015(5)	-0.0010(5)
Br2	0.73	½	0.66049(15)	½	0.0235(4)	0.0420(10)	0.0150(8)	0.0134(9)	0	0.0054(10)	0
Br3	0.89	0.68809(14)	0.98878(14)	0.84773(12)	0.0225(3)	0.0187(6)	0.0316(8)	0.0171(7)	0.0015(6)	0.0033(5)	0.0000(6)
O1	2.02	0.3614(9)	0.5139(7)	0.1150(8)	0.0142(17)	0.016(4)	0.016(4)	0.011(4)	-0.002(4)	0.002(4)	0.003(4)
O2	2.02	0.3227(11)	0.6948(8)	0.0140(9)	0.020(2)	0.023(4)	0.022(5)	0.016(6)	0.006(4)	-0.003(4)	-0.009(4)
O3	2.05	0.1120(10)	0.5803(8)	0.0782(8)	0.0140(19)						

Table 9. Atomic coordinates, displacement parameters (Å^2) and bond-valence sums (in valence units, *vu*) in $Pb_5Cu^{2+}(SeO_3)_4(Br,Cl)_4$

Atom	*B.V.S.*	*x*/*a*	*y*/*b*	*z*/*c*	U_{eq}	U_{11}	U_{22}	U_{33}	U_{23}	U_{13}	U_{12}
Pb1	1.88	0.10398(2)	0.03948(6)	0.17919(2)	0.01721(10)	0.01567(16)	0.02082(18)	0.01594(16)	-0.00114(12)	0.00520(11)	-0.00082(12)
Pb2	1.95	0.26854(2)	-0.00104(6)	0.36598(2)	0.01843(10)	0.01670(17)	0.02071(18)	0.01799(16)	0.00148(12)	0.00409(12)	0.00436(12)
Pb3	2.24	0	0.53164(8)	¼	0.01513(11)	0.0138(2)	0.0177(2)	0.0145(2)	0.000	0.00454(15)	0.000
Se1	3.88	0.16593(3)	0.48374(13)	0.32764(6)	0.01303(17)	0.0119(4)	0.0143(4)	0.0136(4)	-0.0009(3)	0.0043(3)	-0.0009(3)
Se2	3.92	0.04406(3)	-0.01365(13)	0.41225(5)	0.01190(16)	0.0104(3)	0.0138(4)	0.0112(4)	0.0013(3)	0.0020(3)	0.0004(3)
Cu1	1.85	0	½	½	0.0135(3)	0.0137(6)	0.0144(7)	0.0131(6)	0.0042(5)	0.0046(5)	-0.0004(5)
*X*1	0.82	0.30042(4)	0.48992(16)	0.47167(7)	0.0214(4)	0.0195(5)	0.0191(6)	0.0275(6)	-0.0003(4)	0.0095(4)	-0.0008(3)
*X*2	0.77	0.10159(6)	0.5124(3)	0.53341(12)	0.0221(5)	0.0171(8)	0.0229(9)	0.0268(9)	-0.0005(6)	0.0060(6)	0.0000(6)
O1	1.90	0.1844(2)	0.7268(11)	0.2691(4)	0.0197(13)	0.016(3)	0.018(3)	0.025(3)	0.005(2)	0.005(3)	-0.003(2)
O2	2.01	0.0662(2)	0.9088(11)	0.3131(4)	0.0209(13)	0.020(3)	0.028(3)	0.021(3)	-0.001(3)	0.016(2)	-0.002(3)
O3	2.05	0.1992(2)	0.2630(11)	0.2746(4)	0.0189(13)	0.013(3)	0.022(3)	0.022(3)	-0.001(2)	0.005(2)	0.006(2)
O4	2.00	-0.0023(2)	0.2143(10)	0.3761(4)	0.0191(13)	0.013(3)	0.018(3)	0.027(3)	0.006(2)	0.006(2)	0.002(2)
O5	2.05	-0.0061(2)	0.7661(10)	0.4093(4)	0.0158(12)	0.015(3)	0.019(3)	0.013(3)	0.006(2)	0.004(2)	-0.005(2)
O6	2.08	0.1009(2)	0.4126(11)	0.2674(4)	0.0203(13)	0.007(3)	0.022(3)	0.031(3)	-0.005(3)	0.005(2)	-0.002(2)